An in vitro model for the mouse Epiblast to investigate the establishment of the antero-posterior polarity.

Sara Bonavia

Université de Paris
Ecole doctorale Frontières du Vivant ED474
Laboratoire Matière et Systèmes Complexes

An *in vitro* model for the mouse Epiblast to study the establishment of the Antero-posterior polarity

Par Sara Bonavia

Thèse de doctorat de Physique

Dirigée par Jean-Marc Di Meglio
Et par Benoit Sorre

Présentée et soutenue publiquement le 28 Novembre 2019

Devant un jury composé de :

Sylvie Hénon	Université de Paris	Présidente
Iftach Nachman	Tel Aviv University	Rapporteur
Nicolas Rivron	IMBA Vienna	Rapporteur
Benoit Sorre	Université de Paris	Co-directeur de thèse
Jean-Marc Di Meglio	Université de Paris	Directeur de thèse

Titre : Un modèle in vitro de l'Épiblaste de la souris pour l'étude de l'établissement de la polarité antero-posterieure

Résumé :

Le développement d'un embryon est une interaction de phénomènes, impliquant des réarrangements morphogénétiques, mouvement collective et différenciation cellulaire. Comment une forme complexe, composée de nombreux tissus différents, résulte d'un pool symétrique de cellules identiques n'est pas encore totalement dévoilé. Dans cette thèse, nous nous intéressons à comprendre l'un des premiers événements qui brise la symétrie de l'embryon et établit une direction dans laquelle les différents tissus du futur corps seront répartis : l'établissement de la polarité antéro-postérieure (A-P), qui marquera le locus où la gastrulation va commencer. La manière dont cet axe est établi a été partiellement élucidée. Nous savons que le processus est contrôlé par des signaux chimiques, morphogènes, sécrétés par certains sous-groupes de cellules du tissu extra-embryonnaire. Les conditions minimales d'observation de la polarité ne sont cependant pas encore claires. Avec ce travail, nous avons l'intention de construire un système synthétique in vitro pour découvrir les ingrédients minimaux pour observer la brisure de symétrie dans une structure symétrique, qui imite l'épiblaste en morphologie et en expression génétique. Nous observons comment ce système réagit sous stimulation homogène avec des morphogènes. Nous comparons les résultats obtenus, à une situation où la symétrie du stimulus est brisée. Pour stimuler les cellules avec un stimulus directionnel, nous faisons recours à la microfluidique : nous avons développé un dispositif qui nous permet de stimuler notre épiblaste synthétique avec un gradient de morphogènes. Notre dispositif d'origine reposait sur un débit continu pour établir un puits et une source parfaits pour maintenir le gradient. Nous avons observé une perte d'expression du gene Nodal que nous n'avons pas observée en stimulant les organoïdes uniformément. Nous émettons l'hypothèse que le débit continu est responsable de l'élimination d'une partie de la signalisation sécrétée par les cellules. En modifiant le dispositif pour induire une stimulation uniforme, mais en produisant un gradient de molécules sécrétées, nous avons pu observer la polarité des organoïdes d'une manière plus cohérente qu'en les stimulant uniformément. Nous concluons que ces expériences suggèrent l'existence d'un mécanisme d'autorégulation dans l'embryon pour établir la polarité, et que ce mécanisme coopère avec d'autres pour assurer la robustesse de la polarisation, et qu'une source localisée de molécules de signalisation pourrait être pertinente pour augmenter la fréquence de l'observation de la polarité des organoides des cellules souches embryonnaires. Nous prévoyons que d'autres études utilisant des gradients statiques permettront de pousser ce résultat plus loin. Enfin, nous proposons un système qui permettrait d'étudier un aspect sous-investi du développement : le rôle du confinement physique. Comme on le voit, l'embryon précoce est confiné par le tissu extra-embryonnaire, lui appliquant une contrainte. Nous suggérons qu'il serait intéressant d'étudier l'aspect confinement, en le dissociant de l'aspect

signalisation. Pour ce faire, nous proposons d'adapter une méthode d'encapsulation développée à l'origine pour cultiver des organoïdes de cellules cancéreuses, pour encapsuler des cellules souches embryonnaires.

Mots clefs :

biologie du développement, cellules souches, organoids, synthetic embryology, microfluidique, morphogenèse, gradients

Title : An in vitro model for the mouse Epiblast to investigate the establishment of the antero-posterior polarity

Abstract :

The development of an embryo is an interplay of phenomena, involving morphogenetic rearrangements, collective migration and cell differentiation. How a complex shape, made of many different tissues, arises from a symmetric pool of identical cells is still not fully unveiled. In this thesis, we are interested in understanding one of the first events that breaks the symmetry of the embryo and establishes a direction along which, the different tissues of the future body will be allocated: the establishment of the Antero-Posterior polarity (A-P), that will mark the locus at will gastrulation will start. How this axis is established has been partly elucidated. We know that the process is controlled by some chemical signalling, morphogens, released by some subgroups of cells in the extra-embryonic tissue. The minimal conditions for observing polarity however are still not clear. With this work we intend to build a synthetic in vitro system to find out the minimal ingredients to observe symmetry breaking in a symmetrical structure, that mimics the Epiblast in morphology and gene expression. We observe how this system reacts under homogeneous stimulation with morphogens. We compare the results obtained, to a situation where the symmetry of the stimulus is broken. To feed the cells with a directional stimulus, we make use of microfluidics: we developed a device that allows us to stimulate our synthetic Epiblast with a gradient of morphogens. Our original device was relying on continuous flow to establish a perfect sink and source to maintain the gradient. We observed a loss of Nodal expression that we did not observe when stimulating the organoids in bulk. We hypothesise the continuous flow to be accountable for washing out some secreted signalling downstream of the signal we induce differentiation with. By modifying the device to induce a uniform stimulation, but producing a gradient of secreted molecules, we were able to observe polarity arising in the organoids in a more consistent way than in bulk. We conclude that these experiments hint to the existence of a self-regulated mechanism in the embryo to establish polarity, and that this mechanism co-operate with others to ensure the robustness of the polarisation, and that a localised source of signalling molecules could be relevant to increase the frequency of observation of polarity in Embryonic Stem Cells only organoids. We anticipate that further studies making use of static gradients devices would allow to push this result further. Last, we propose a system that would allow

the study of an underinvestigated aspect of development: the role pf physical confinement. As seen, the early embryo is confined by the Extra-embryonic tissue, applying a constraint to it. We suggest that it would be interesting to study the confinement aspect, uncoupling it from the signalling aspect. To do so, we propose to adapt an encapsulation method originally developed to grow cancer cells organoids, to encapsulate Embryonic Stem Cells.

Keywords :

developmental biology, stem cells, organoids, synthetic embryology, microfluidics, morphogenesis, gradients

An *in vitro* model for the mouse Epiblast to investigate the establishment of the antero-posterior polarity

Sara Bonavia

Advisor: Benoit Sorre

Advisor: Jean-Marc Di Meglio

Contents

List of Figures

1 Introduction

The development of an embryo is an interplay of phenomena, involving morphogenetic rearrangements, collective migration and cell differentiation. How a complex shape, made of many different tissues, arises from a symmetric pool of identical cells is still not fully unveiled.

In this thesis, we are interested in understanding one of the first events that breaks the symmetry of the embryo and establishes a direction along which, the different tissues of the future body will be allocated: the establishment of the Antero-Posterior polarity (A-P), that will mark the locus at will gastrulation will start. How this axis is established has been partly elucidated. We know that the process is controlled by some chemical signalling, morphogens, released by some subgroups of cells in the extra-embryonic tissue. The minimal conditions for observing polarity however are still not clear.

With this work we intend to build a synthetic *in vitro* system to find out the minimal ingredients to observe symmetry breaking in a symmetrical structure, that mimics the Epiblast in morphology and gene expression. We observe how this system reacts under homogeneous stimulation with morphogens. We compare the results obtained, to a situation where the symmetry of the stimulus is broken. To feed the cells with a directional stimulus, we make use of microfluidics: we developed a device that allows us to stimulate our synthetic Epiblast with a gradient of morphogens. Our original device was relying on continuous flow to establish a perfect sink and source to maintain the gradient. We observed a loss of Nodal expression that we did never observed when stimulating the organoids in bulk. We hypothesise the continuous flow to be accountable for washing out some secreted signalling downstream of the signal we induce differentiation with. By modifying the device to induce a uniform stimulation, but producing a gradient of secreted molecules, we were able to observe polarity arising in the organoids in a more consistent way than in bulk. We conclude that these experiments hint to the existence of a self-regulated mechanism in the embryo to establish polarity, and that this mechanism co-operate with others to ensure

the robustness of the polarisation, and that a localised source of signalling molecules could be relevant to increase the frequency of observation of polarity in Embryonic Stem Cells only organoids. We anticipate that further studies making use of static gradients devices would allow to push this result further.

Last, we propose a system that would allow the study of an underinvestigated aspect of development: the role pf physical confinement. As seen, the early embryo is confined by the Extra-embryonic tissue, applying a constraint to it. We suggest that it would be interesting to study the confinement aspect, uncoupling it from the signalling aspect. To do so, we propose to adapt an encapsulation method originally developed to grow cancer cells organoids, to encapsulate Embryonic Stem Cells.

The thesis is organised as follows: in Section 2, I sketch some basic concepts in mouse developmental biology, that we will make use of in the following, introduce the latest results in the rapidly growing field of synthetic embryology, providing the rationale for the study here discussed. Then in Section 3, I detail our synthetic model of the Epiblast and discuss what kind of expression patterns it is possible to observe when a uniform stimulus is applied. I compare these results with what we obtain when we expose the same system to a gradient of signalling molecules in Section 4). In Section 5, I describe a possible method to investigate the role of confinement in early development.

Lastly, I draw some conclusions and sketch some future directions to undertake to follow up this study.

2 From Embryology to Developmental Biology to the Stem cell era

> Science, like life itself, indeed like history, itself, is a historical phenomenon. It can build itself only out of its past.
>
> Jane Oppenheimer

The history of embryology is as fascinating and wide and complicated as embryology itself.
Wondering about how we 'come to being' has kept human kind busy along, we could say, its entire existence (Figures 2.1 and 2.2 report illustrations of gestation respectively found in New Guinea and Japan) [Wallingford, 2019]. And whether answers have been provided from time to time by religion, philosophy or science, it is that urgency for answers that represents the common thread that connects primitive beliefs to Aristotelian theories and their first observations, to Preformationism and Epigenesis and their opposite fundamental concepts, to Leonardo's first dissection of the human fetus, to embryology in Germany during the 19th century, to Ethel Browne's experiments and discoveries (still not fully acknowledged [Lenhoff, 1991]) on what Mangold and Spemann will later call the organizer, to Developmental Biology and its genetic approach, and now to Stem Cell Biology.

In what follows, we will summarise the main facts we consider established about the development of the mouse embryo up to the gastrulation stage, and argue what we can hope to add to that, by means of the synthetic model we developed.

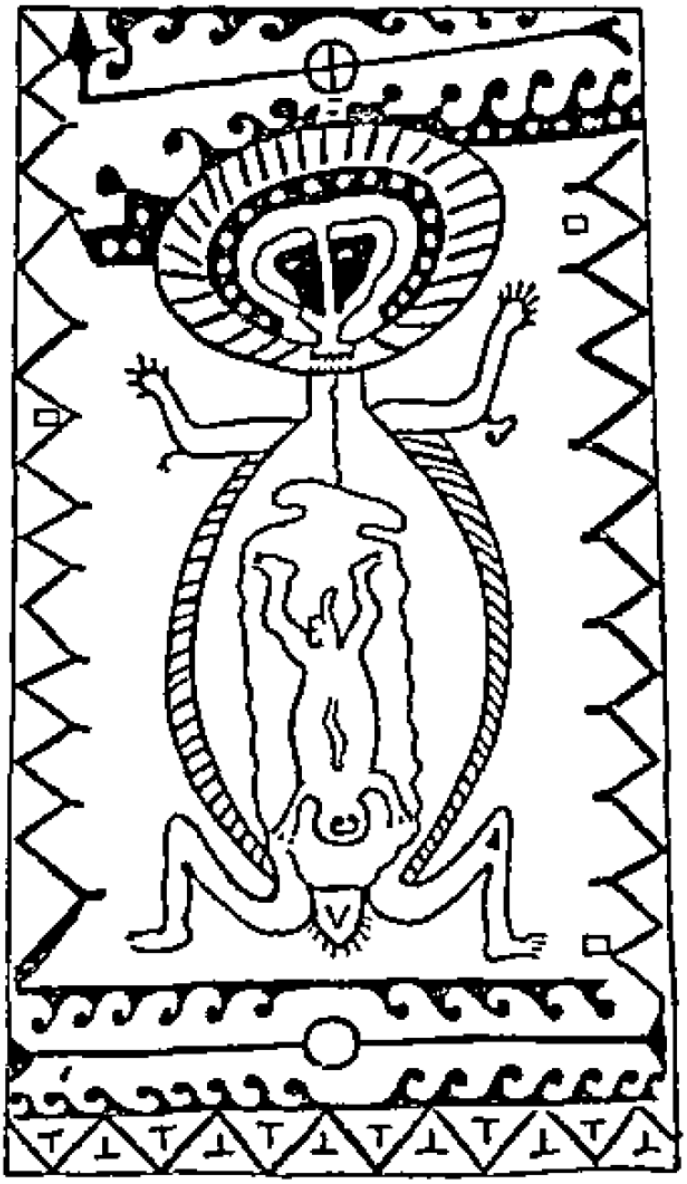

Figure 2.1: **Representation of gestation, New Guinea** Painted and carved door from New Guinea, according to [Needham, 1959], who erroneously attributes it to [De Clerq and Schmelz, 1983]. It is not known whether the cord connecting the fetus to upper part of the body of the mother reflects some local knowledge on gestation

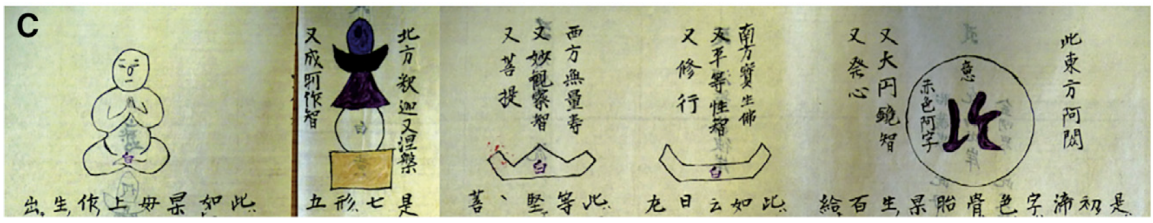

Figure 2.2: **Five stages of gestation in Buddhist belief** Estimated from 14th century, conserved in the Jindaiji Temple in Tokyo, Japan. Reported from [Wallingford, 2019]

2.1 A brief history of Early development in the Mouse: from the Zygote to the Late Blastocyst

The early development of the mouse embryo is a succession of cell fate specification steps and cell rearrangements.

In this section, which does not intend to be an exhaustive discussion on what is known about mouse development (which on the other hand can be found for example in [Rossant, 2004] or [Arnold and Robertson, 2009]), I will mainly focus on the main characteristics and events that are most significant to motivate what we will discuss later and elucidate what features of the real embryo we aim to capture with our models. Particularly I will try to highlight those aspects on which we still lack knowledge, and how we expect it may be possible to better understand the underlying mechanisms that produce them, with the *in vitro* model that we present later.

This section is organised as follows: a brief recap of the events that lead to the late blastocyst formation, followed by a discussion on the main signalling pathways involved in the gastrulation process.

Up to implantation, which takes place around the end of E4.0 [Yoshinaga, 2013] [Matsumoto, 2017], the embryo will specify three different cell lineages, the Epiblast, which is the embryo proper, and two extra-embryonic lineages, the Extra-embryonic Ectoderm, which will give rise to the placenta and the Visceral Endoderm, which will generate the yolk sac. But first, the zygote undergoes three rounds of cell division. Up to the 8-cells stage, the cells that form the embryo (morula, at this stage), are

called blastomers, and do not present any substantial difference in morphology nor gene expression. Cell division up to this stage produces cells that are progressively smaller, while the total volume of the embryo does not change [Cockburn and Rossant, 2010]. The embryo at this stage can be described as a clump of cells that is overall spherically symmetric.

The first morphological change, is called compaction and it occurs at the late 8-cell stage. During compaction the morula becomes a compacted, full sphere of cells. This rearrangement happens as adherens and tight junctions are established at the cell-cell contact. Cells appear to have then a flattened morphology. E-cadherin being the main player in establishing adherens junctions, and considering that embryos lacking E-cadherin would fail to maintain the epithelial morphology beyond the morula stage [Riethmacher et al., 1995], while still being able to compact in the first place thanks to maternal E-cadherin, compaction has long being thought to be regulated by E-cadherin. A recent study [Maître et al., 2015] showed that this process seems to be controlled rather by an increase of tension at the cell-cell contact, mainly due to acto-myosin contractility.

Up to E3.5 and around the 32-cell stage two main events, that are shown in Figure 2.3, take place: two cell lineages are specified, the Trophectoderm (TE), an extra-embryonic tissue that surrounds the embryo, and the Inner Cell Mass (ICM), which is the embryo proper, and a cavity, the blastocoel, is formed at the interface of the two tissues.

It is known that a pool of genes that are relevant to the fate specification are OCT4, Sox2, Nanog (for the ICM) and CDX2 (for the TE). These genes are first co-expressed among the blastomers, and then become segregated respectively in the Inner Cell Mass and the Trophectoderm (Figure 2.3). This segregation is first established as Cdx2 starts being expressed exclusively in outer cells in the embryo and is later maintained by the reciprocal repression of this two pools of genes and their auto-regulation.

To explain how these two cell lineages are specified and what produces this asymmetric expression in Cdx2, it has been proposed by [Maître et al., 2016] that the

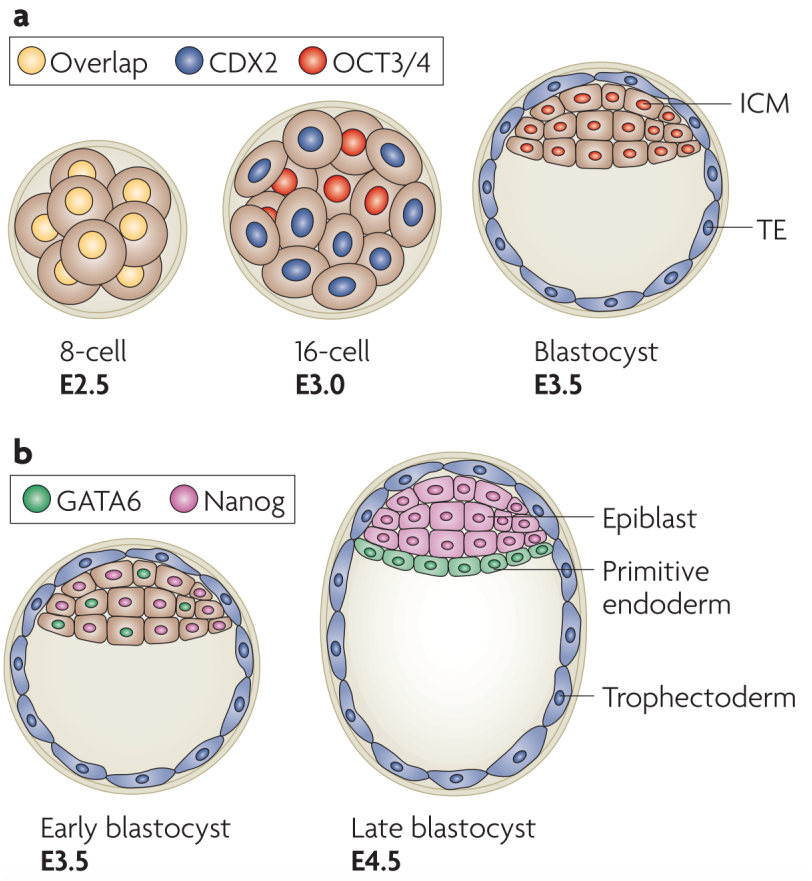

Figure 2.3: **The mouse embryo, from fertilisation to implantation stage** From fertilisation to implantation stage, the mouse embryo specifies three lineages. The fist morphological change is compaction, by which the morula acquires its flatten and compact layout. Then, the first cell fate specification takes place around E3.5: two lineages are specified, the Inner Cell Mass (embryonic) and the Trophectoderm (extra-embryonic). At this stage the embryo is called (early) blastocyst. Then, around E4.5, another two lineages are specified from the ICM: the Visceral Endoderm (extra-embryonic) and the Epiblast (embryonic). The figure highlights that asymmetries in gene expression arise before the lineages are fully specified. Figure is adapted from [Arnold and Robertson, 2009]

mechanism underlying cell sorting and resulting in the TE encapsulating the ICM would be regulated by a difference in contractility resulting from an asymmetric segregation of apical domain among the blastomers.

The second event we mentioned is the formation of a fluid filled cavity, called blastocoel, at the interface of the two tissues. The formation of a cavity on one side of the embryo represents the first symmetry breaking in the up to now spherically symmetric structure of the embryo. The mechanical aspect of how the blastocoel is formed and positioned has been again recently described by [Dumortier et al., 2019], where they show that many micro holes are dynamically formed at the cell-cell interface, breaking cell-cell contacts with pressurised fluid, and one finally prevails, in a way that they model as an Ostwald ripening process (the process by which in emulsions the droplets of the disperse phase coarsen into bigger structures that minimise the surface to volume ratio, in order to minimise the total surface tension), where fluid discharge toward one peculiar cavity is driven by differences in cell contractility.

At this stage the embryo, composed by two lineages and a cavity separating them, is referred to as early blastocyst.

During the following day another two-cell fate specification takes place among the cells of the Inner Cell Mass, and two lineages appear: en extra-embryonic tissue, the Primitive Endoderm (PE) and the embryo proper, the Epiblast (EPI). By the end of E4.5 the PE is established as an epithelium surrounding the Epiblast, in an outer versus inner cell rearrangement that is similar to the first ICM-TE specification. The relevant genes that specify and identify these two subpopulations are Gata4 and Gata6, from the Gata family, that are necessary for establishing and maintaining the PE and Nanog, a pluripotency marker that is found expressed in the EPI. These genes are found expressed already at E3.5 in the ICM in a mutually exclusive way, meaning that most of cells express only either of them. At this point though, as represented in Figure 2.3, they lack spatial organisation and they are dispersed in a 'salt and pepper' arrangement among the ICM. By E4.5 they are found segregated in two well-defined region of the ICM. Differently from another pluripotency marker, Oct4, which is still found expressed all over the cells of the ICM, Nanog expression is

found restricted to a subgroup of cells of the ICM (the EPI), while Gata4 and Gata6 are found restricted to the region of the ICM that is in contact with the blastocoel, the hypoblast, the prospective PE. Their mutual exclusion, plus the fact that experiments run on Nanog knockout embryos show that they fail to recapitulate both EPI and PE [Silva et al., 2009], suggests that Nanog is required not only to specify the EPI, but also for establishing the PE, hinting to a mechanism of mutual repression between Gata4-Gata6 and Nanog, similar to what has been found for Oct4 and Cdx2, although the existence of such a mechanism has not been proved yet.

2.1.1 Toward the onset of Gastrulation: the role of Nodal, Wnt and BMP in establishing the Antero-Posterior Polarity

The late blastocyst features three lineages, the Extra-embryonic tissues, the Primitive Endoderm and the Trophectoderm and the Epiblast which will give rise to the somatic and germ cells. At this point the Trophectoderm will regulate implantation and give rise to the Extra-embryonic Ectoderm, while the Primitive Endoderm will differentiate into two distinct tissues, the Parietal Endoderm, which will be in contact with the maternal tissues and the Visceral Endoderm, a monolayer surrounding both the Epiblast and the Extra-embryonic Ectoderm.

All these different tissues are represented in Figure 2.4.

From this stage, two main axes will be specified: the Proximal-Distal (P-D) and the Antero-Posterior (A-P) axis.

First the P-D axis is defined by the elongation of the cavity, following the epithelialisation of the Epiblast. The Epiblast then elongates to form a conical structure, referred to as the egg-cylinder. The direction of the elongation defines the P-D axis with the Proximal side in contact with the Extra-embryonic Ectoderm. At this stage the Epiblast is a monolayer of cells.

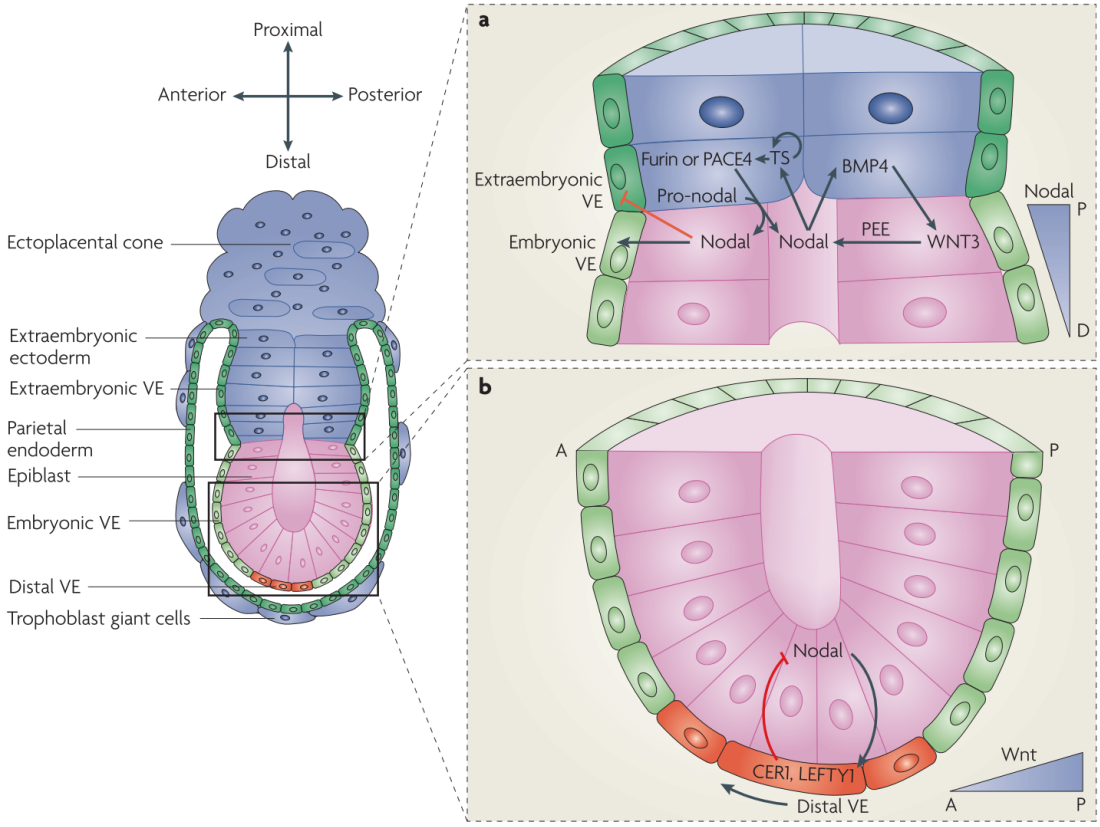

Figure 2.4: **Morphology and signalling pathways in late mouse blastocyst** Around E5.5, in the mouse blastocyst three tissues are present: the Epiblast (an epithelium that represents the embryo proper) the Extra-embryonic Ectoderm, the Visceral Endoderm (two extra-embryonic lineages). The cavity formation and invagination of the Epiblast specifies the Proximal-Distal axis. The Figure shows how Nodal activity will contribute to establishing what will be the Antero-Posterior polarity. Nodal induces BMP in the ExE, that in turn sustains Nodal in the proximal Epiblast, and induces its own inhibitors in the VE, that migrating toward the prospective anterior pole contributes to the restriction of Nodal to the posterior proximal side of the embryo. Adapted from [Arnold and Robertson, 2009]

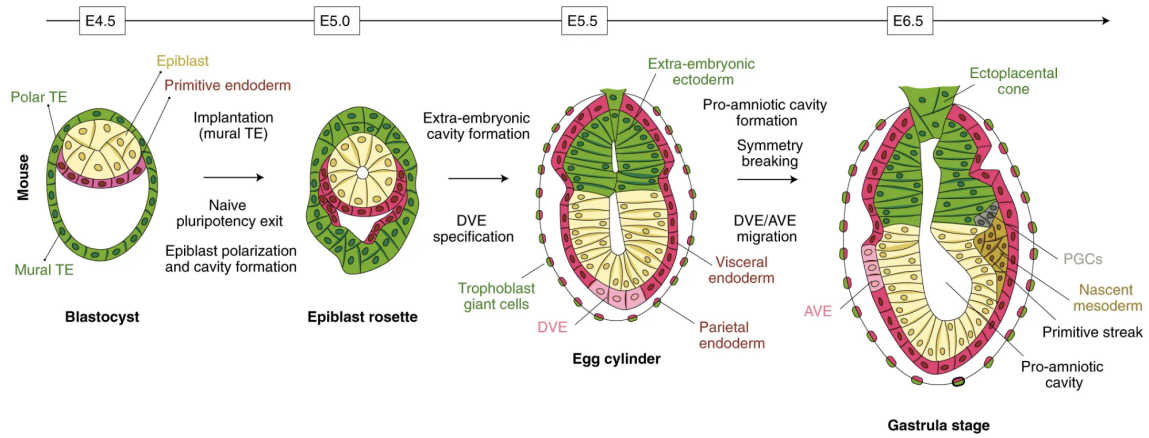

Figure 2.5: **Luminogenesis in the Epiblast** Luminogenesis and following elongation of the Epiblast around E4 establishes the Proximal-Distal axis. A cavity is initially formed in the Epi compartment, following epithelialisation of the Epi, by a mechanism described in [Shahbazi et al., 2017] and relying on the ECM provided by the VE, then a cavity is also formed in the ExE compartment. By E6 at the onset of gastrulation the two cavities are fused together. Adapted from [Shahbazi and Zernicka-Goetz, 2018]

The luminogenesis in the EPI and its elongation are shown in Figure 2.5. The same Figure also shows the formation and subsequent elongation of a cavity also in the ExE compartment at the Proximal side. The two cavities later fuse into one. At this stage the Embryo is composed of three epithelia, the ExE, the EPI and the VE. Cross-talk between these three tissues will result in asymmetries in the gene expression patterns in different parts of the embryo and finally in establishing the A-P polarity. This cross-talk is regulated by the morphogens of the TGF-β family, which includes Activins, Nodals, Bone Morphogenetic Proteins (BMPs), and Wnt. The first molecular asymmetry is reported along the P-D axis. The establishment of the reference axis can be considered as the starting point for successive changes and tissue specification. This set of axes will serve as a reference frame for the following gastrulation, the process by which the embryo will allocate the three germ layers that will later give rise to the somatic tissues.

Among the TGF-β family members we will focus here on Nodal and BMP that together with Wnt are responsible of driving this early pattern formation. Their mutual interactions are sketched on top of Figure 2.4, that shows that Nodal sustains the

expression of BMP, that in turn induces Nodal through the activation of Wnt. At E5, Nodal is expressed all over the Epiblast [Brennan et al., 2001]. The Epiblast is radially symmetric. At this stage also Wnt is expressed radially among the cells of the proximal Epiblast (and defines a gene expression pattern along the P-D axis). Later, macroscopic cell rearrangements will break the radial symmetry and trigger the establishment of the Primitive Streak (PS) that will mark the starting point of gastrulation and fix the prospective Posterior side of the Epiblast.

The Primitive Streak, as shown in Figure 2.6 is formed by cell movements that result in a clustering of cells at the proximal Epiblast that undergo an Epithelial-to-Mesenchymal Transition (EMT). Migrating cells, moving toward the Anterior side of the Embryo, will establish the Mesoderm Germ Layer. So, cells in the Primitive Streak start expressing Mesendoderm markers such as Brachyury. The positioning of the Primitive Streak is preceded by an asymmetry in gene expression, with genes, previously expressed all over the Epiblast like Nodal, or all over the Proximal Epiblast, like Wnt, being restricted to the proximal posterior side.

Figures 2.7 and 2.8, show the gene expressions patterns, when the A-P polarity is established, as well as mutant Embryos for Nodal and Wnt failing to establishing it. From data shown in [Brennan et al., 2001] and [Arnold and Robertson, 2009], the Antero-Posterior polarity is established as Nodal is restricted to the Posterior side and Wnt is expressed on the posterior proximal side of the Epiblast.

The mechanism underlying the restriction of Nodal to the Poserior side of the Embryo is not fully elucidated yet, but it has been proposed that Nodal and BMP cooperate to establish the polarity in two main ways, that involve the extra-embryonic tissues present in the late blastocyst. On one side Nodal induces the expression of the Bone Morphogenetic Protein BMP, in the Extra-Embryonic Ectoderm (as shown in Figure 2.7), that reciprocally sustains Nodal expression through activation of Wnt3. BMP is also required to pattern the Proximal Visceral Endoderm, and it is known to induce Cdx2, an extra-embryonic marker, that we can find restricted (Figure 2.7) in the posterior proximal side of the VE at the onset of gastrulation. Embryos lacking

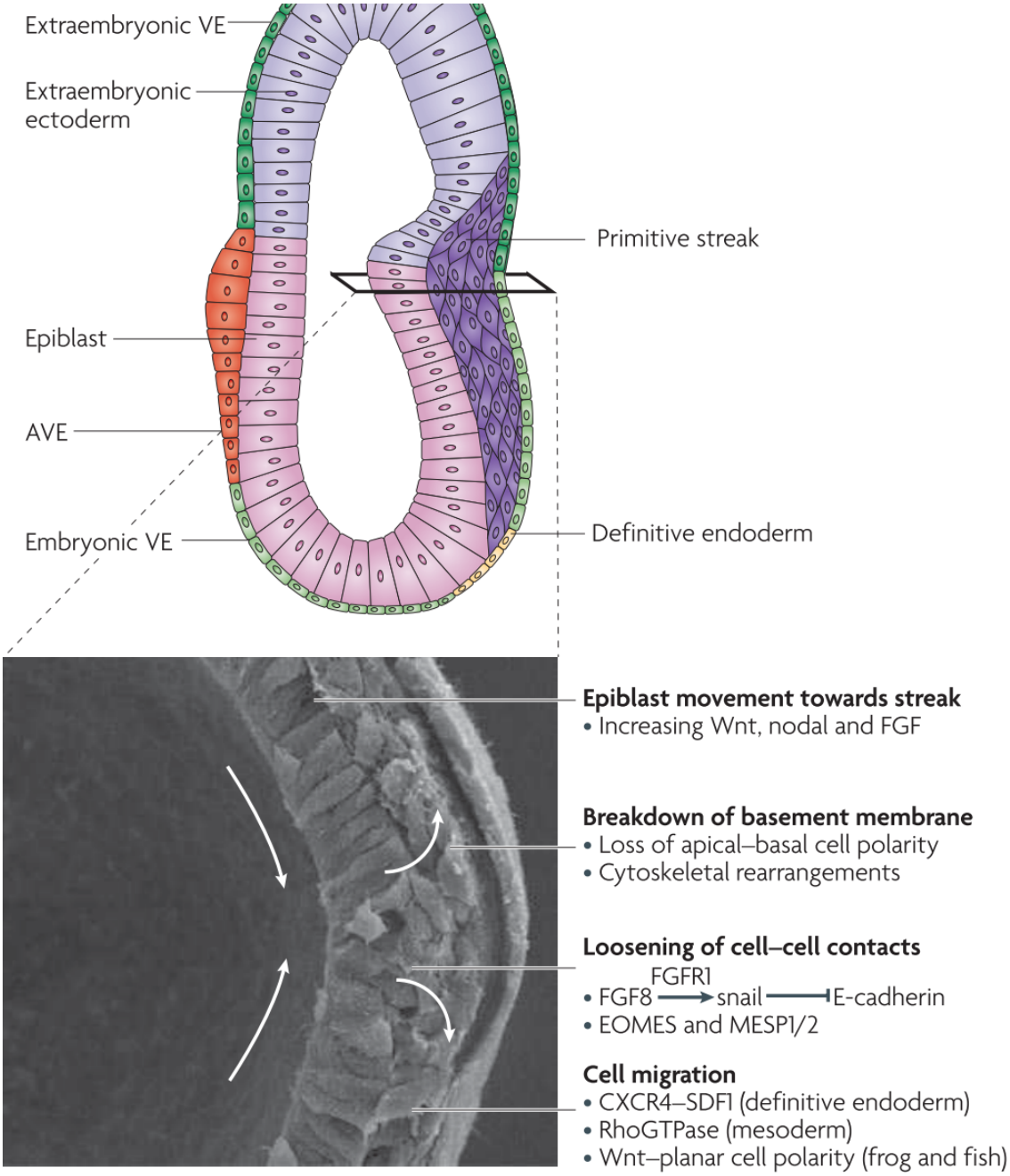

Figure 2.6: **Cells cluster at the posterior side of the embryo and undergo EMT at the onset of gastrulation** The Figure shows the inward movement of cells from the Epiblast toward the Primitive Streak locus, and the outward movement of cells undergoing EMT from the Primitive Streak, that will give rise to the Mesoderm and the Endoderm. Adapted from [Arnold and Robertson, 2009]

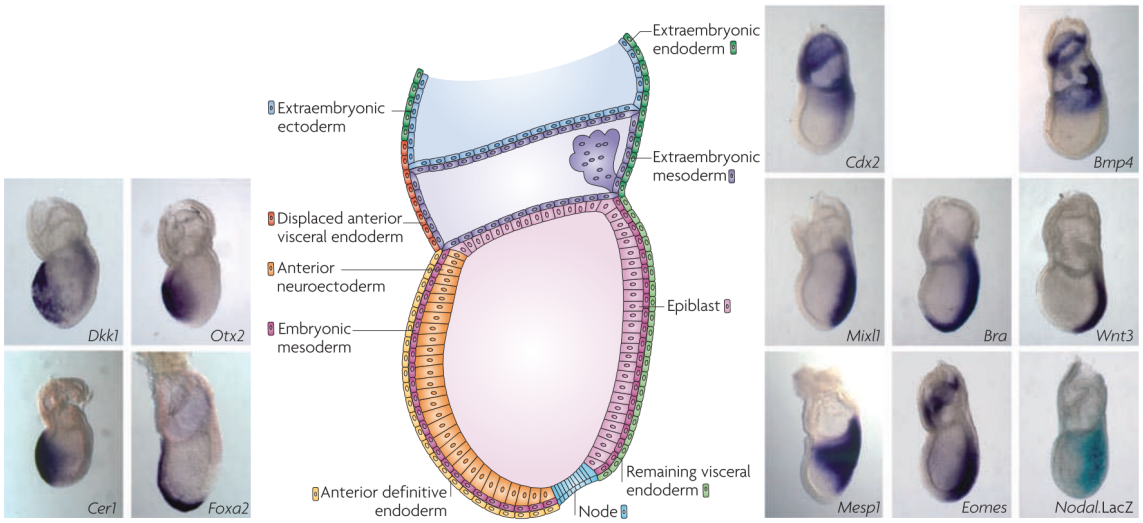

Figure 2.7: **Gene Expression shows Antero-Posterior polarity at E6.5-E7.5** At E6.5-E7.5 Gastrulation has resulted in the allocation of the three germ layers, Mesoderm, Endoderm and Ectoderm. The Gene Expression all over the embryo shows clearly the establishment of the Antero-Posterior polarity, with different markers restricted only to the Posterior side, as Nodal, Brachyury and Wnt or the Anterior side, as FoxA2, Dkk1, and Cer1. BMP is still present in the Extra-embryonic Ectoderm at the Proximal side of the Embryo. Note the population of cells in the Primitive Streak, which originates an extra-embryonic tissue, the Extra-embryonic Mesoderm, which is Cdx2 positive in response to BMP. Adapted from [Arnold and Robertson, 2009]

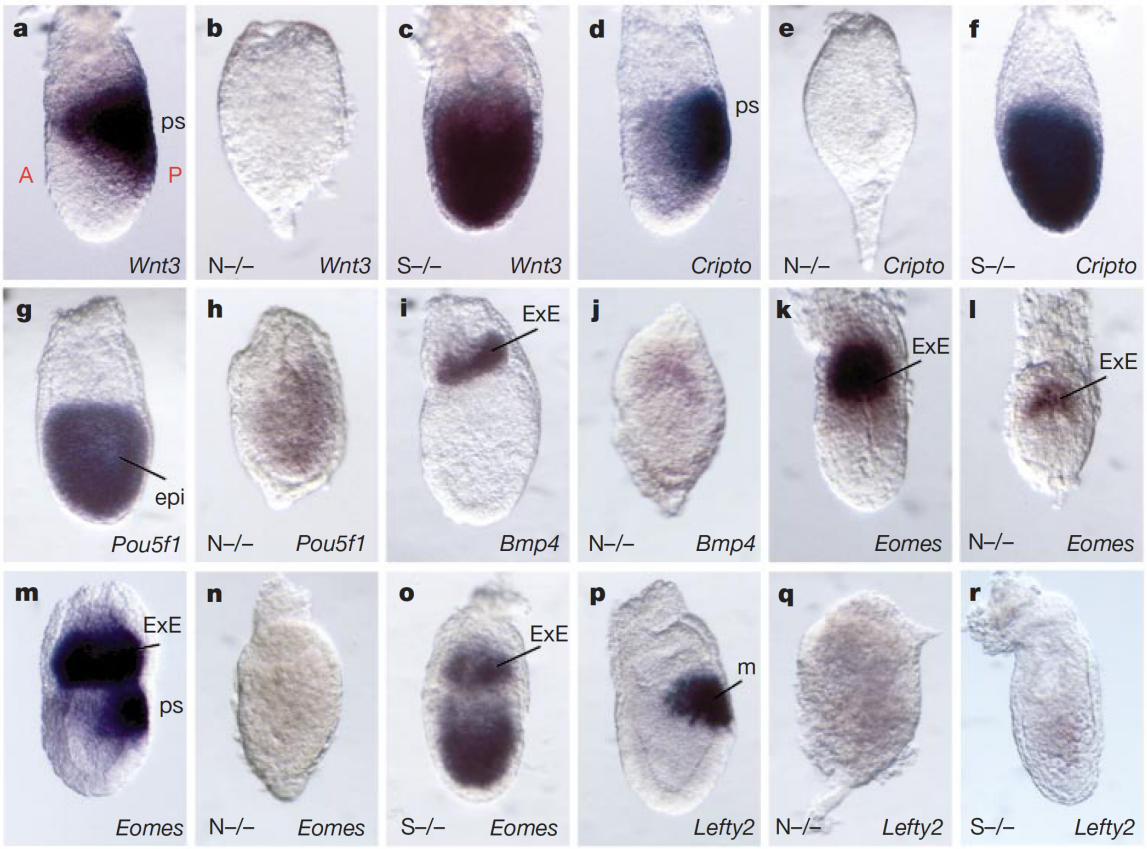

Figure 2.8: **Nodal is necessary for pattern formation and polarity establishment in the late Blastocyst** Pictures hown are from embryos at E6.5 (a-j, m-r) and E5.5 (k-l). The Figure shows that embryos lacking Nodal or its effector Smad2 fail to establish the expression pattern typical of the late Blastocyst and to set up the Antero-Possterior polarity. Particularly, Nodal results necessary to the proper expression of BMP in the Extra-embryonic Ectoderm, to the restriction of Wnt to the posterior side, and to the expression of its own inhibitor Lefty. Figures are reported from [Brennan et al., 2001].

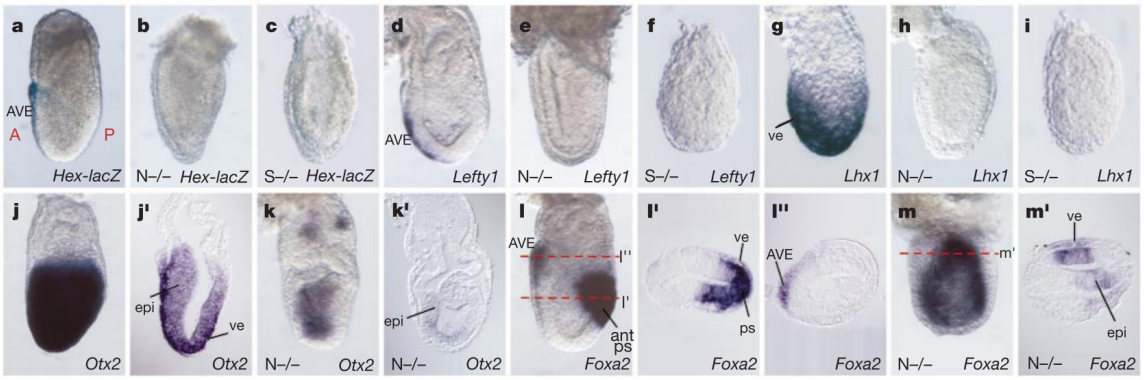

Figure 2.9: **Nodal is necessary for patterning the anterior side of the Visceral Endoderm** Figures show that embryos lacking Nodal or its effector Smad2 fail to pattern the anterior side of the Visceral Endoderm. Particularly, they do not restrict FoxA2, and they do not show any expression of Nodal inhibitor Lefty1. Figures are reported from [Brennan et al., 2001].

the ExE fail to restrict the DVE, whose role in patterning the embryo is connected to the second role of Nodal in establishing the A-P polarity. In fact, the Anterior Visceral Endoderm is needed for patterning the Anterior side of the embryo [Thomas and Beddington, 1996] [Lu and Robertson, 2004], and its formation is again mediated by Nodal. Nodal activates in the migrating Distal Visceral Endoderm its own inhibitors Cerberus and Lefty1. The migration of the DVE toward the prospective Anterior side of the Embryo would be responsible for the restriction of Nodal to the Posterior side. This assumption is reinforced by the observation that in Embryo lacking Lefty or Cerberus, multiple Primitive Streaks are formed [Perea-Gomez et al., 2002] [Yamamoto et al., 2004].

In what follows, we test this assumption and we ask whether it is possible to observe a polarised expression of Nodal even in absence of Extra-embryonic tissues. We will model the ExE as a source of BMP morphogen, first uniform then localised, and we will show under which condition we can restore a polarity.

2.1.2 Does physical confinement have a role in patterning the embryo?

We have seen that the fundamental ingredients to observe the A-P polarity seem to be the two extra-embryonic tissues the Extra-embryonic Ectoderm that provides the

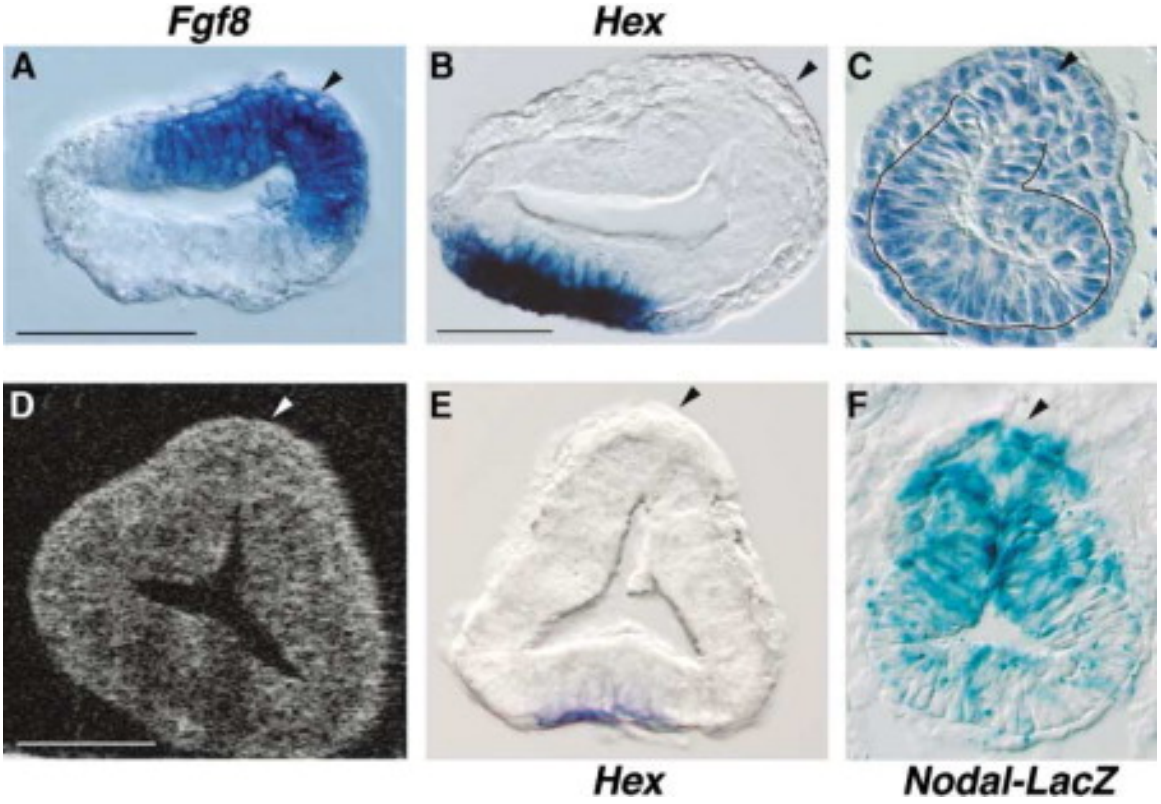

Figure 2.10: **The Visceral Endoderm confines the Epiblast** The Figure shows different transverse sections of the mouse Embryo at the Gastrulation stage. The arrow show the Primitive Streak locus in B-C-F. From all of them it is possible to see that the Visceral Endoderm is applying a confinement to the Epiblast, so that it deforms and buckles under this constraint. Particularly in C, at the PS site it is possible to recognise cells undergoing EMT and the Epiblast buckling inward. Adapted from [Perea-Gomez et al., 2004]

BMP that is responsible for patterning the proximal posterior side of the Epiblast and of the Visceral Endoderm, and later for inducing Mesoderm cell fate in cells in the Primitive Streak, and the Distal Visceral Endoderm, that, in response to Nodal induction releases, Nodal inhibitors Cerberus and Lefty1, that pattern the Anterior side of the Epiblast and restrict Nodal to the Posterior side of the Epiblast. This role of the extra-embryonic tissues has been well-investigated.

Here, we want to introduce another possible aspect that might also play a role. As shown in Figure 2.10, the Visceral Endoderm encapsulates the Epiblast. Looking at the picture it is possible to see that the Epiblast is buckling under what it is possible to assume to be the stress applied by the confining Visceral Endoderm.

During this thesis, we tried to setup a system that would allow the study of the differentiation in the Epiblast under physical confinement. The system is presented in Section 5. Concerning confinement playing a role in patterning the embryo it is interesting to briefly discuss the results presented in [Hiramatsu et al., 2013]. Here, researchers have found that the establishment of the A-P polarity in *ex vivo* growing embryos was strongly dependent on whether a stress was applied. Only embryos cultivated inside narrow wells were able to establish a polarised expression of posterior and anterior markers. Moreover the polarity was found to be more evident in stiffer wells. In this study though the compression aims to model that applied to the embryo by the uterus.

Interestingly, these findings have been challenged by [Bedzhov et al., 2015], where they report being able to grow mouse embryos *in vitro* and observing the establishment of the Antero-posterior polarity in the absence of maternal cues.

Nonetheless, we think that it would be interesting to apply the same principle to investigate the role of the Visceral Endoderm in compressing the Epiblast. To uncouple its confining role, by its behaviour as a source of Nodal inhibitors, we tried to set up a system, by adapting the Capsule technology [Alessandri et al., 2013] to cultivate Embryonic Stem cells. Our preliminary results are described in Section 5.

2.2 Stem Cells: a new path to developmental biology

Most of what we know on mouse early development, and that we have discussed in Section 2.1, comes from *ex vivo* experiments, from different mutants that made it possible to establish the role of the main genes in early development. The availability of Embryonic Stem cells (ESCs) introduced indeed many new possibilities to developmental biology [Keller, 2005] and broadened the range of possible manipulations. As said, ESCs made it possible to engineer mutants to unravel the genetic aspects of development, and their plasticity and pluripotency (i.e.) made it possible to characterise the relevant molecular aspects of cell fate specification.

Mouse Embryonic Stem Cells are derived from the Epiblast of the mouse Blastocyst around E3.5, as illustrated in Figure 2.11. They have been first isolated in the '80s by two independent teams [Evans and Kaufman, 1981] [Martin, 1981]. They are defined by two specific characteristics: self-renewal and pluripotency. In fact, they can be maintained in culture and conditions have been defined under which they maintain their initial state and differentiation potential. Embryonic Stem Cells can be found to conserve a normal karyotype in long term culture, unlike cancer cells, even though they can present chromosomal abnormalities, that have been widely studied, and found to be dependent on, among other factors, amplifying successive passages and enzymatic methods for cell detaching [Gaztelumendi and Nogués, 2014]. Their pluripotency means that they maintain the potential to differentiate toward all the cells of the adult body, either *in vivo* where transplanted into the blastocyst and in culture, where protocols have been optimised that trigger ES differentiation toward many adult cell types.

Beyond the possibility of modifying the mouse genome, and of investigating the molecular mechanisms underlying differentiation, in the last 10 years ESCs proved themselves to be a very promising tool to establish synthetic *in vitro* models of embryos that allow observations and manipulations that were previously impossible, par-

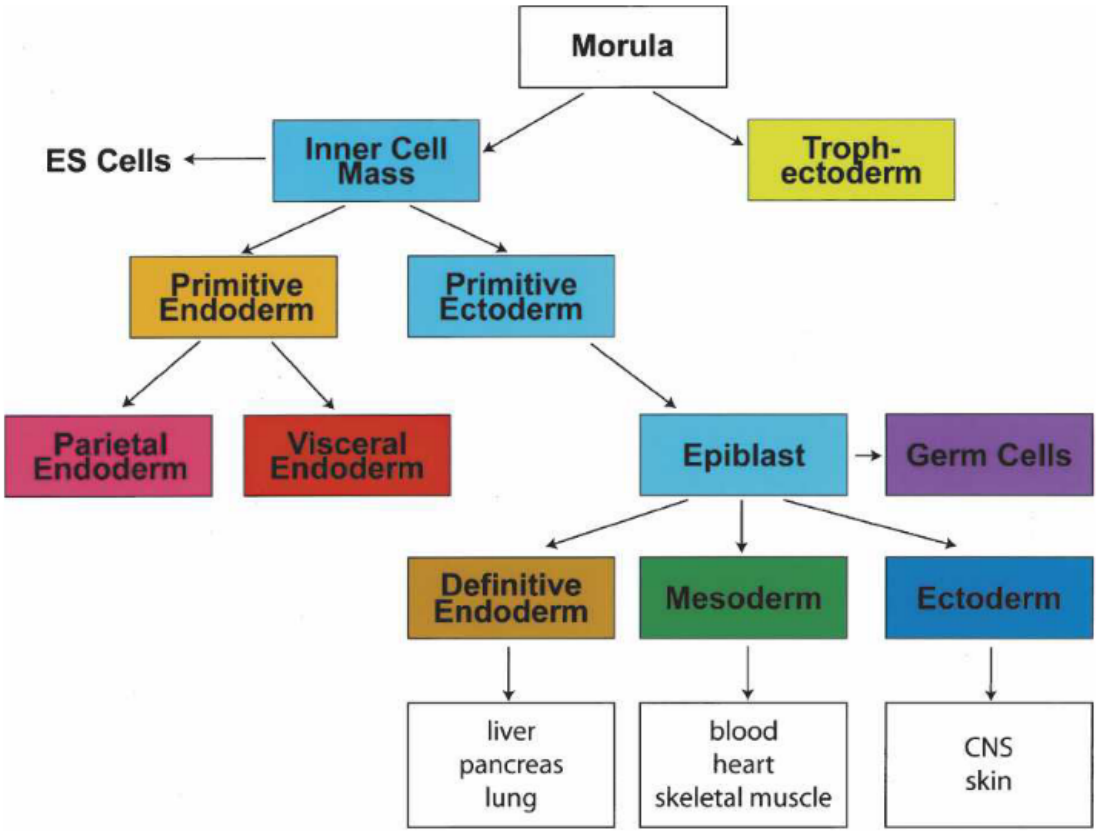

Figure 2.11: **ESCs are derived from the Inner Cells Mass of the Early Blastocyst at E3.5** The scheme reports the lineage specification occurring in the mouse from the Morula stage to the specification of the three germ layers, and it highlights the stage at which Embryonic Stem cells are derived from the Inner Cell Mass, at the early Blastocyst stage, around E3.5. Adapted from [Keller, 2005]

ticularly in mammals where the availability of the embryo to observation is strongly limited by its development taking place inside the uterus, and in humans for obvious ethical reasons. The importance of these novel culture systems relies in the fact that they capture more physiological aspects of the embryo (like in 3D models may capture the three-dimensional spacial reorganisation of the embryo) and allow the investigation of not only the signalling pathways that lead to differentiation, but also the self-organisation events that take place in the embryo in a way that is not possible in standard 2-dimensional culture conditions. We review the major systems developed during the last 10 years in the next Section.

2.2.1 Embryonic Stem Cells and Development: toward Synthetic Embryology

As said in the previous section, Embryonic Stem cells are showing to have self-organising properties that make them a precious tool to investigate mechanical, morphogenetic and chemical aspects of development, in a way that was impossible to traditional developmental biology. This approach to development as been described as 'bottom-up' to highlight what I believe it to be its main characteristic: building complexity step by step, starting from the main constitutive blocks, i.e. Stem cells. This is a dramatic change of perspective from traditional developmental biology, that tries to unravel the fundamental mechanisms underlying a very complex object, i.e. the embryo. Of course these two approaches are not mutually exclusive, but absolutely complementary. Somehow, development is the result of continuous exchange in between the unfolding of an instructive programme and self-organisation. I think these two approaches permit the capture of both these aspects. Particularly, synthetic systems are incredibly valuable for they allow us to uncouple and study separately aspects that are impossible to separate in the embryo: I am referring here to the respective role of the embryonic or the extra-embryonic tissues, or of a single signalling molecule. The possibility of coupling engineering and development, allows us to imagine novel culture systems that make it possible to study not only the devel-

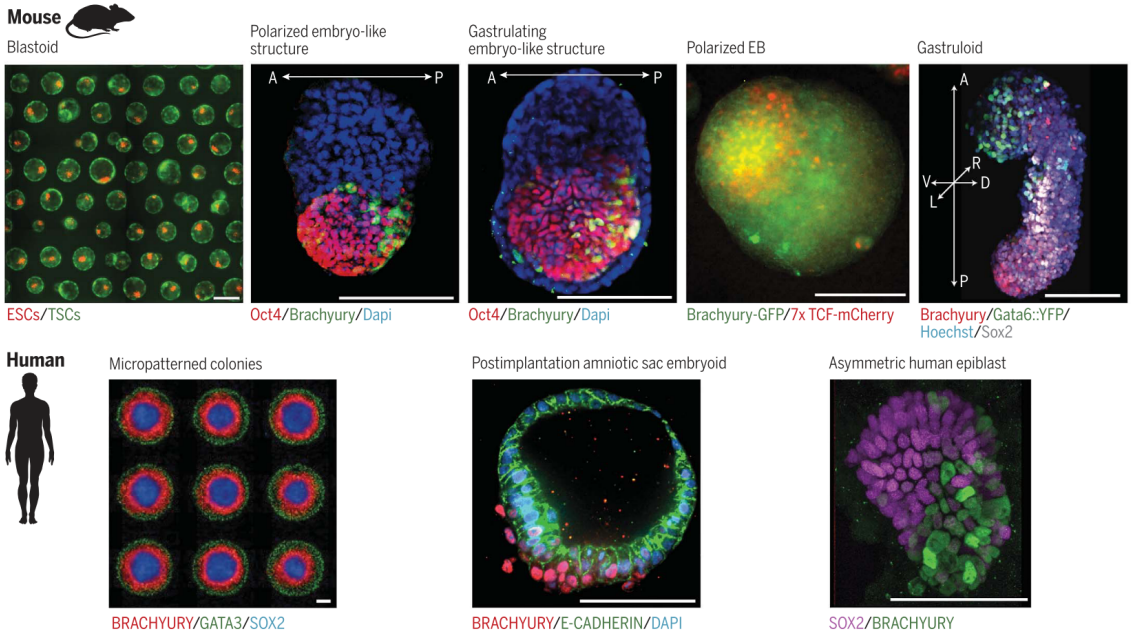

Figure 2.12: **Overview on established *in vitro* synthetic models for the early embryogenesis of mouse and human** Among mouse models, from left to right: the self-assembly of Embryonic Stem cell and Trophoblast Stem cells gives in non-adherent conditions gives rise to the Blastoid, reminiscent of the Early Blastocyst. The self-assembly of Embryonic Stem Cells and Trophoblast Stem cells when proteins from the ECM are provided gives rise to the ETS-embryos, reminiscent of the egg-cylinder stage but lacking the Visceral Endoderm. The self-assembly of Embryonic Stem cells, Trophoblast Stem cells and Extra-embryonic Endoderm Stem cells (XEN) gives rise to the ETX-embryos, reminiscent of the Late Blastocyst. Embryoid Bodies are clumps of Stem cells that are grown in non-adherent conditions and that show some ability to polarise the expression of posterior markers such as Brachyury. Gastruloids are structure made of Embryonic Stem cells grown in non-adherent condition, that, according to precise conditions of cell density and bio-chemical stimulation show an elongated phenotype and a polarised gene expression. Among human models, from left to right: micropatterned cell colonies proved the ability to self-organise into concentric rings of different tissues (from the outside inward, Extra-embryonic/Trophectoderm-like, Endoderm, Mesoderm/PS-like, Ectoderm) when stimulated with uniform BMP4. Humans Stem cells when grown in/on Matrigel develop into cysts that, if properly stimulated, develop into asymmetric cysts recapitulating the formation of the amniotic sac, with an Epiblast-like side and an extra-embryonic-like side. Human Embryonic Stem cells when embedded in Matrigel and stimulated with BMP spontaneously break the Symmetry and a polarity is established with two poles alternatively expressing Sox2 (pluripotent marker) or Brachyury (Posterior/PS-marker). Adapted from [Shahbazi et al., 2019]

oping embryo, but also what is its environment's impact on development. This field of research has been growing very fast in the last 5-10 years, and the many systems developed have allowed us to understand more fully the self-organisation potential of stem cells in response to different stimuli: differentiation inducing molecules, geometrical confinement, mechanical aspects of the environment, co-culture of embryonic and extra-embryonic cells. These models capture different aspects and are able to recapitulate different events taking place at early developmental stages. Recently, many of the recent advances in the field have been reviewed by [Shahbazi et al., 2019], while a more comprehensive history of development and stem cells can be found in [Shahbazi and Zernicka-Goetz, 2018]. Here, we are going through the most relevant of these recently developed systems, adding to this fast-growing list the latest results in this very prolific research environment. We will restrain ourselves to systems relevant to the study of embryo early development, but the organoids field exploiting adult and embryonic stem cells to investigate organogenesis is very wide and diverse. A review on these models can be found in [Lancaster and Knoblich, 2014].
Lastly, after having highlighted all the interesting and promising aspect of what we could define as the rising field of Synthetic Embryology rising field, I would like to focus on its main critical aspect: the lack reproducibility and the big variability, that represent an omnipresent issue within the field of organoid biology. The last result we present in this Section though is very encouraging in this sense, and opens up the idea that finer tailoring of our culture systems will lead us to a better control on these systems that will result in an improved reproducibility.

It is difficult to catalogue the multiplicity of systems that have been developed, especially because each of them captures a very specific aspect of early development, so we will have a topological distinction and we will analyse first recent results obtained by means of micropatterned culture system, and what conclusions can be drawn from them and later discuss those systems that aim to capture the tri-dimensional aspect of the Epiblast, and finally the models that aim to capture the totality of the Embryo by using self-organised co-culture of Embryonic and Extra-embryonic Stem cells. Ap-

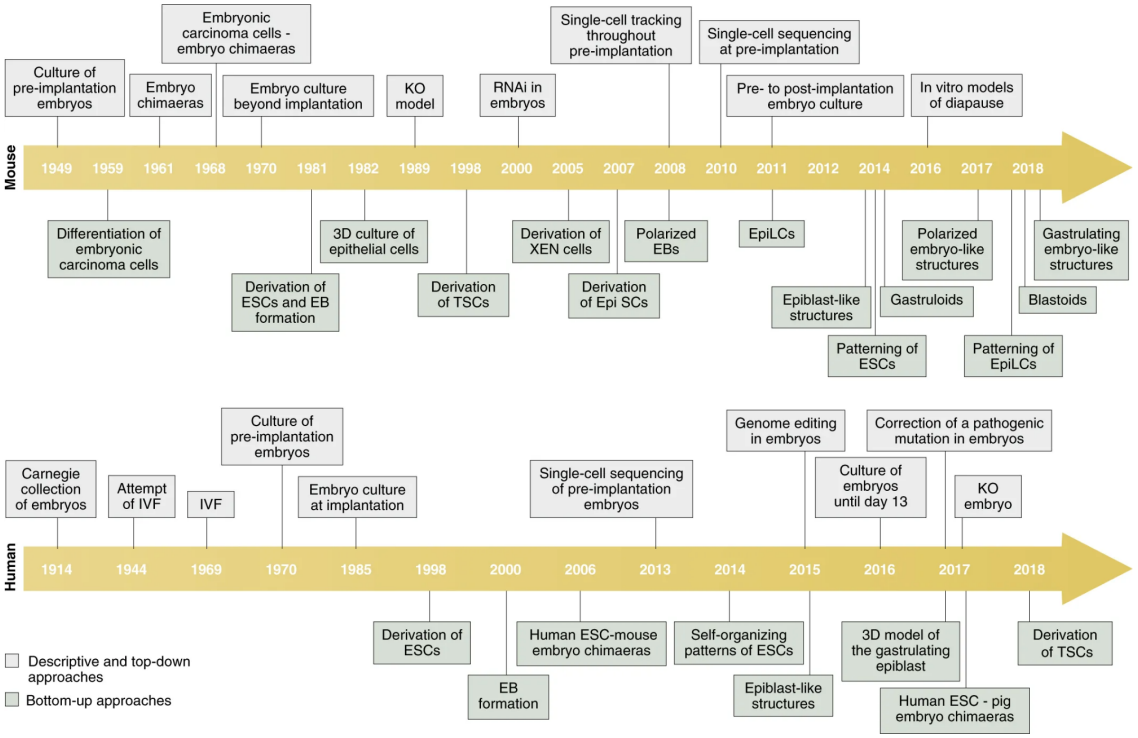

Figure 2.13: **Timeline of milestones in Developmental Biology and Stem Cells Biology** The timeline recapitulates the major discoveries or advancements in Developmental Biology of the Mouse and Human, following a traditional top-down approach and by means of the innovative bottom-up approach, made it possible by the derivation of Embryonic and Extra-embryonic Stem cells. Adapted from [Shahbazi and Zernicka-Goetz, 2018]

plying this order of growing complexity to our presentation, we loose the chronological order in which these systems have been established, and we will oscillate from mouse models to human and vice versa, without rigorous distinction. To make up for this, we report the Figure 2.13 from [Shahbazi and Zernicka-Goetz, 2018], that represents an exhaustive timeline that thoroughly recap the history of Stem cells biology and its crossover with developmental biology establishing a parallel between mouse and human case.

2.2.2 2D models: micropatterns

Imposing geometrical confinement to human Embryonic Stem cells, by growing them on micropatterns of circular forms [Warmflash et al., 2014] was shown to trigger self-organisation resulting in a organised differentiation in concentric rings of endoderm, mesoderm and ectoderm (an example is shown in Figure 2.12 on the bottom left), when stimulated with BMP4. This system makes it possible to dissect the cell response to different molecular signalling [Yoney et al., 2018], [Heemskerk et al., 2019],[Martyn et al., 2019] and also to understand the mechanism underlying this edge-based response epithelium, based on the localisation of BMP receptors on the basolateral side of the epithelium [Etoc et al., 2016] [Zhang et al., 2019], and therefore only available to ligands at the edge of the colonies.
The same technology has been applied to investigating differentiation under neuroectoderm inducing stimulation conditions [Britton et al., 2019], and coupling micropattern and chemical stimulation to a mechanical stimulus [Xue et al., 2018] proved a relevant impact of mechanics on patterning.
Recently then, results obtained with human Embryonic Stem cells have been also extended to mouse, by [Morgani et al., 2018].

2.2.3 Capturing 3Dness: from Embryoid Bodies to Gastruloids

As said before, initially research on pluripotent Stem Cells has been focused on dissecting the molecular mechanisms of differentiation. The aim was mainly then to identify a reproducible protocol to obtain a pure population of differentiated cells

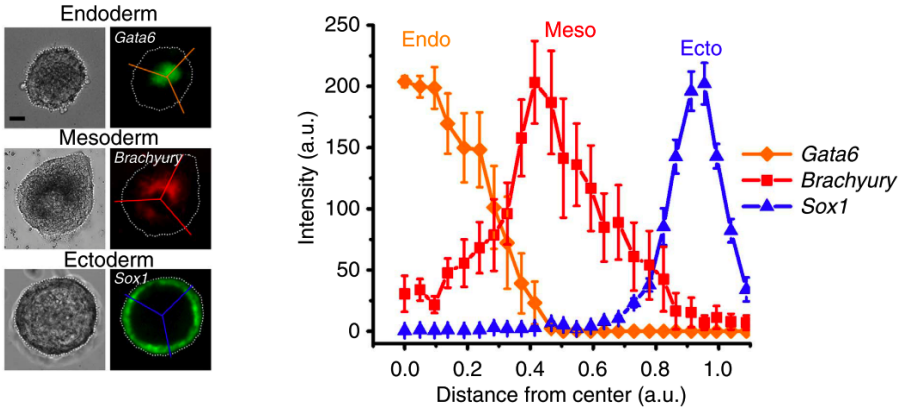

Figure 2.14: **Generation of three germ layers starting from a single Embryonic Stem cell** Organoids of mouse Embryonic Stem cells grown on adherent substrate recapitulate the formation of the three germ layers. Though the allocation of the three germ layers is not reminiscent of the *in vivo* reorganisation of the Epiblast. Results reported from [Poh et al., 2014]

starting from ESCs [Murry and Keller, 2008]. Among different culture methods, non-adherent suspension culture systems were employed, resulting in the formation of tridimensional clusters of cells, later called Embryoid Bodies. Embryoid Bodies have been used for years to investigate differentiation [Burkert et al., 1991] [Doetschman et al., 1985], but it has been only the pioneer work of [ten Berge et al., 2008] to show that in response to a polarised endogenous activation of the Wnt signalling, it was possible to observe not only random differentiating cells but a polarisation of posterior-like cells expressing Brachyury, which is a mesoderm marker and a direct Wnt target in mouse Embryonic Stem cells derived Embryoid Bodies. Interestingly, researchers reported sometimes the presence of two Wnt positive loci in the Embryoid bodies, suggesting that the lack of Extra-embryonic tissue signalling could result in multiple primitive Streak-like regions as it happens in mouse mutants for Nodal inhibitors. An example of e polarised Embryoid Bodies from this study can be found in Figure 2.12 in the fourth position counting clockwise.

This study paved the way for a novel approach to studying differentiation, and since new systems have been established that recapitulate to some extent the symmetry breaking and differentiation pattern of the peri-gastrulation mouse embryo.

Development is the outcome of the interplay of chemical and mechanical stimuli. Proving this assumption, this study [Poh et al., 2014] has shown that growing ES in soft fibrin gel and anchoring them to a stiffer matrix they differentiate into the three germ layers of Endoderm (interior), Mesoderm (middle) and Ectoderm. An example of this result is shown in Figure 2.14.

Continuing on the line of non-adhesive culture systems, in the lab of Alfonso Martinez-Arias [van den Brink et al., 2014] [Turner et al., 2017] [Beccari et al., 2018] they have been able to establish a system for mouse development, that interestingly does not only recapitulate a polarised gene expression, but also shows an elongation reminiscent of the antero-posterior axis formation that takes place in mouse after gastrulation. The phenotype observed strongly depends on the initial number of cells. These structures have been called Gastruloids, to highlight the fact that as during gastrulation a Brachyury positive pole is formed, where cells cluster and initiate EMT. An example of a Gastruloid can be found in Figure 2.12 on the top right.

This promising system has been investigated further by [Boxman et al., 2016] [Sagy et al., 2018]. They have tried to understand the mechanism underlying the positioning of the Brachyury positive locus, that positions the posterior side of the embryo and that sets the antero-posterior polarity along which the antero-posterior axis will develop. It is worth remembering in fact that the polarisation arises following a uniform biochemical stimulus in the form of Wnt induction pulses. They proved that the positioning of the Brachyury positive site depends on the contact between the EB and its surrounding, and acting on this parameter they were able to control the positioning of one or multiple Brachyury positive loci, by engineering a microwell system. Such studies prove that it is important to pursue a deeper understanding of these complex systems, if we aim to go beyond a pure phenomenological description of the self-organising potential of ES *in vitro*.

Differently from EB cultures, ES have later started being grown in adherent conditions, by means of Extra-Cellular Matrix support. The work done in Magdalena Zernicka-Goetz's lab in Cambridge [Bedzhov and Zernicka-Goetz, 2014] [Shahbazi et al., 2017], comparing embryos and Embryonic Stem cells embedded inside Ma-

trigel, leads to greater understanding of the cavity formation in the mouse Epiblast, forming at around E5, in a way that was previously not possible. It has long been believed in fact that this cavity was formed by activation of programmed death by the cells situated at the interior part of the Inner cell mass of the Early Blastocyst. Those study demonstrated that cavitation is a phenomenon connected to the presence of the Extra-cellular Matrix, and starts with the organisation of the spherical epithelium in a rosette. Later on the same luminogenesis, again triggered by the establishment of the apico-basal polarity, due to the presence of the ECM has been observed in human Embryonic Stem cells [Taniguchi et al., 2015].

Another interesting study, involving growing human Embryonic Stem cells and providing them with Matrigel [Shao et al., 2016] [Shao et al., 2017] has shown that cells can develop into asymmetric cysts reminiscent of the amniotic sac formation stage of the human embryo. These cysts, of which one example is shown in Figure 2.12 (bottom middle), present an asymmetric morphology, featuring on one side a monolayer of columnar cells, that recapitulate the human Epiblast in morphology and gene expression, including Brachyury positive cells undergoing EMT, and on the other a more flat epithelium, reminiscent of the Trophectoderm. Recently this study has been updated [Zheng et al., 2019], but we will discuss these recent results in the last dedicated section of this review as it helps the drawing of conclusions that are valuable to the whole field of organoids research, beyond the impact on the single study.

Again, human Embryonic Stem cells have been used by [Simunovic et al., 2019] to obtain cysts of Epiblast-like tissue, that spontaneously break the symmetry of gene expression, when exposed to BMP. The rate at which the symmetry breaking is observed is strongly dependent on the BMP concentration. Despite lacking a clear corresponding equivalent *in vivo*, this system might be valuable in the future for unravelling the mechanism of the symmetry breaking, as the segregation of two domains exclusively expressing Brachyury (Primitive Streak/Mesoderm marker) or Sox2 (core pluripotency marker) follows homogeneous and isotropic stimulation with BMP.

Embryonic Stem cells have not only been used to investigate the earliest stages of development, but also to understand the mechanisms of later organogenesis. These

studies [Meinhardt et al., 2014] [Ranga et al., 2016] have shown that growing mouse Embryonic Stem cells inside ECM, and feeding them with neural inducing media, results in cysts that recapitulate the morphology and expression pattern of early neurogenesis.

2.2.4 Self-assembly of Embryonic and Extra-embryonic Stem cells Blastoids, ET-embryos and ETX embryos

All the models described up to now capture some aspects of the development of the Epiblast. They fail though to recapitulate the complexity of the whole embryo, as they completely lack the extra-embryonic tissues. To expand those model, different studies have explored the self-assembly potential of embryonic Stem cells when grown together with Stem cells derived from the Extra-embryonic tissues.

A first study [Harrison et al., 2017] combined Embryonic Stem cells and Trophoblast Stem cells. They proved that when these two cell types were grown together in Matrigel, that provided the ECM, they assembled spontaneously into structures, closely resembling the egg-cylinder stage of the mouse embryo, lacking though the Visceral Endoderm. An example of these so called ET-embryos can be found in Figure 2.12. This important result is instructive on two aspects: first, it confirms that Stem cells both from the Epiblast and from the Trophoblast behave as their *in vivo* counterparts, and they are able to self-assemble to reconstruct a structure very similar to the real embryo. Moreover, the fact that the ET-embryos express Brachyury at the interface of the two compartments (Figure 2.15) confirms the role of the Extra-embryonic Ectoderm in inducing the symmetry breaking of the Epiblast.

Following up on this study, the same team [Sozen et al., 2018] showed that when also cells derived from the Extra-embryonic Endoderm (XEN) were included in the co-culture, the three types of Stem cells would self-assemble into structures resembling the embryo in its late blastocyst stage with both the two extra-embryonic tissues, the Extra-embryonic ectoderm and the Visceral Endoderm enveloping the Epiblast (XEN cells compartment). The team proved that adding the XEN compartment was sufficient to observe the starting of gastrulation as cells coming from the pool

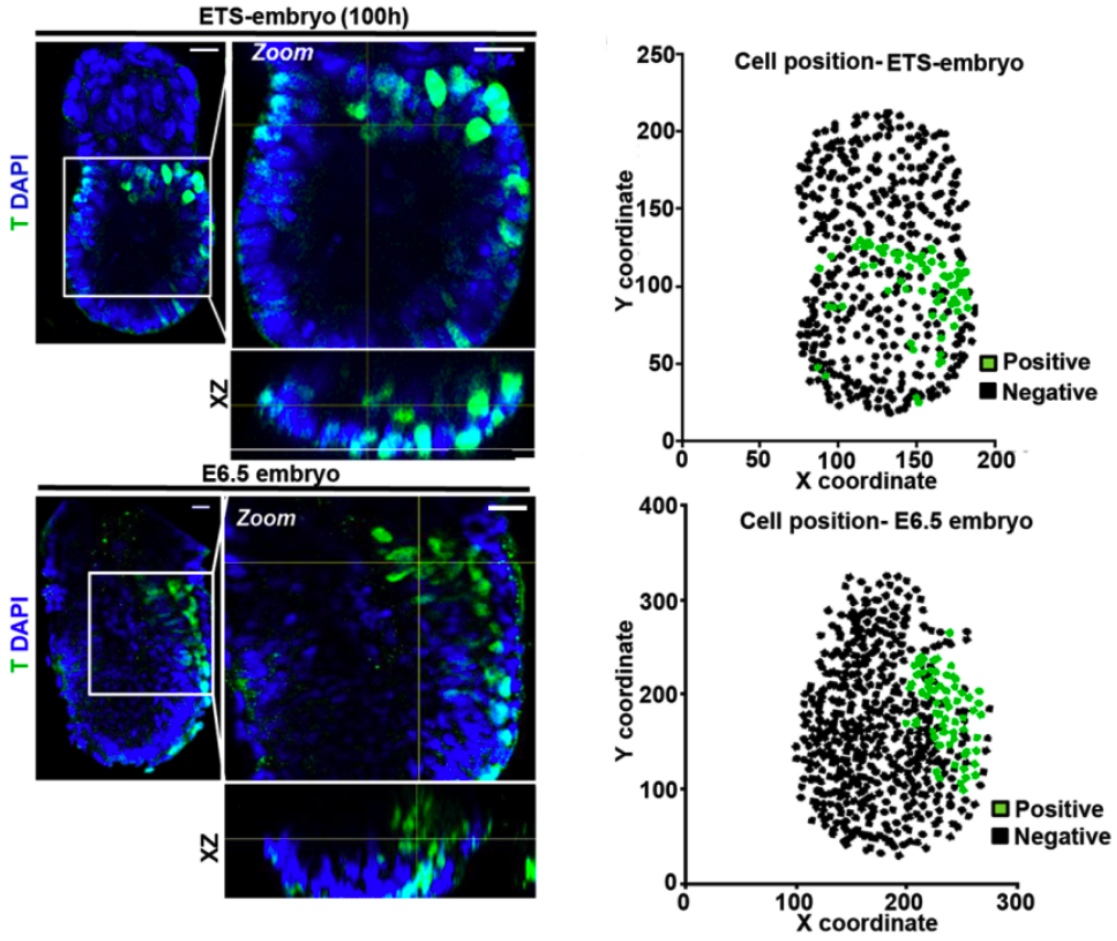

Figure 2.15: **ET-embryos express Brachyury at the interface between Trophoblast Stem Cells and Embryonic Stem Cells compartments** The fact that ET-embryos express Brachyury at the interface of the Extra-embryonic and Embryonic compartments seems to confirm the importance of the Extra-embryonic Ectoderm in inducing posterior/Primitive Streak-like markers such as Brachyury in the proximal side of the Epiblast. Adapted from [Harrison et al., 2017]

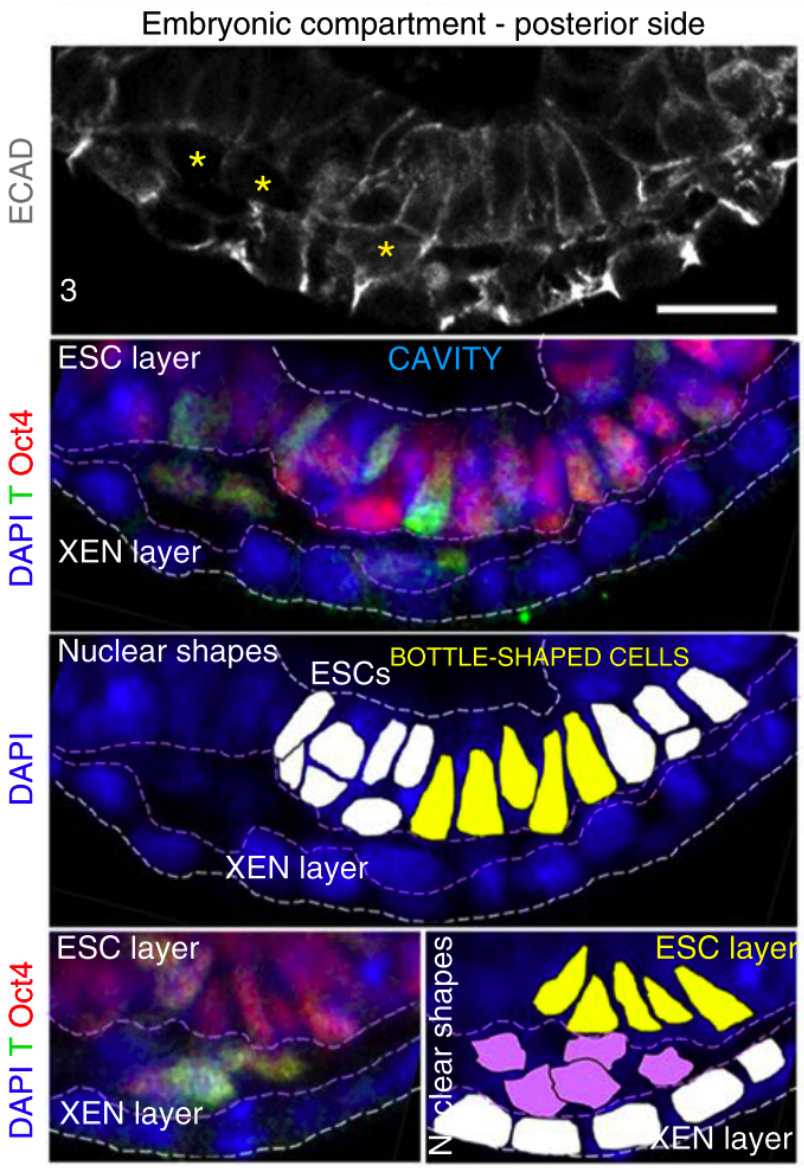

Figure 2.16: **ETX-embryos present cells that undergo EMT.** Cellas undergoing EMT in ETX-embryos are reminiscent of cells leaving the Epiblast from the Primitive Streak to form Mesoderm and Endoderm, during Gastrulation

of positive Brachyury cells at the interface between TS and ES compartment would start undergoing EMT, as shown in Figure 2.16. Moreover, cells undergoing EMT and situated distally would also express markers of the Definite Endoderm, proving the ETX-embryo were not only forming the mesoderm layer but also contributing to the prospective Anterior Visceral Endoderm. This result has been confirmed and reproduced by [Zhang et al., 2019]. In parallel to this study, another model has been developed [Rivron et al., 2018], that recapitulate the morphology of the early mouse blastocyst: when Embryonic Stem Cells are mixed with Trophoblast Stem cells they self-assemble into Blastocyst-like structures, then called Blastoids (an example of which is shown in Figure 2.12, top left). These structures reproduce the two separate compartments, embryonic and extra-embryonic as well as the cavity that separates them starting from E3.5 *in vivo*. It is interesting to notice that the same co-culture of the same fundamental ingredients, ES and TS, results in two systems, [Harrison et al., 2017] and [Rivron et al., 2018], that are clearly reminiscent of two different stages of mouse development. The main difference between the two culture systems relies on the presence (ET-embryos) or absence (Blastoids) of externally added ECM. Indeed in the ETS-embryos, Matrigel is intended to replace the ECM provided to the Inner Cell Mass by the future Visceral Endoderm, which is instead not specified yet at the early blastocyst stage. This proves again that the ECM has a fundamental role in instructing morphological changes through the epithelialisation of the tissues.

2.2.5 Improving reproducibility: a challenge for the Organoids community

I anticipated an update [Zheng et al., 2019] to the study [Shao et al., 2017] describing the formation of human Stem cells derived cysts that recapitulates the amniotic sac asymmetric morphology. The reason why I believe this is worth discussing separately is because the advances described in [Zheng et al., 2019] do not introduce any novelty with the respect to the phenomenology of the observations. They introduced though a microfluidic system, which is shown in Figure 2.17, for growing the cysts in a more controllable way. This change of paradigm for the culture conditions, introduced a

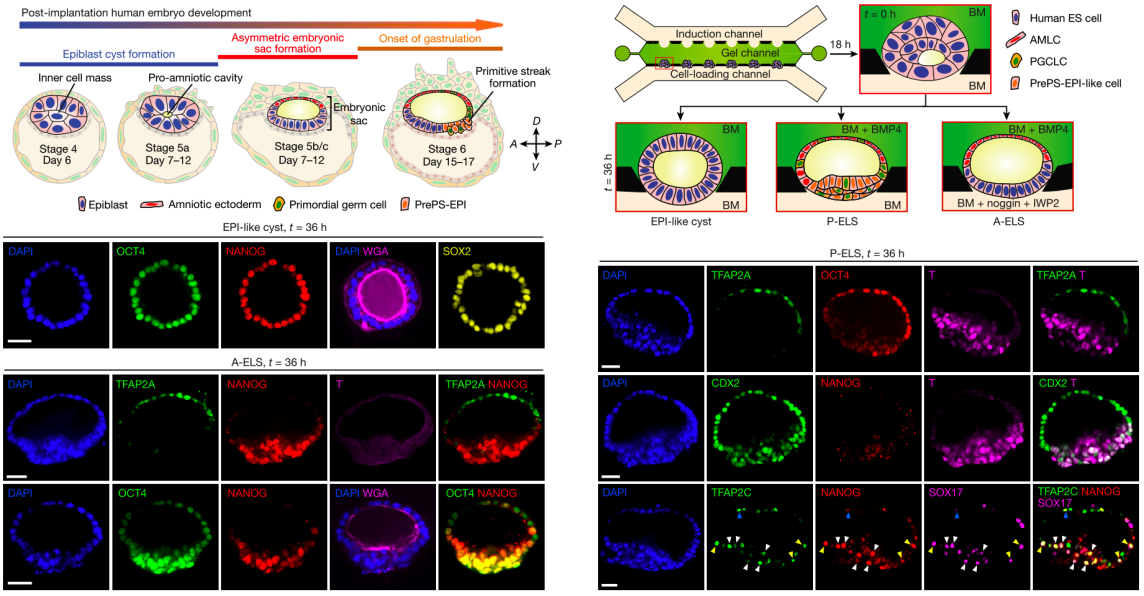

Figure 2.17: **A microfluidic device for controllable formation of asymmetric hESCs cysts, reminiscent of the amniotic sac formation** Introducing this microfluidic device to the previous essay that was proving the emergence of this asymmetric phenotype when cysts where grown on traditional 2D surfaces coated with Matrigel, increased the frequency at which the phenotype was observed from 5% to 96% of the times. Adapted from [Zheng et al., 2019]

dramatic change in the frequency at which the interesting asymmetric phenotype is observed, passing from $\approx 5\%$ of times of the original paper, to 96% in the one that introduces the microfluidic device.

This striking increase in reproducibility is the result of introducing a device that allows the precise positioning of single human Embryonic Stem cells into equally spaced cavities, and the application of a stimulus inducing either anterior or posterior fate on one side of the cysts, while in the previous essay cysts were differentiated on Petri dishes by providing uniformly the differentiation media.

I think that results like this are crucial to the field, because they prove that an effort in engineering novel culture systems that better define culture conditions and narrow down degrees of freedom of the system, directly translates to an increase in controllability of the system and reduces the variability, which is a constitutive feature of the whole organoids field of research. And clearly, reproducibility also improves the predictive power of these systems and their reliability and opens up to them being effective models by means of which it will be possible to gain knowledge about the mechanisms of differentiation an pattern formation.

2.3 A synthetic model for investigating the role of Extra-embryonic tissues in patterning the embryo at the peri-gastrulation stage

We have seen that, before the onset of gastrulation and the emerging of the Primitive Streak, a molecular asymmetry is already established in the mouse Epiblast.

At this time, in the embryo three lineages have already been specified: the Epiblast that will give rise to the embryo proper and two extra-embryonic tissues, the Visceral Endoderm that surrounds the Epiblast and the Extra-embryonic Ectoderm at the proximal side of the Epiblast. Around E4.5, the Epiblast is a spherically symmetric clump of pluripotent columnar cells that do not show any pre-patterned molecular asymmetry (2.5). This symmetry is then manifestly broken, immediately before the Primitive Streak is formed.

The symmetry breaking happens under the control of morphogens of the TGF-β family, Nodal and BMP4 and Wnt family [Arnold and Robertson, 2009][Brennan et al., 2001][Cockburn and Rossant, 2010]. Before Gastrulation, Nodal, previously expressed along the whole Epiblast is restricted to the prospective posterior side. The precise mechanisms underlying this symmetry breaking and how the embryo reliably sets the body axes are not fully unveiled yet, but it has been elucidated a double role of Nodal, provided by the Epiblast on the two extra-embryonic tissues present in the embryo at this stage. In fact, Nodal induces BMP in the Extra-embryonic Ectoderm, which in turn sustains the expression of Nodal and induce differentiation toward posterior embryonic fate (embryonic mesoderm, Brachyury positive) and posterior extra-embryonic fate (extra-embryonic mesoderm, Cdx2 positive). Moreover, Nodal induces its own inhibitors Lefty1 and Cerberus in the migrating Visceral Endoderm, and they are believed to be necessary to the restriction of Nodal to the posterior domain.

In what follows, we explore these assumptions, by testing them on a synthetic model for the Epiblast. We will compare the situation where our synthetic Epiblast is stimulated with a uniform chemical stimulus to the situation where the Epiblast is stimulated by a gradient of chemical induction.
Doing so, we aim to be able to find out what the minimal condition to observe a clear symmetry breaking in the Epiblast are and whether it is possible to establish the Antero-posterior polarity in absence of Extra-embryonic Ectoderm and Anterior Visceral Endoderm.

3 A minimal model for the Epiblast to investigate what conditions trigger the establishment of Antero-Posterior polarity in the mouse

We have summarised in Section 2.2 a number of recent studies, that address the question of what shapes the embryo on a molecular and mechanical level and, to tackle such questions, make use of *in vitro* models based on different three-dimensional culture systems.

A number of studies have already investigated the establishment of the antero-posterior polarity in the embryo, with different findings. [Harrison et al., 2017] and [Sozen et al., 2018] have shown that Extra-embryonic Stem cells are needed to observe the polarisation of posterior markers in a consistent manner. In fact, when they grew aggregates made of only Embryonic Stem Cells in the same medium as the ETS-embryos (which does not contain gastrulation inducing signalling), they observed Brachyury in a significantly less recurrent way. Other studies, [van den Brink et al., 2014] [Beccari et al., 2018], have shown that antero-posterior polarity is observed together with elongation, and in the absence of extra-embryonic tissues, when mouse Embryonic Stem Cells are grown in non-adherent conditions. Finally in human Embryonic Stem cells, it has been shown [Simunovic et al., 2019], that cells grown in adherent conditions can consistently break the symmetry, when stimulated with BMP, in a concentration dependent way.

Here, we propose to study the setting up of the Antero-posterior polarity though a minimal system of the Epiblast only, that allows us to deconstruct the complexity of the cross-talk between the Extra-embryonic tissues and the Epiblast, and to study their role as signalling sources only. In doing so, we use a model that recapitulate the epithelialisation of the Epiblast and the consequent luminogenesis it undergoes *in vivo* around E4.5, and then we stimulate these Epiblast-like structures with BMP, known to be a key factor in inducing the antero-posterior polarity.

In this section, we discuss how growing mouse Embryonic Stem cells embedded in

an Extra-cellular Matrix gel (Geltrex), in a similar way to what has already been done in mouse [Shahbazi et al., 2017] and human [Simunovic et al., 2019], allows for establishing a minimal model of the mouse Epiblast that recapitulate some of the morphogenetic rearrangements of the Epiblast, like compaction, apico-basal polarisation and luminogenesis. Then, we ask if it is possible to induce symmetry breaking in these Epiblast-like organoids, by applying a uniform BMP stimulus. We will detail what we were able to learn from this system, under what conditions we could observe a polarisation arising and what are the future directions to undertake to develop it further. We will finally highlight some limitations, and the way we hypothesised to overcome them by using tools from microfluidics, that will be extensively discussed in Section 4 of this thesis.

The goal of these experiments is to establish a minimal model of the mouse Epiblast at the peri-implantation stage to investigate the minimal conditions to observe some gene expression asymmetry reminiscent of the setting up of the antero-posterior polarity.

We are interested here in investigating the role of the Extra-embryonic tissues in establishing this polarity. From the literature we know that the role of the Visceral Endoderm in patterning the embryo consists in providing the Epiblast with inhibitors of Wnt and Nodal, that restrict Nodal domain to the prospective posterior side of the embryo, while the VE migrates toward the prospective anterior side, to establish the Anterior Visceral Endoderm. However the establishment of a polarity has been observed *in vitro* by [Harrison et al., 2017] in the absence of the Anterior Visceral Endoderm, but only when an Extra-embryonic Ectoderm compartment is provided.

We want to find the minimal conditions to observe the establishment of the Antero-posterior polarity. We need a system then, which allows the uncoupling of the role of the morphogens from that of the Extra-embryonic tissue, which would make it possible to investigate under what conditions it is possible to observe the morphogenetic rearrangements and the asymmetric molecular expression that the Epiblast shows at the onset of gastrulation. We provide a model for the Epiblast only. Making the

hypothesis that the role of the Trophectoderm is to provide BMP to the Epiblast, can we replace it by feeding directly BMP to our synthetic Epiblast? Is it a sufficient condition to trigger a polarised expression of posterior markers?

3.1 First step: seeding cells in Geltrex

To recapitulate the topology and morphology of the Epiblast, a polarised epithelium with its apical side facing a cavity and its basal side in contact with the Extra-cellular Matrix provided by the Visceral Endoderm, a suitable substrate is needed, to replace the role of the Visceral Endoderm in providing the ECM.

In what follows, such a substrate will be Geltrex, a commercially available product, which is extracted from Engelbreth-Holm-Swarm (EHS) mouse sarcoma and contains different proteins from the Extra-Cellular Matrix, mainly collagen and laminin, and some growth factors.

This gel, which appears in the form of a viscous liquid at +4°C, solidifies into a very soft gel already at room temperature. Providing both the basal membrane that cells need to adhere on and a three-dimensional structure, soft enough that cells are still able to move through it, Geltrex appears to be the perfect candidate for a minimal 3D culture system (cell stiffness being around 500Pa is the same order of magnitude of Geltrex).

Nonetheless, it is necessary to discuss briefly the animal origin of such a product, and its ubiquity in Stem Cell culture. The first consequence of using products of animal origin is that they can be inhomogeneous within the batch and quite variable from batch to batch. There is a big research effort in trying to develop synthetic alternatives, that would allow a finer control on every component and the possibility to uncouple the relevance and the impact of any of them. Different hydrogels, functionalised with adhesion proteins to allow the cells to attach and spread on them, have been proposed to overcome this issue. An example of those is sodium alginate, a bio-polymer that cross-links in the presence of divalent ions and that can be functionalised with monomers from adhesion proteins such as fibronectin. We will

discuss alginate in Section 5, when we will introduce a system to study the confinement applied by the Extra-embryonic tissues on the Epiblast. Among synthetic gels that are commercially available, we tested Mebiol and Hystem-C. For different, and partly unknown, reasons, though, they do not perform as well as Geltrex. Cells viability is manifestly decreased. Plus, the stiffness of Hystem-c, which is reported to be tunable in the range 11-3500Pa [Vanderhooft et al., 2009] by varying the relative amount of the cross-linker, would need a dedicated study to find the optimal conditions. It has already been shown [Poh et al., 2014] in fact, that the stiffness of the substrate has a relevant impact on the proliferation and the size of Embryonic Stem cells clusters. In what follows, cells have then always been embedded in 100% Geltrex, whose stiffness has been measured in the range 400-500Pa [Soofi et al., 2009].

In order to get monoclonal organoids, cells need to be resuspended as single cells before being embedded in gel. To do so, 5 minutes in Trypsin are sufficient to separate them. Trypsin is washed out by resuspending cells in DMEM (plus FBS to neutralise the Trypsin), centrifuging, and aspiring the supernatant, cells can be resuspended directly in Geltrex to be then plated.
To do so, they have first to be resuspended at a density of 1-2million/ml in normal mouse Embryonic Stem cells culture medium (N2B27). This density is enough to ensure later to have many cysts per plate, but not too many that cells would assemble in non-monoclonal cysts, which would result in overgrowing cysts and cysts fusing with each other into bigger disorganised structures.
Prior to mixing cells with Geltrex, it is preferable to cool them down, in order not to raise abruptly the gel's temperature, that would quickly make it undergo gelification, making it impossible then to disperse the cells homogeneously and to later spread the gel on a dish. To avoid Geltrex cross-linking, cells can be kept on ice for 3-5minutes. When ready, 20µl of cells suspension have to be mixed with 100µl Geltrex. Again to avoid raising the temperature, it is preferable to use pipette tips that are stored at -20°C.
To reach a homogeneous cell density throughout the gel, cells have to be mixed thor-

oughly, but without inserting bubbles in the gel. To ensure that, it is safer to reverse pipette only 50µl when first aspiring, and then aspire from the bottom of the tube and release on top of it. To check that the cell density is uniform, 10µl of solution can be plated on a slide and checked under a microscope. Then, the cells suspension can be plated on a Petri dish, or as we do here to run live experiments, on a 10-well commercially available glass-bottom dish. For a 96-wells Petri dish, we plate 10µl per well. The gel needs to be spread uniformly to get a thin flat layer, but it is important to avoid touching the walls, if using a small surface well, such as a well in a 96-wells Petri dish, otherwise the solution will tend to stick and accumulate to the walls, resulting in fewer cells in the middle of the chamber and hence making it difficult to live image. Once cells are plated, the gel needs to solidify for 5-10 minutes in the incubator at 37°C, but this time has not to be exceeded as otherwise the gel will dry out. To ensure that the gel does not dry out, it is sufficient to fill the external wells with PBS, or to put a PBS reservoir close to it, to ensure humidity.
Once the Geltrex is solidified, the wells can be filled with culture medium.

3.2 Results

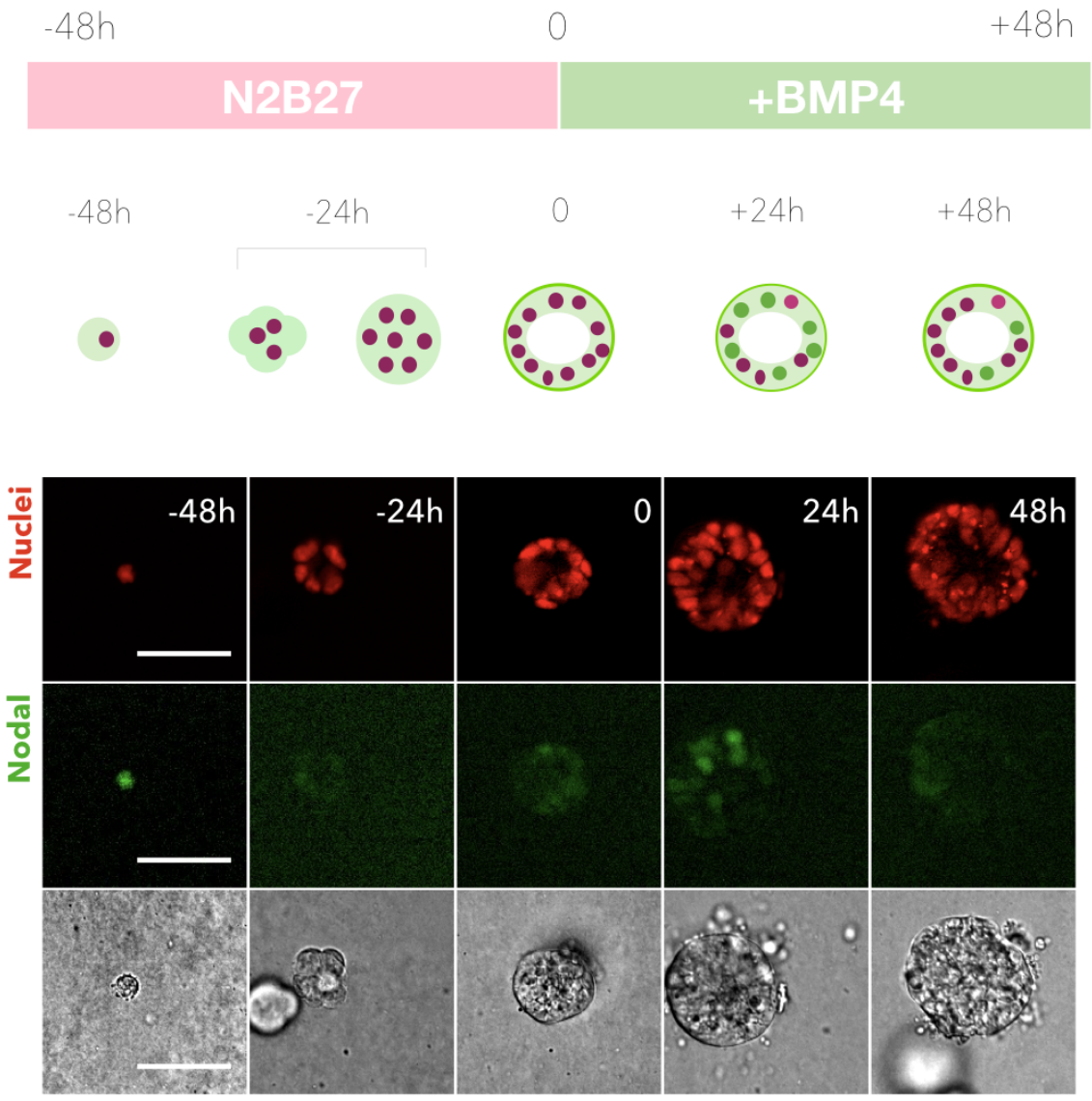

Figure 3.1: **Making of a synthetic Epiblast: experimental protocol** On top of the picture the experimental protocol is schematised. In the middle, a sketch represents the system at each stage. On the bottom, a representative example is shown for each time point, showing the compaction, the formation of the cavity and the dynamical expression of Nodal. Scale bar is 50µm.

Here, we first confirm that, as already shown in [Shahbazi et al., 2017], providing a basal membrane is the necessary minimal condition to observe mESCs reorganise into a polarised epithelium. Epithelialisation is the requirement for luminogenesis,

which is observed 24-36h after seeding. Luminogenesis in similar conditions has been observed also with human Embryonic and Pluripotent Stem Cells [Taniguchi et al., 2015] [Simunovic et al., 2019].
We discuss how this system responds to stimulation with gastrulation inducing morphogens such as BMP, when provided uniformly in the media, in order to simulate the Extra-Embryonic Ectoderm as a source of morphogens. We explore different stimulation configurations, we present the results and we draw some conclusions, highlighting what needs still to be done, discuss the limitations of such a model and what we think could be a possible way to overcome them, by introducing a microfluidic setup, that will be extensively discussed in the last chapter of this thesis.

Our protocol (as reported in Figure 3.1) runs over 4 days. During the first two days we remove from the medium the 2i/LIF, the molecules that keep cells in their naive pluripotent state, to allow them to differentiate. We grow them adding the Fibroblast Growth Factor FGF (10ng/ml) and the KnockOut Serum Replacement (KSR) , a serum replacement, to N2B27. This step is needed to differentiate mouse Embryonic Stem cells to Epiblast-like Stem cells (EpiLCs), which are considered similar in gene expression and pluripotency to Epiblast Stem cells (EpiSCs). Either EpiSCs and EpiLCs can generate teratomas, but they are unable to generate chimeras. During this 48h the pluripotency switch from the naive pluripotency of ESCs to the primed pluripotency of EpiSCs/EpiLCs [Guo et al., 2009].
After 48h, we stimulate them for 48h with BMP4, known to be a morphogen responsible for inducing gastrulation in the mouse [Arnold and Robertson, 2009], as detailed in Section 3. One experiment is shown where mESCs organoids have been stimulated with Wnt, known as well to be a relevant player in orchestrating gastrulation. More details on cell culture are discussed in Appendix A.1.

3.2.1 The first 48h: generating a synthetic Epiblast

During the first two days after seeding in Geltrex, the observations we were able to make can be summed up in four main phenomena: cells proliferate, establish the

apico-basal polarity, compact and undergo luminogenesis.

As described by [Shahbazi et al., 2017], where they detail that epithelialisation of mouse Embryonic Stem Cells in Matrigel and the formation of a rosette are followed by lumen formation, this process is reminiscent of the morphological changes of the mouse embryo around implantation, when, between E3.5 and E5.5, the Inner Cell Mass of the mouse embryo transforms from a spherical compact clump of cells to an epithelium, the Epiblast, which has its basal side in contact with the Visceral Endoderm, that envelops it (cf. Figures 2.3 and 2.4).

We observed, Figure 3.1, that the organoids undergo 2-3 rounds of cell division, where they grow in 'raspberry-like' structures. Then adhesion between cells increases and they compact to form a spherical full clump of cells. Providing basal proteins results in establishing the apico-basal polarity, with the basal side of the cells in contact with the ECM.

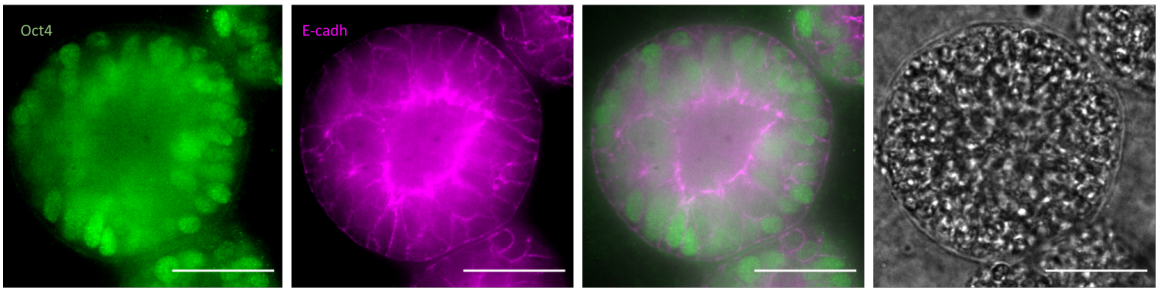

Figure 3.2: **A section of a Synthetic Epiblast** A representative example of a hollow cyst is shown after the 4 days protocol. The inner cavity is formed during the first 24-48h. No necrotic core is visible, so the cavity is not formed by apoptosis of the inner cells. Scale bar is 50μm.

Between 24-36h after seeding, cells undergo luminogenesis and a cavity is formed. A section of a hollow cyst is shown in Figure 3.2. As shown in the picture, at this stage cells still express the core pluripotency marker Oct4, meaning that pluripotency is conserved.

From these observations we can first confirm that a key factor to obtain luminogenesis is providing proteins from the Extra-cellular Matrix, i.e. inducing the apical-basal polarisation.

Among the cyst population there is a certain size variation, but the cysts being monoclonal, the average size after the 4-days protocol peaks around 50-100μm diameter. We were interested in assessing any size dependence in luminogenesis and further expression patterning.

To be able to perturb the size of this system, we thought first of extending the protocol, allowing the cells an extra-day in N2B27. We observed though that cells cannot survive long in this condition, and cell death was observed surrounding the cysts. We proceeded then differently, introducing a preliminary 24-48h step, where cells are plated in Geltrex, fed with N2B27 provided with 2i/LIF.

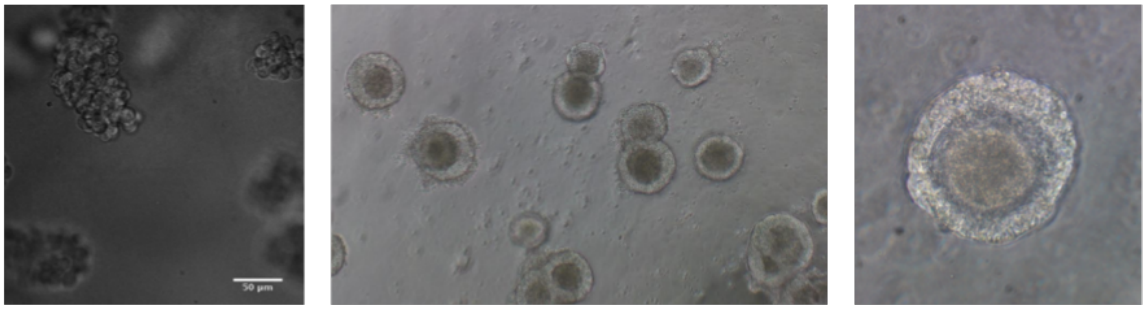

Figure 3.3: **2i/LIF prevent the formation of the synthetic Epiblast, even if Geltrex is provided** Left: cells grown in Geltrex do not compact nor undergo luminogenesis, unless 2i/LIF are removed. Instead, they keep proliferating in 'raspberry-like' structures that do not show any degree of morphogenetic organisation. Right: if 2i/LIF are given transiently to the cells, the cysts will compact when 2i/LIF are removed, but they will undergo a disrupted luminogenesis and a necrotic core will be visible inside the cavity.

The result of growing cells in Geltrex when 2i and LIF are provided is shown in Figure 3.3. We could conclude first that, growing cells in 2i results in no compaction nor luminogenesis at all: cells keep proliferating but they do not compact, giving rise to disorganised 'raspberry-like' structures.

Also, when we tried to provide 2i and LIF transiently, releasing them after 24-48h and proceeding then with the standard protocol (48h FGF, 48h BMP4), we could observe that cells restored compaction, but the luminogenesis was compromised and

the cavity filled with a necrotic core.
As described by [Shahbazi et al., 2017], where they do not observe luminogenesis unless 2i/LIF are removed from the medium but they confirm that cell polarisation still takes place, we can conclude that the presence of the ECM is not sufficient to ensure luminogenesis, despite being sufficient to ensure cell polarisation.
There are two necessary co-factors for cells to self-organise into hollow spherical structures that resemble the Epiblast: providing the ECM, that triggers the the apico-basal polarity and starts the epithelialisation, and releasing the 2i/LIF, that allows cells to compact and then open the cavity. It would be possible to argue that cells need to be in their primed pluripotent state to cavitate, but to confirm that further experiments would be needed like releasing 2i, but not providing FGF that triggers the conversion of ESCs to EpiLCs.

3.2.2 Inducing differentiation on a Synthetic Epiblast: the role of BMP

After 48h in Geltrex, cysts present the characteristics of the peri-gastrulation Epiblast: they are uniformly Oct4 positive and they underwent epithelialisation and luminogenesis.
In the second part of the experiment, we stimulate cells to differentiate by providing BMP4 along with the culture media for 48h. BMP4, as detailed in Section 3, is known to induce Primitive Streak formation, and cell fate specification toward mesendoderm fate.
Nodal and Brachyury are two relevant posterior markers. When antero-posterior polarity is established, across E6.5 and E7.5, Nodal is found restricted to the posterior side, and cells that will form the Primitive Streak start upregulating Brachyury. Moreover, Nodal is known to be necessary for the expression of Brachyury (among other posterior markers such as Wnt and Eomes) as experiments run on Nodal knockout mouse embryos were able to prove [Brennan et al., 2001].

For these reasons, we will mainly use these two genes as a readout of BMP stimulation. By means of two reporter lines Nodal-YFP and Bra-GFP, we have been able

to track over time Nodal and Brachyury expression.

The aim is to be able to establish the role of BMP in inducing posterior cell fate specification and whether and to what extent it is possible to observe symmetry breaking in the absence of the Extra-embryonic tissues or of an asymmetric stimulation.

It is important to recall here, the study conducted in the lab of Alfonso Martinez-Arias [van den Brink et al., 2014] [Beccari et al., 2018], where indeed they were able to observe a polarised expression of Brachyury, and an elongation of the structures along the antero-posterior axis, in response to a uniform stimulation with the Wnt agonist Chir. They called the obtained elongated structures 'gastruloids'. The main difference that distinguishes this system from ours, it is in the culture methods: gastruloids are not monoclonal, they arise from seeding 50-100 mES cells that are grown in low adhesion conditions and where Matrigel is not provided if not in small amounts in solution with the media.

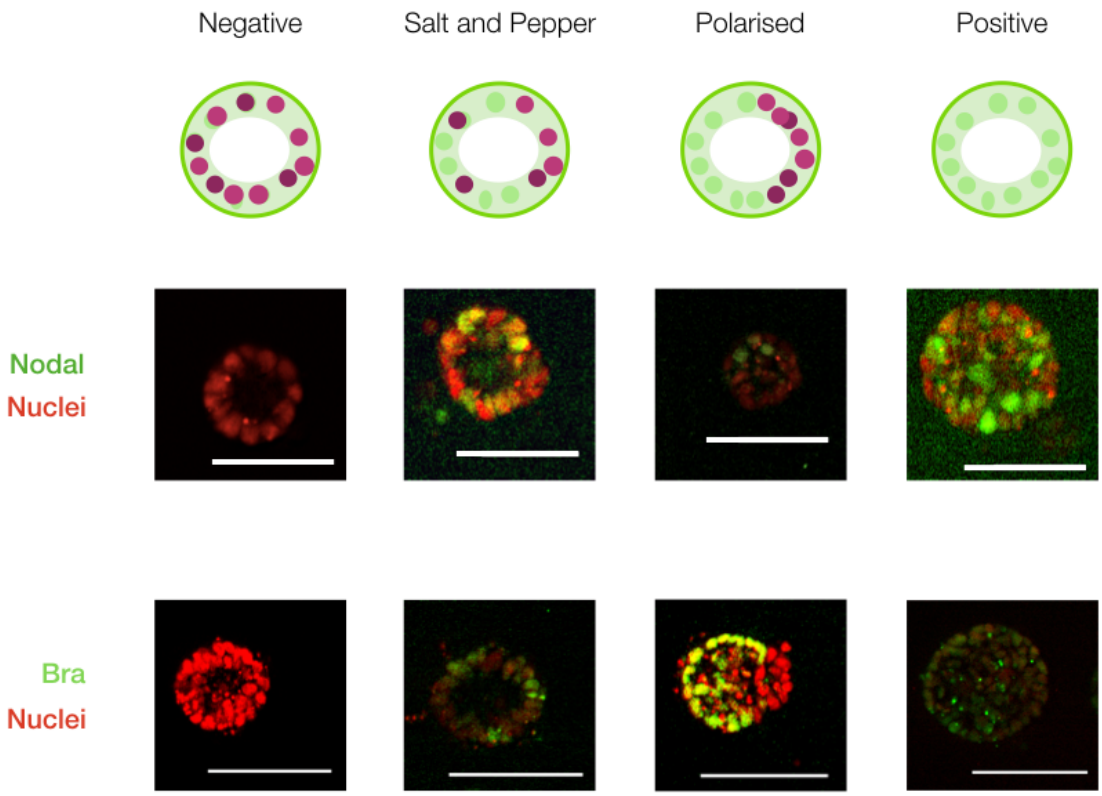

Figure 3.4: **Uniform stimulation with BMP results in four phenotypes for the expression patterns of Nodal and Brachyury** After 48h of stimulation, we observe 4 different phenotypes for Brachyury and Nodal (here only examples for Nodal are shown, but the same applies to Brachyury), a negative one where no signal is detected, a 'salt and pepper' where the signal is not constant across the organoid but does not show any preferred direction, a polarised one where the signal is polarised on one side of the cysts and a positive one where the signal is on across the whole organoid. Scale bar is 50μm

The results of our experiments are quantified in the following section, where we explore how the response changes with varying BMP concentration, but qualitatively we can sum up our observations into four different phenotype classes, that are defined in Figure 3.4: a fully positive phenotype, where all cells in the organoid express the gene under consideration, a 'salt and pepper' phenotype where the gene is expressed over all of the cyst in an isotropic manner, but not all cells are positive, a polarised phenotype where we indeed observe symmetry breaking and gene expression appears polarised, and a negative phenotype, where we do not observe any expression at all. Nodal and Brachyury appear to have complex dynamics over the 48h stimulation,

which is manifestly BMP concentration dependent. We do not observe any preferential direction in the polarisation, which is in agreement with an isotropic stimulus.

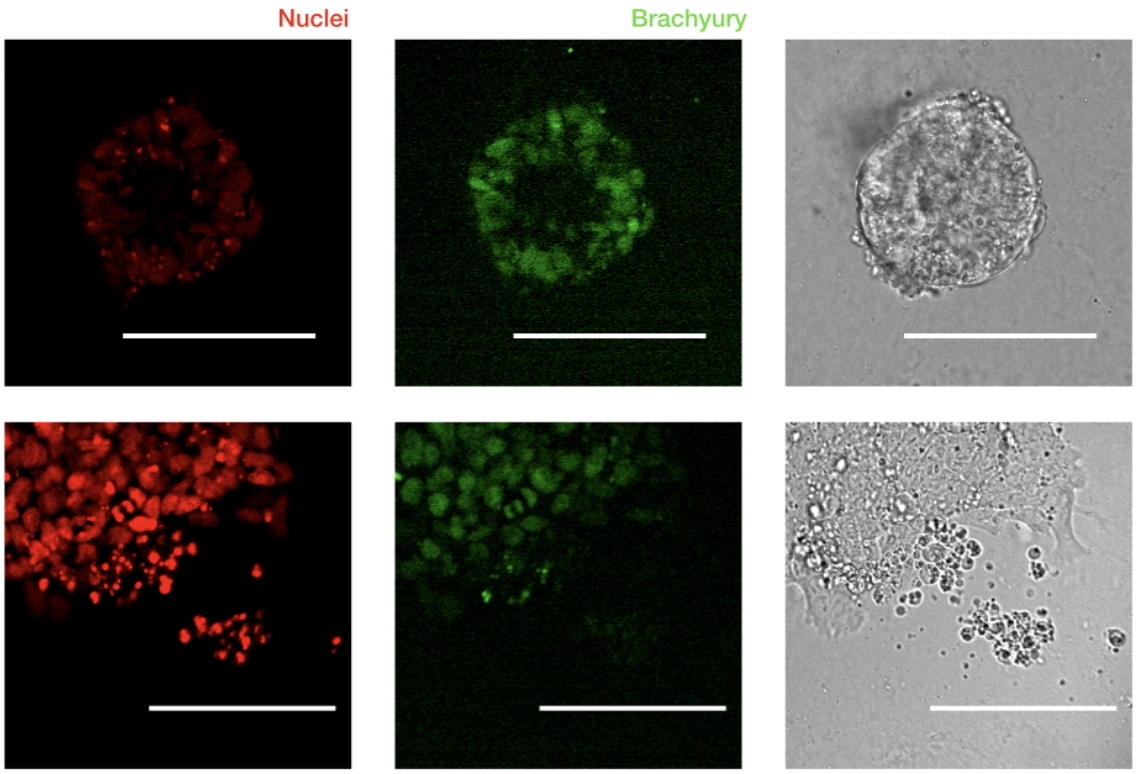

Figure 3.5: **Upon stimulation with BMP cells tend to undergo EMT and spread on the substrate** Top: a fully positive cyst. Bottom: cells start undergoing EMT, breaking up the cyst and spreading on the substrate. Scale bar is 50μm

Lastly, it is worth mentioning, that the following quantification takes into account only those organoids, that kept their morphological structure intact at any time point. In fact, over time, we observe that cells tend to undergo an Epithelial to Mesenchymal Transition (EMT) and to adhere to the surface and spread on the substrate, leaving and disrupting the cyst structure as shown in Figure 3.5. This happens in every condition we tested, but it seems to be more relevant in higher BMP concentrations, which can be considered as expected, as cells in the embryo undergo EMT at the onset of gastrulation, where a subgroup of cells starting expressing Early Mesoderm markers leave the Epiblast to establish the Mesoderm layer. Further investigations, anyway, would be needed to quantify the impact of BMP on inducing EMT in cysts. Brachyury positive cells undergoing EMT and leaving their aggregate have been al-

ready reported in Gastruloids [van den Brink et al., 2014] upon induction of Wnt and also in human organoids upon stimulation with BMP [Simunovic et al., 2019].

3.2.3 A dose response curve experiment: population behaviour for different concentrations of BMP

In this section we discuss the dynamic response of these Epiblast-like organoids when stimulated with BMP4.

To explore the landscape of response we observe live the evolution of the dynamics of Nodal and Brachyury in the population of cysts throughout stimulation.

We decided to explore a range of different concentrations for BMP in order to find out what is the minimal induction that results in the appearance of Posterior-like cells. The main reason behind this was to understand if cells could sense different concentrations of morphogens and how their response would vary accordingly. Moreover, it has been shown in human ESCs [Simunovic et al., 2019] that BMP concentration is a relevant parameter in determining the emerging of polarisation and its frequency.

It has been shown that cells can distinguish temporal and spatial patterns of morphogens [Sorre et al., 2014].

Also, in previous studies [Etoc et al., 2016] [Nallet-Staub et al., 2015] [Zhang et al., 2018] the localisation of BMP receptors has been investigated and it has been found that they are located at the basolateral site of the membrane, both in human Embryonic Stem cells and in the mouse embryo. In traditional 2D culture systems, this translates to a strong cell density dependent response to stimulation, as high density condition would prevent the accessibility of ligands to the receptors, due to establishment of tight junctions at cell-cell contacts. In our case the basal side of the cells is facing the ECM and is thus fully exposed to ligands. It is reasonable then to ask how the morphogen concentration itself affects the cellular response.

We tested three configurations where BMP is provided at a concentration of 0.1ng/ml, 1ng/ml and 10ng/ml. As a control we keep one sample of cells in N2B27 for the whole 4 days. FgF and KSR are provided over the whole 96h.

We discuss first the dynamics of Nodal and then that of Brachyury whose expression

is delayed with respect to Nodal, as we will see.

Then we discuss what we could learn from repeating this experiment.

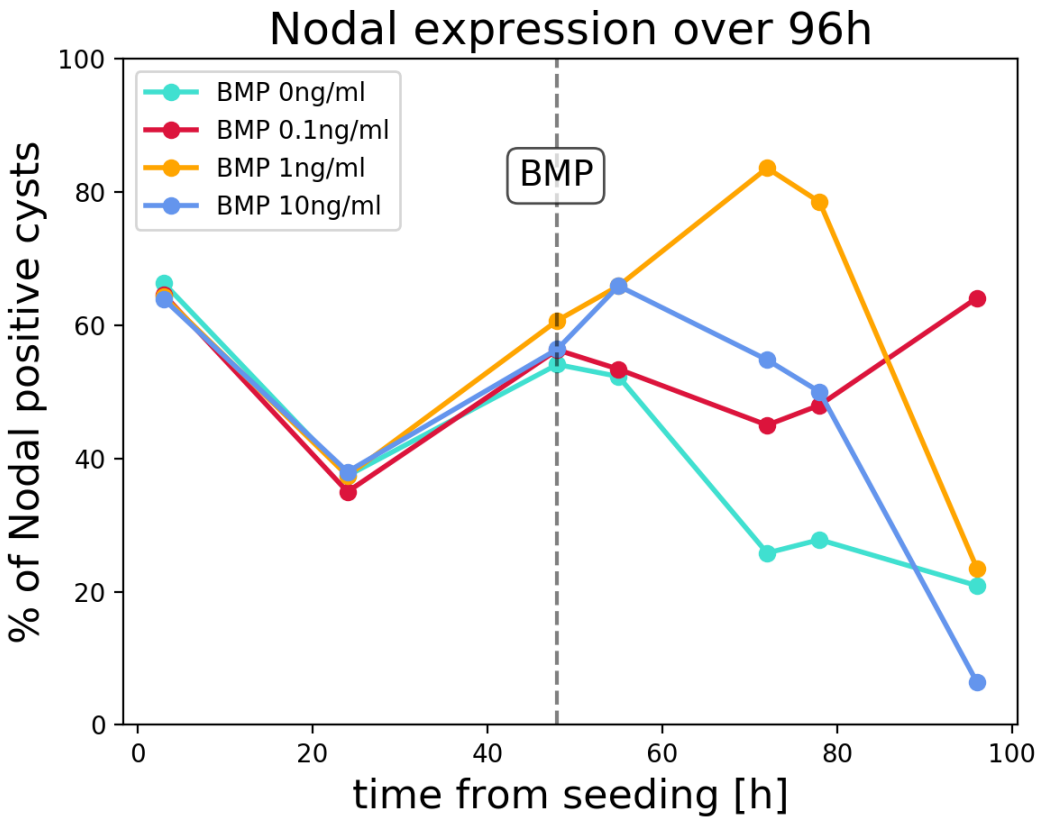

Figure 3.6: **Nodal dynamics over 96h for different BMP concentrations** Only 1ng/ml and 10ng/ml BMP concentrations are able to significantly induce Nodal among the whole population over the first 24h stimulation. Nodal is then turned off during the last 24h.

The dynamics of Nodal expression over the four days of our protocol, i.e two days before stimulation and two days in BMP4, is represented in Figure 3.6: here, all the cysts that present Nodal positive cells are taken into account. In the following, it will be detailed to what extent, part of those show a polarised expression of Nodal, but for now we are interested in addressing to what extent BMP is inducing and sustaining Nodal expression.

The first observation we were able to make is that before stimulation, at the start of our experiment, all the four samples show the same behaviour, showing strong

reproducibility in Nodal expression pattern during transition from ESCs to EpiLCs, while forming cysts.

Particularly, when cells are seeded a majority of them are already expressing Nodal. Then Nodal expression drops down during the first day and is partly re-established at the end of the second. This behaviour, Nodal high when 2i and LIF are removed from the medium, and then dropping over 24h, has been confirmed also in flat culture (data not shown, Furfaro et al., Plouhinec et al., in preparation).

As we can see, upon stimulation with BMP, Nodal dynamics presents significant differences according to different BMP concentrations: in the control configuration (no BMP), we cannot observe any induction of Nodal, and Nodal expression drops significantly over 48h. This confirms that BMP4 is necessary to sustain Nodal expression in the posterior pole of the Epiblast. On the opposite side, high concentrations of BMP4 such as 1ng/ml and 10ng/ml are found to actively induce and sustain Nodal expression over the first 24h stimulation. After that, despite keeping providing BMP, Nodal expression drops to the same frequency of expression of the control. Also this pattern has been confirmed in flat cultures (data not shown, Plouhinec et al., in preparation). We observed that stimulating the system with a concentration of 0.1ng/ml BMP was not sufficient to induce a significant expression over the first 24h, but produced an increased expression during the second, corresponding to the time we observed a drop in Nodal in high concentration conditions.

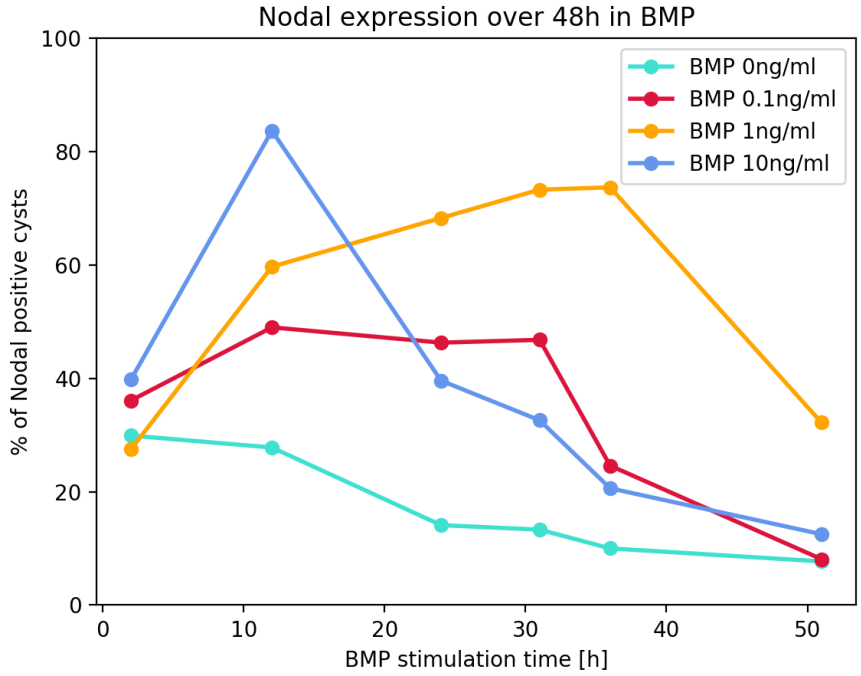

Figure 3.7: **Repeated experiment shows that 1ng/ml BMP induces reproducible temporal patterns in Nodal expression** A repeated experiment showed a conserved profile for BMP 1ng/ml and BMP 10ng/ml, but BMP 0.1ng/ml fails to induce the late spike of Nodal expression previously observed.

We repeated the experiment (results shown in Figure 3.7) and we could confirm that 1ng/ml and 10ng/ml BMP concentration induce and sustain Nodal during the first day of stimulation and that in these two cases Nodal is found dropping during the second day. Again, no significant Nodal expression could be found in the control, confirming that BMP is not only sustaining, but actively inducing Nodal expression. We could not observe, though, the late spike in Nodal in the low concentration case. The reason for this phenomenon suggests an indirect mechanism, but will require further investigation to be fully understood. As we will discuss further later in this and following chapters, we hypothesised that the density of organoids also plays a role: we found evidence from our experiment in the gradient device (see Section 4) that secreted factors from the synthetic Epiblast play a role in sustaining Nodal and inducing Brachyury. In that sense, the density of cysts could represent a parameter to be investigated as cysts (that are not isolated in these experiments, as they are in

others by plating on microwells etc.) could impact on each other gene expression. It is possible then, that there would be other effects connected to the local density of (Nodal expressing) cysts that would affect the expression patterns of neighbours, and we hypothesise that this effect might be even more visible in the low concentration situation. We leave to the conclusion a further discussion on this hypothesis.

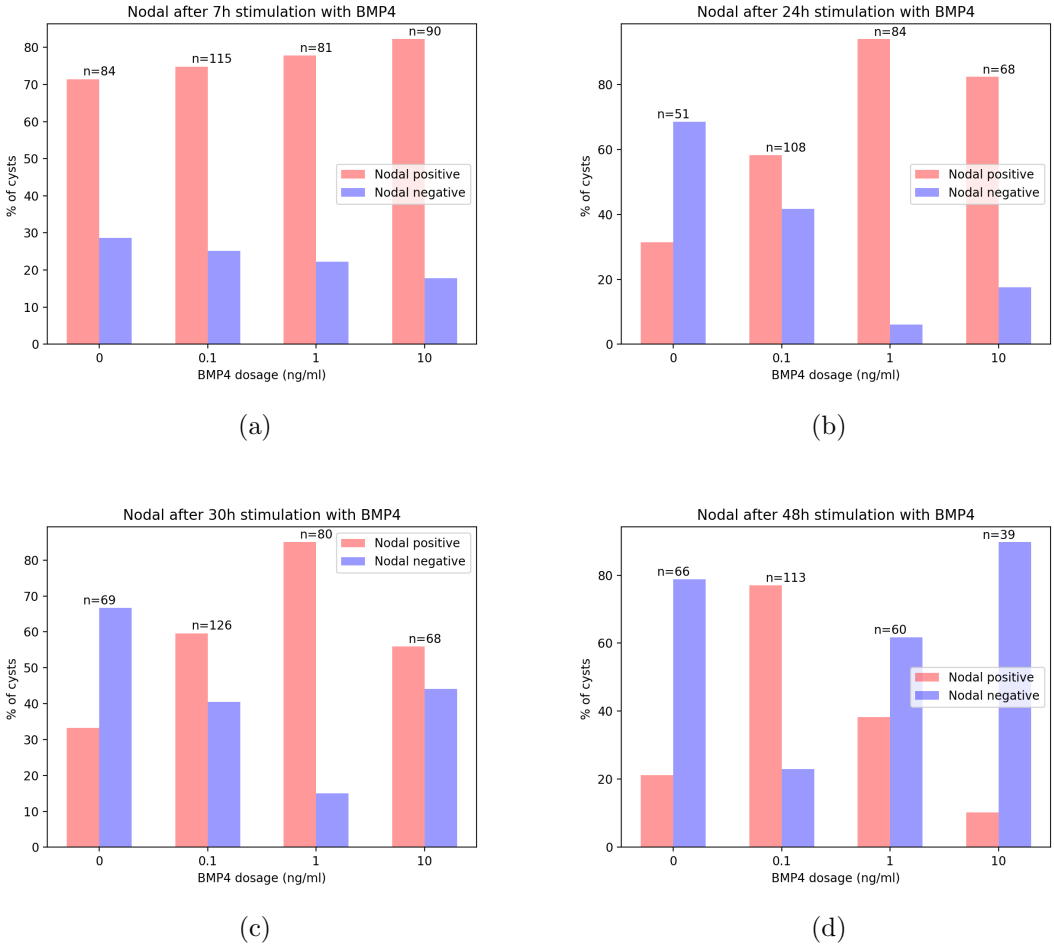

Figure 3.8: **Nodal expression for the population of cysts over different time points during 48h stimulation with BMP** We see that higher concentration of BMP sustain Nodal over the first 30h stimulation. Nodal is then turned off in all condition, but in 0.1ng/ml where it shows a delayed induction. On top of each couple of columns it is specified the total amount of organoids taken into account per condition.

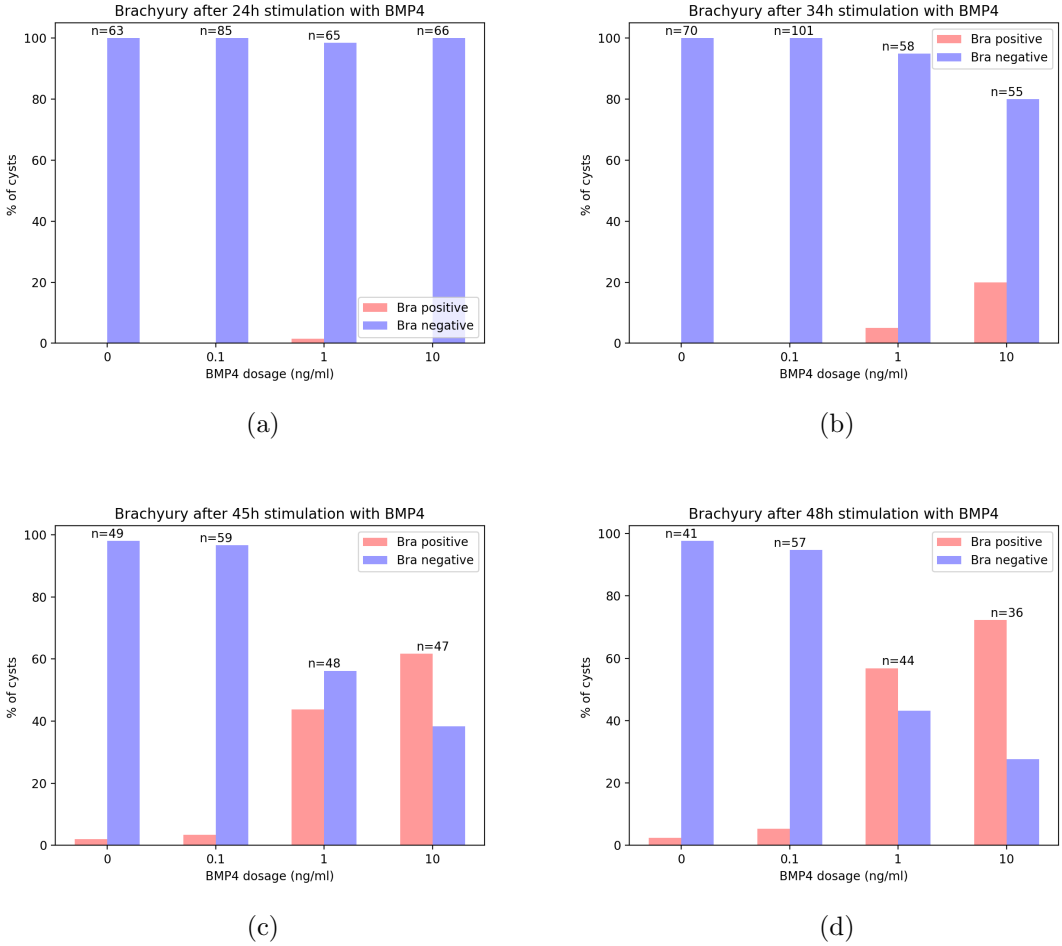

Figure 3.9: **Nodal expression for the population of cysts over different time points during 48h stimulation with BMP** Brachyury is found to be induced by high concentration of BMP over the last 24h stimulation. It takes 24h for BMP to induce Brachyury. Low concentration of BMP, such as 0.1ng/ml, is found not sufficient to induce Brachyury. On top of each couple of columns it is specified the total amount of organoids taken into account.

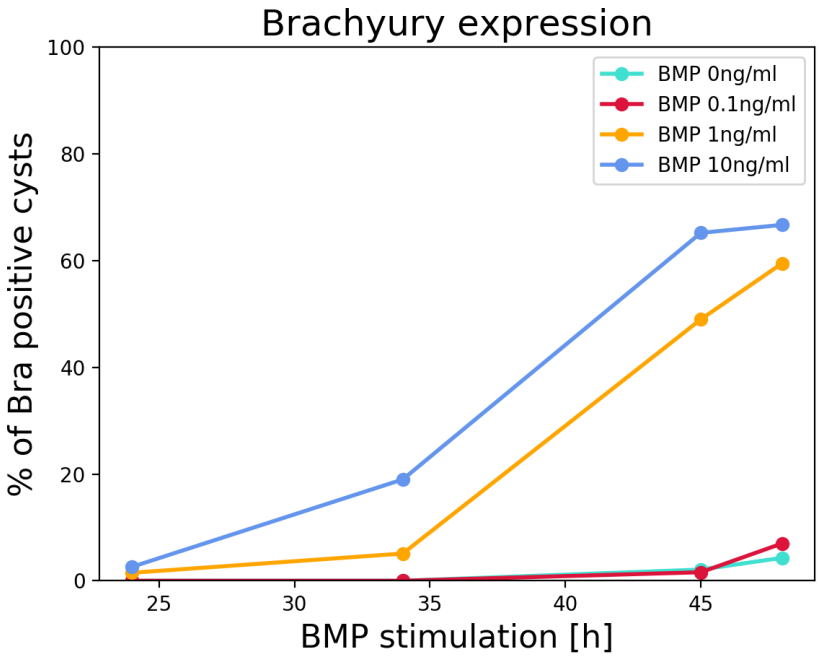

Figure 3.10: **Brachyury dynamics over 48h BMP stimulation** BMP induces Brachyury in a significant amount of synthetic epiblasts, during starting from after 24h stimulation. Only high concentrations BMP are found to induce Brachyury expression

In Figure 3.8 the relative amount of Nodal positive cysts is shown at each time point, highlighting the number of cysts analysed.

The same experiment has been repeated with a Bra-GFP reporter line to highlight the dynamics of Brachyury, and the results are reported in Figure 3.10.

We found out that only high concentrations of BMP (1ng/ml and 10ng/ml) were able to induce significant Brachyury expression, where none or no significant expression was observable in the 0.1ng/ml BMP4 case nor in the control. We could observe that the induction of Brachyury is shifted with respect to the Nodal profile. Indeed Brachyury positive cells start appearing after 24h stimulation. The fact that BMP induces Brachyury after 24h stimulation has been already observed in human and mouse on micropatterned 2D cultures [Warmflash et al., 2014] [Morgani et al., 2018] and in human ES organoids [Simunovic et al., 2019].

In a repeated experiment (Figure 3.10) we observed induction of Brachyury also for the low concentration sample. This will need though further investigation to be con-

firmed, but it is not completely surprising as in the ETS-embryos study [Harrison et al., 2017], they reported some activation of Brachyury in mESCs organoids even if no active stimulation was provided: they intended to assess that, in their system, TS cells were reponsible for inducing Brachyury expression, so they kept mESCs only organoids in same culture conditions as the ETS-embryos and they observed still some Brachyury expression even though with strongly less significant frequency than when in the presence of TS cells.

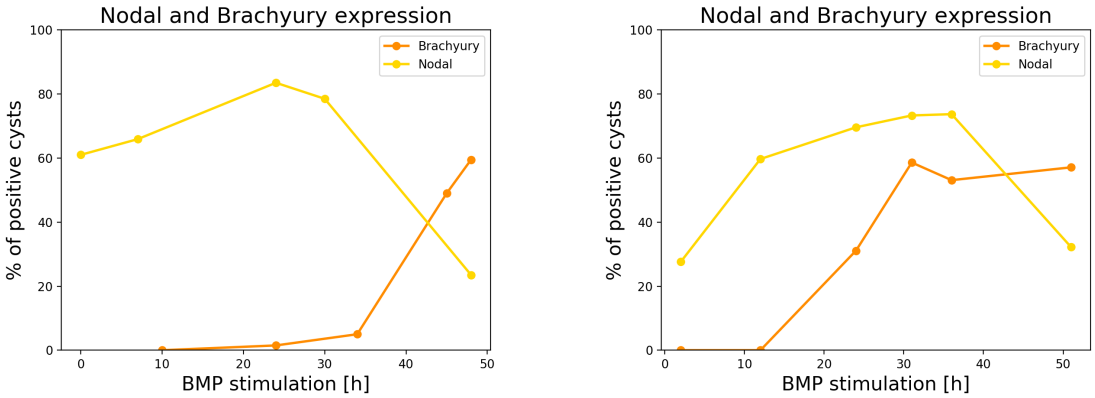

Figure 3.11: **The induction of Brachyury is delayed of 24h from the start of BMP stimulation** Superimposing the profiles of Nodal and Brachyury expressions in two independent experiments allows to confirm that the induction of Brachyury is shifted of 24h with respect to the stimulation. When Brachyury is on Nodal is being turned off.

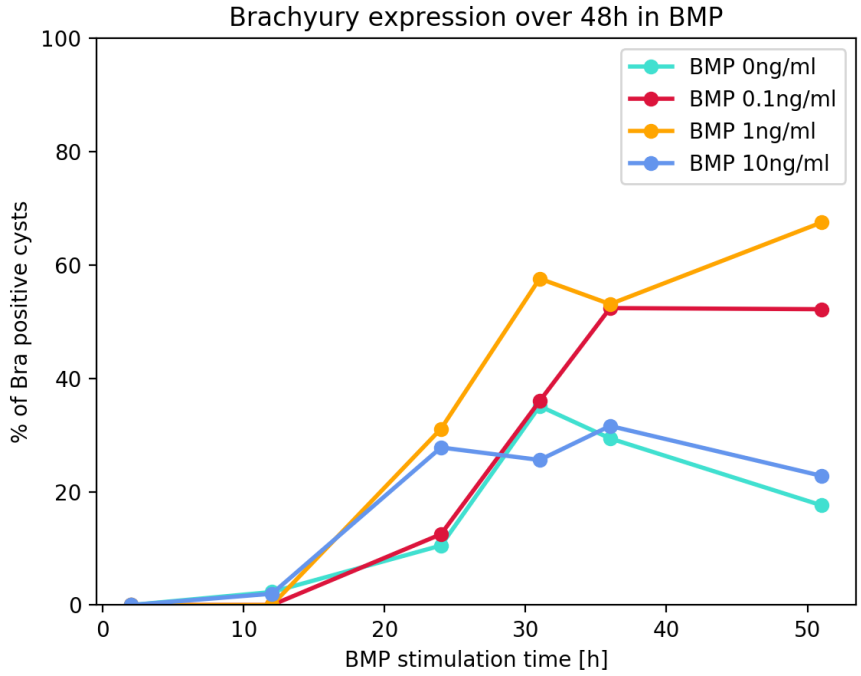

Figure 3.12: **Repeated experiment shows that 1ng/ml BMP induces reproducible temporal patterns in Brachyury expression** a repeated experiment showed a conserved profile for BMP 1ng/ml that induces Brachyury after 24h stimulation.

What was conserved though across the two experiments is the behaviour in the 1ng/ml BMP concentration case. To visualise that better, we superimpose the profile of Nodal and Brachyury in both experiments in Figure 3.12, where it is possible to recognise Nodal expression increasing over the first 24h, followed during the second day, by an induction of Brachyury which corresponds to a decrease in Nodal. It would be interesting in the future to understand better the relationship between Nodal and Brachyury: by immunofluorescence experiments we could assess to what extent Nodal and Brachyury expression overlap at different time points.

3.2.4 Observing symmetry breaking upon an isotropic stimulus

Up to this point, we have been looking at what we could define as the overall expression of posterior markers Nodal and Brachyury over time. In what follows, we discuss in further detail the different phenotypes observed among the class of positive

organoids. We wanted to refine this analysis to see if some symmetry breaking reminiscent of the antero-posterior polarity could be observed upon a uniform stimulus. We recall from Figure 3.4, that we can divide the positive phenotypes in three subtypes: *positive*, meaning that the gene of interest is uniformly expressed across the cyst, *'salt and pepper'* meaning that the expression is not uniform but still isotropic and not polarised, and *polarised*, where we can observe a polarised expression of Nodal and Brachyury.

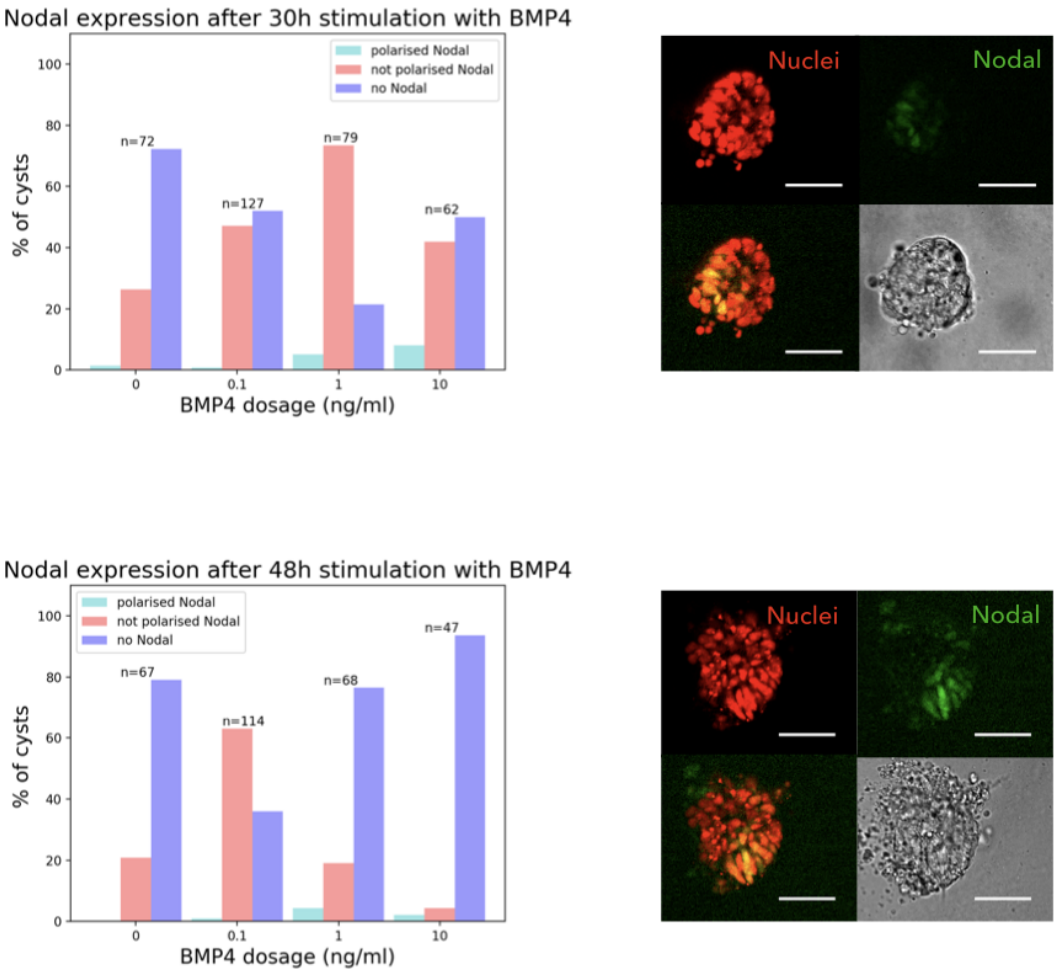

Figure 3.13: **Frequency of observation of the polarised phenotype and a representative example of a Nodal polarised synthetic Epiblast** The histograms show the relative frequency of polarised, not polarised and negative cysts for the time points 30h and 48h after BMP stimulation. Frequency of observation is lower than $\approx$ 10% of the total amount of cysts analysed and particularly do not exceeds the $\approx$ 20% of the cysts overall expressing Nodal, in a polarised or unpolarised fashion. On the left a representative example of a polarised cyst. Scale bar is 50µm

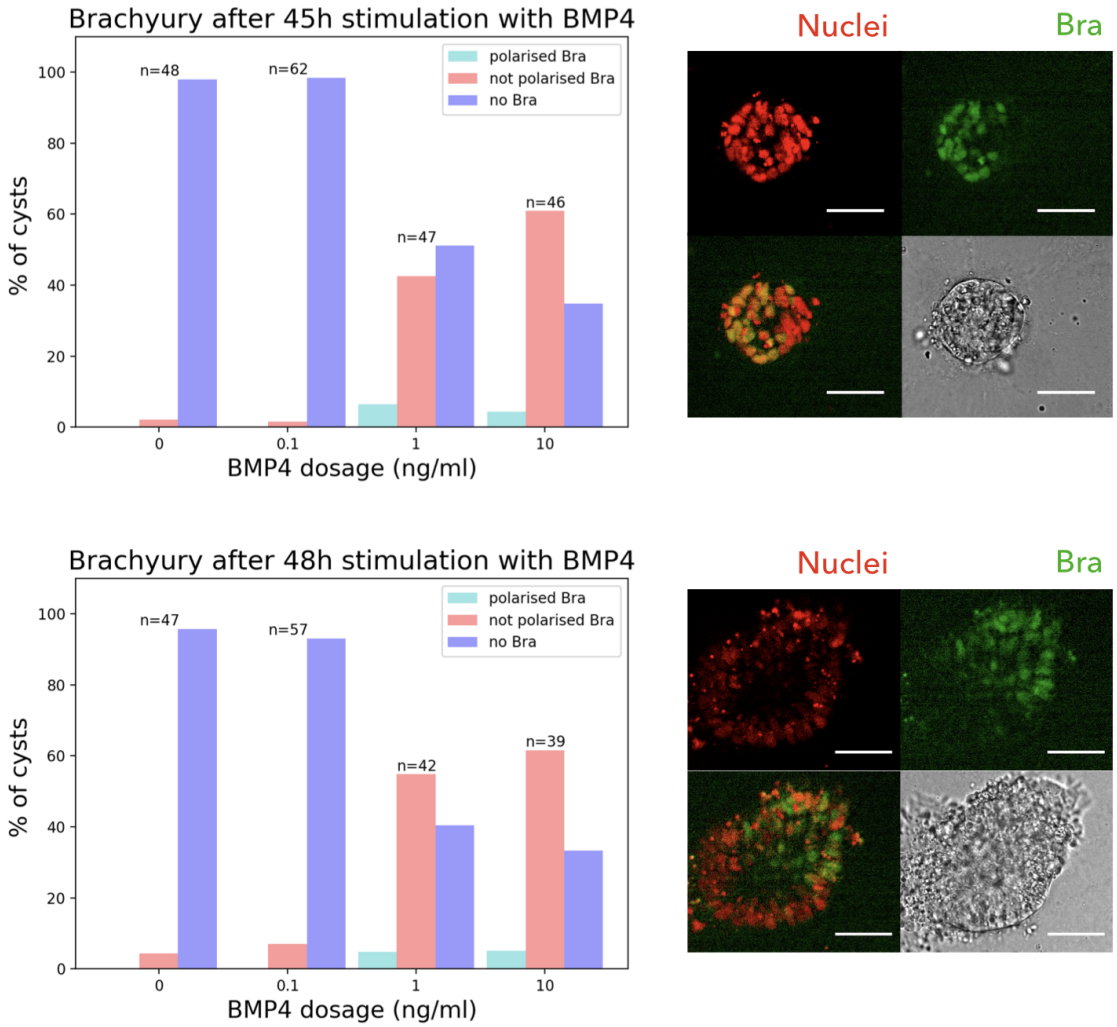

Figure 3.14: **Frequency of observation of the polarised phenotype and a representative example of a Brachyury polarised synthetic Epiblast** The histograms show the relative frequency of polarised, not polarised and negative cysts for 45h and 48h after BMP stimulation. Also in this case, as in Nodal analysis, Brachyury polarised cysts represent a small fraction of the total (polarised and not polarised) amount of cysts that are Brachyury positive. On the left a representative example of a polarised cyst. Scale bar is 50μm

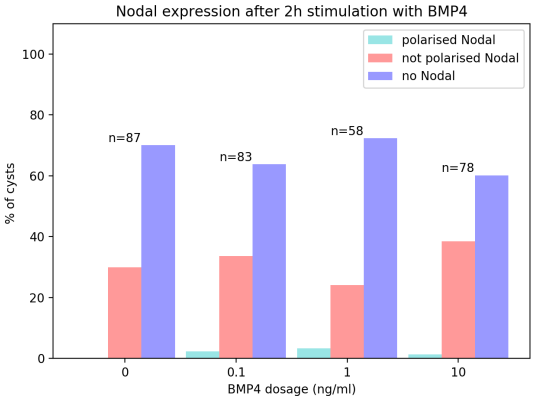
Nodal expression after 2h stimulation with BMP4
polarised Nodal
not polarised Nodal
no Nodal
% of cysts
BMP4 dosage (ng/ml)
n=87
n=83
n=58
n=78

(a)

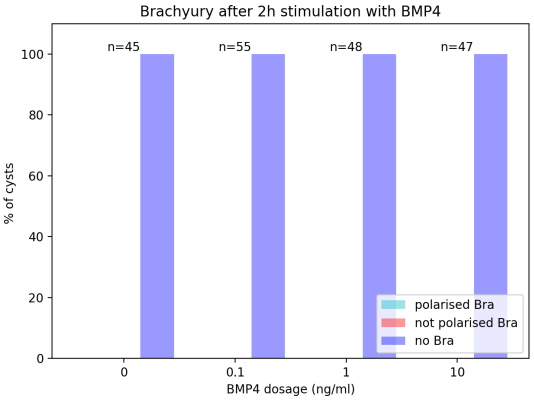
Brachyury after 2h stimulation with BMP4
polarised Bra
not polarised Bra
no Bra
% of cysts
BMP4 dosage (ng/ml)
n=45
n=55
n=48
n=47

(b)

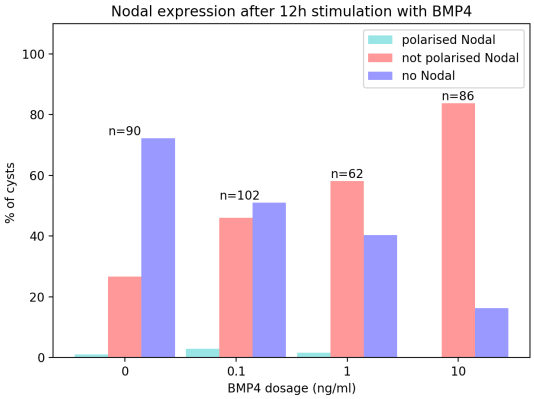
Nodal expression after 12h stimulation with BMP4
polarised Nodal
not polarised Nodal
no Nodal
% of cysts
BMP4 dosage (ng/ml)
n=90
n=102
n=62
n=86

(c)

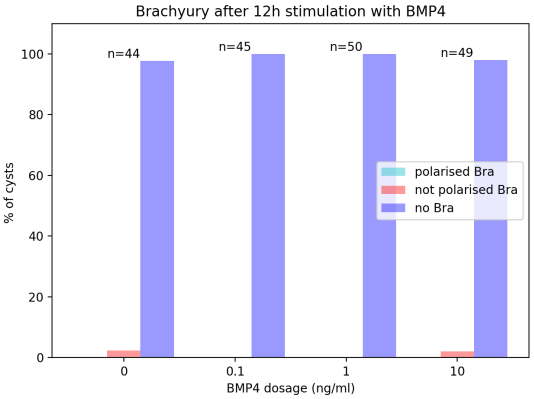
Brachyury after 12h stimulation with BMP4
polarised Bra
not polarised Bra
no Bra
% of cysts
BMP4 dosage (ng/ml)
n=44
n=45
n=50
n=49

(d)

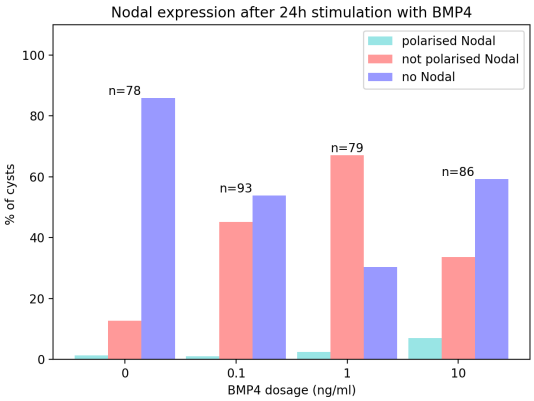
Nodal expression after 24h stimulation with BMP4
polarised Nodal
not polarised Nodal
no Nodal
% of cysts
BMP4 dosage (ng/ml)
n=78
n=93
n=79
n=86

(e)

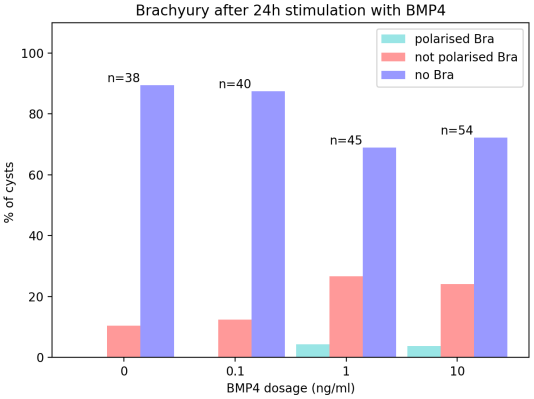
Brachyury after 24h stimulation with BMP4
polarised Bra
not polarised Bra
no Bra
% of cysts
BMP4 dosage (ng/ml)
n=38
n=40
n=45
n=54

(f)

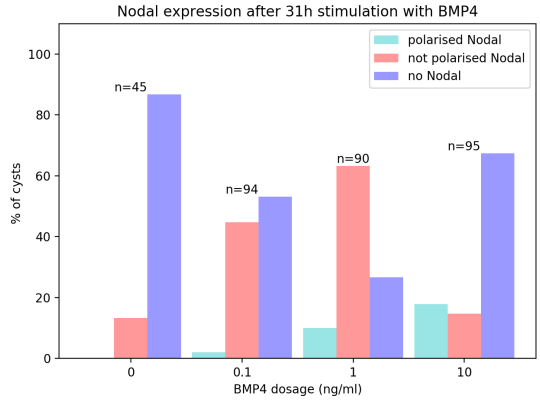

(g)

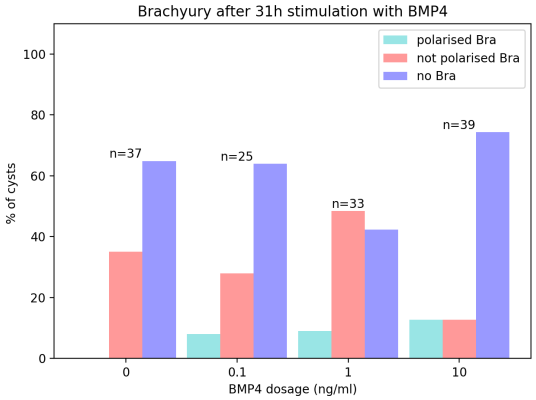

(h)

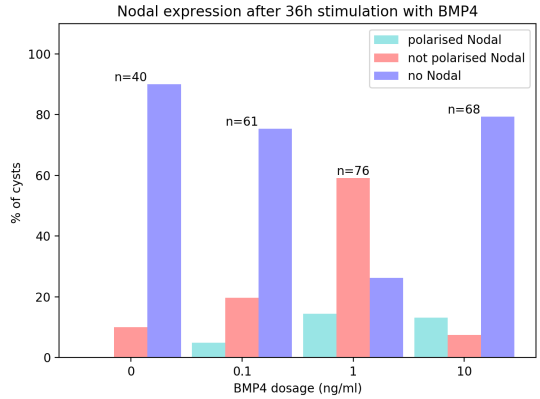

(i)

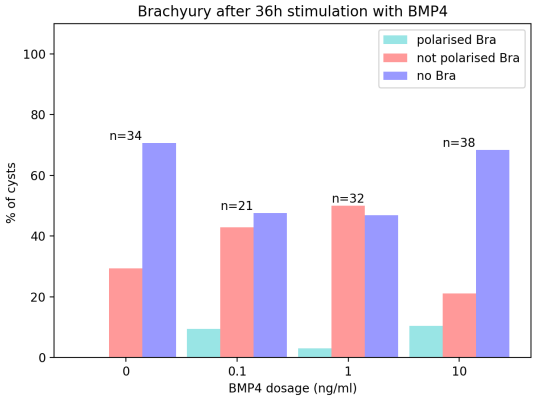

(j)

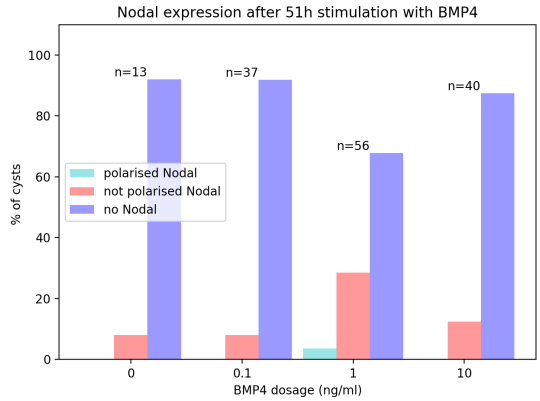

(k)

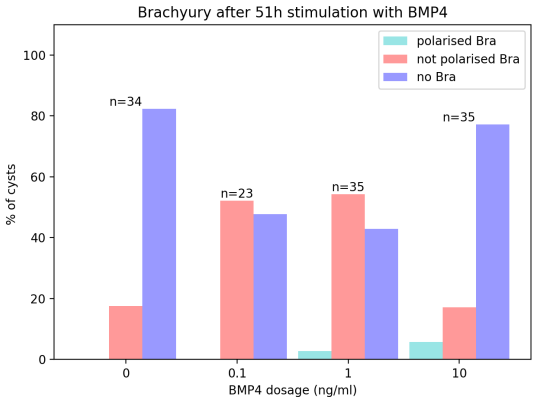

(l)

Figure 3.15: **Frequency of observation of the polarised phenotype for Nodal and Brachyury for all time points detected** The histograms show the relative frequency of polarised, not polarised and negative cysts for Nodal (left) and Brachyury (right) for all the time points detected. For t=31h and t=36h, we observe the largest occurrence of polarised cysts, but only for high concentration of BMP (10ng/ml) the relative amount of polarised cysts is compared to the relative amount of positive cysts.

We have been able to observe in a sub-population of organoids a spontaneous symmetry breaking event, following uniform stimulation with BMP. In the charts presented in Figures 3.13, 3.14, 3.15), we highlight the percentage of cysts that present a polarised gene expression.

It has to be noted though that the frequency at which this event occurs is quite small, usually around 5% and never bigger than 15% of the total amount of cysts analysed. It is interesting here to compare this work to the work of [Simunovic et al., 2019], where they make use of a culture system for human Embryonic Stem cells, that is the analogue to what we do here for mouse cells. They were able to observe that uniform stimulation with BMP resulted in a significant symmetry breaking where cysts polarise into two domains exclusively expressing Sox2, a pluripotent marker, or Brachyury. The frequency at which they are able to observe this symmetry breaking event is found to be strongly dependent on BMP concentration, but they found that for a concentration of 1ng/ml $\approx 50\%$ of the cysts were showing the polarisation of Brachyury and Sox2. This is pointing out to some differences in how molecular mechanism regulate the induction of gastrulation between the two species.

The fact that a majority of the positive cysts express Nodal or Brachyury with no preferred direction seems to confirm the necessity for a local asymmetric stimulus to restrict the signal to a posterior domain.

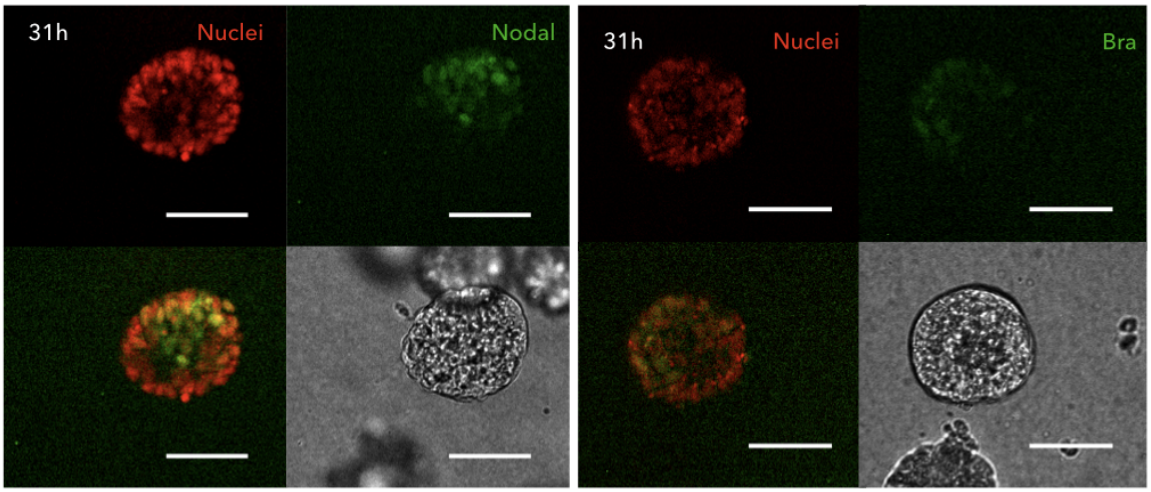

Figure 3.16: **Nodal and Brachyury polarised cysts following uniform stimulation with BMP** A representative example of a Nodal (left) and Brachyury (right) polarised cyst at t=31h after BMP stimulation. Scale bar is 50 μm

Repeating the experiment (results reported in Figure 3.15), we found the same result, a small fraction of polarised cysts, in all conditions and time points, except, surprisingly, around 30h after high dose (10ng/ml) BMP stimulation, where the number of polarised cysts is comparable to the number of uniformly positive ones. Representative examples of polarised cysts are shown in 3.16. The reason behind this increased frequency of observation of the polarised phenotype, is not clear, but it is worth noticing that the total amount of positive organoids, both uniform and polarised, is lower than that that was reasonable to expect based on the previous experiment. We anticipate that further experiments will be needed to keep investigating conditions under which a polarisation arises. As anticipated also before, we intend to investigate the role of other parameters that might be relevant such as the density of cysts, and to further check the existence of an optimal configuration of concentration of BMP, that is found to induce best a symmetry broken expression of posterior markers. Particularly if signalling from neighbours turned up to be a relevant parameters, that stimulus would be somehow directional as we could interpret our plated organoids as point-like sources.

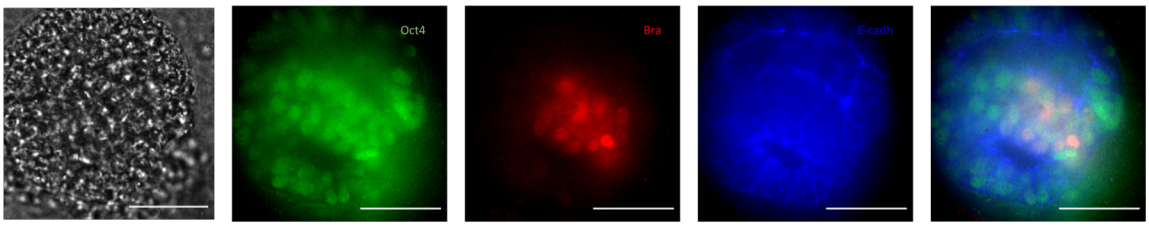

Figure 3.17: **A representative example of two cysts coalescing** Brachyury is polarised at the interface of the two cysts. Both sides present Brachyury positive cells. Scale bar is 50μm

Indeed, we were able to make an interesting observation, that points out in the direction of a cross-talk between organoids and an active role of the Epiblast itself in inducing and/or sustaining the local expression of Brachyury. In our system, as detailed before, cysts are not isolated from each other. It happens then that they fuse in one single hollow cyst, moving toward each other as there was some kind of attractive force. When this happens, before the cysts completely fuse, when they are in contact, we observe the polarisation of Brachyury at the interface between them, with Brachyury positive cells found on both sides of the interface. An example is reported in Figure 3.17.

3.3 Discussion: what's missing in this model, introducing the gradient

Summarising, we have seen that growing Embryonic Stem cells in Geltrex provides the necessary conditions to observe the formation of hollow spherical structures with the basal side exposed toward the exterior in contact with the Extra-Cellular Matrix, that are reminiscent of the Epiblast at the peri-implantation stage.
We have observed that stimulation with BMP4 triggers the expression of Nodal that peaks during the first day followed during the second day by the induction of Brachyury, both of which are markers of the posterior side of the embryo.
In a subgroup of organoids the expression of Brachyury and Nodal appears to be polarised on one side of the cysts, as it would be in the embryo at the onset of gastrulation. The fact that it is possible to observe symmetry breaking with an isotropic

stimulation suggests the existence of a self-regulated mechanism from the Epiblast to sustain the differentiation toward posterior-like fate. Nonetheless, the rather small frequency at which this event takes place suggests that something is missing to ensure that the Antero-posterior polarity is reliably established. Based on the literature, we hypothesised that a localised source of morphogens could be necessary to ensure the polarisation, and we will discuss in Section 4 how to set up a system for stimulating locally our synthetic Epiblast.
Nonetheless, we believe that this simple model for the Epiblast is valuable in its simplicity to address quickly and with high-throughput the response of the Epiblast-like organoids to different concentrations of different morphogens and/or their inhibitors. Nevertheless, we think that engineering systems that allow a better control of the environment in which the organoids are grown could help narrowing down the variability observed, that is an issue to address across all organoids research.

In what follows, we introduce a microfluidic chip that we have developed to grow organoids in Geltrex, and expose them to a gradient of morphogens. We will detail how this has an impact on the frequency of polarisation among the organoids population.

4 The gradient device: a microfluidic tool to stimulate mESc organoids with gradients of morphogens

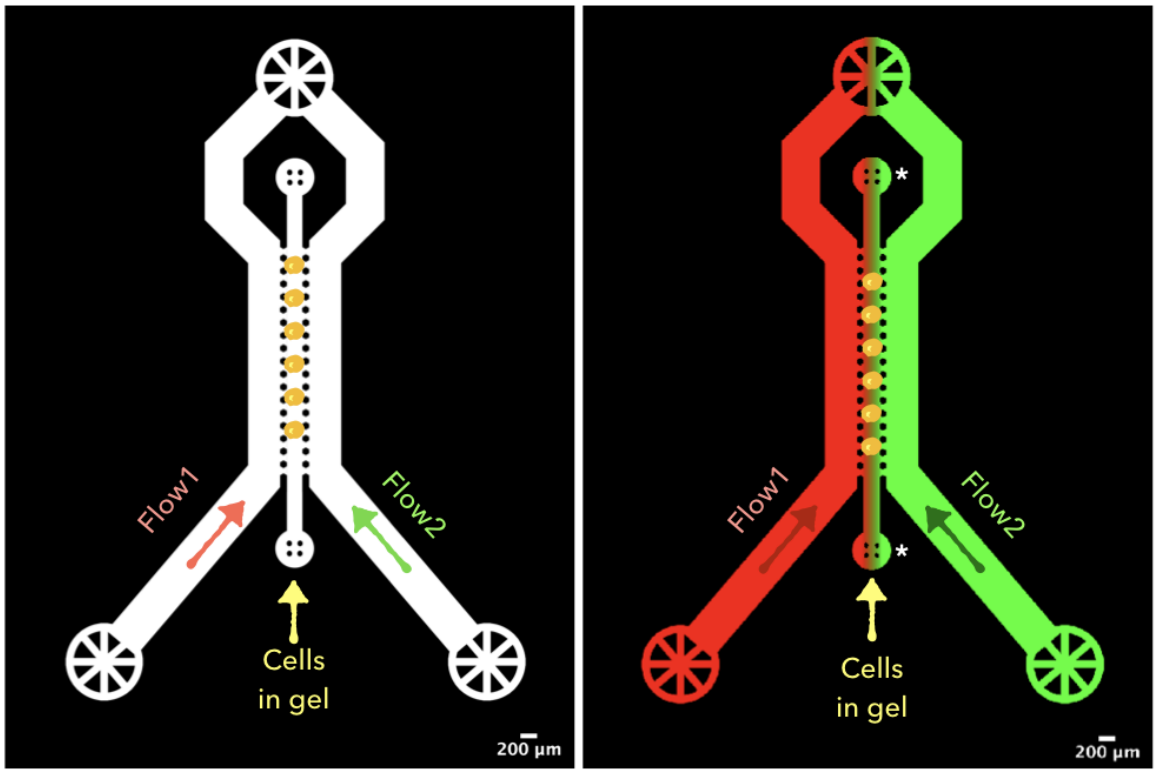

Figure 4.1: **Scheme of the gradient device.** This microfluidic chip is used to generate linear gradients of chemicals over the length scale of the middle channel, here 200µm. The middle chamber is filled in with a gel. The hexagonal pillars confine the gel and prevent it from spilling into the two flow channels. Pushing two media with different chemical composition in the two flow channels results in the chemicals diffusing through the gel and establishing a linear gradient of concentration between one channel that acts as an infinite source and the other that acts as a perfect sink. *The picture represents a simplification. We will discuss later, that in these regions, that are not in contact with the flow channels, there is no gradient, but rather a uniform intermediate concentration.

After concluding from the previous Section that uniform stimulation with BMP4 was not sufficient to ensure robust antero-posterior polarisation, as it seems to be for the human [Simunovic et al., 2019], we hypothesised that having a localised source,

therefore biasing the directionality of the signalling, would have had a role in imposing the symmetry breaking. Indeed in the mouse embryo, BMP is provided from the Extra-embryonic Ectoderm at the proximal side of the Epiblast, and it has been recently hypothesised [Zhang et al., 2019] that the geometry of the embryo coupled to basal positioning of BMP receptors would be responsible for the establishment of a gradient of BMP along the Proximal-Distal axis. From the literature this gradient of BMP coupled to a gradient of Nodal inhibitors on the A-P axis is considered responsible for setting up the Antero-Posterior polarity. We thought of designing a device to stimulate our synthetic model of the Epiblast with a gradient of BMP, in order to mimic the gradient established by the Extra-embryonic Ectoderm. We introduce here a microfluidic device to generate gradients of morphogens over the length scale of the mouse Embryonic Organoids that we have introduced in Section 3. The design of such a device is schematically shown in Figure 4.1 and will be presented in detail in Section 4.2.

During recent years many different devices have been proposed to provide a gradient of different molecules to cells in a controlled way in space and time, in order to study different phenomena from chemotaxis to morphogenesis. In Section 4.1 we provide a short overview over some of them, that are the most relevant for describing the system we are going to present later. Here, we evaluate whether a localised source of differentiation inducing signal translates to inducing symmetry breaking in the Epiblast, in a more consistent way than what we were able to observe by providing a uniform and isotropic stimulus.

By studying this stimulation configuration, we expect to gain information on what conditions are necessary to observe symmetry breaking in the Epiblast, and particularly the respective role of morphogens and the Extra-embryonic tissues in establishing the Antero-posterior axis. In the literature, a double role for the Extra-embryonic tissues in patterning the A-P polarity has been identified: providing BMP from the ExE, that induces posterior markers such as Brachyury, and providing Nodal inhibitors from the migrating AVE, that would be responsible for confining Nodal to the posterior side. However it has been shown in mouse [Harrison et al., 2017] that

having Trophoblast Stem cells was sufficient to induce Brachyury localised expression in the absence of the AVE.

Here, we want to find out if it is possible to observe this restriction in the absence of the AVE and, consequently, of the correlated Nodal inhibitors, and if it is possible to mimic the role of the ExE by engineering a localised and controlled source of BMP. In what follows, we introduce the devices already existing, and to which the one presented here is inspired, highlighting the main changes we introduced to adapt it to our requirements, then we provide a description of our gradient device, and how to operate it. Then, we discuss the observations we were able to make and we compare them to what we were able to conclude from our bulk experiments. Last, we sketch the guidelines for what we believe it is important to do next, to improve this setup, with a particular attention to possible ways of improving the reproducibility of the results observed and overcome the issues we encountered.

4.1 Generating a gradient: an overview on existing devices

Devices to generate gradients have been extensively sought after during recent years to investigate different biological phenomena, where molecular gradients play an important role, from morphogenesis and development [Demers et al., 2016] [Regier et al., 2019] [Manfrin et al., 2019], to chemotaxis [Saadi et al., 2007] [Diao et al., 2006] [Atencia et al., 2009] [Shamloo et al., 2008], to capillary morphogenesis [Vickerman et al., 2008].

We first introduce the working principles of such devices and divide them according to some technical characteristics. In a second part, we highlight some results they made it possible to achieve. We will mainly focus on systems used to investigate stem cell patterning as they are the most relevant to this work.

In fact, Embryogenesis is known to be regulated by molecules, morphogens, released by certain type of cells and that diffuse in the surrounding media, with a well defined temporal pattern.

To mimic these processes, a number of systems have been already exploited and it is about those, we are mainly going to talk about at the end of this section.

4.1.1 How to generate a gradient

The whole family of Gradient generating devices can be divided into two sub-families: those devices that establish a gradient by diffusion [Saadi et al., 2007] and those that rely on flow-focusing [Li Jeon et al., 2002]. There are advantages and drawbacks in both, and the choice depends much on the characteristics of the system under investigation: in fact, systems that rely on flow-focusing have the great advantage of generating a gradient over a very short timescale, allowing for dynamical evolution of the stimulation, but expose the cells to shear stress, that can in some case damage cells. On the other hand, systems relying on diffusion do not present the shear stress issue, but establishing a gradient can take a long time, depending on the length scale over which the gradient is wanted, not allowing then a dynamical almost instantaneous control over it.

In Figure 4.2 and 4.3, we show an example of co-flowing-like and diffusion-like gradient generating device, respectively.
From here on, we are going to talk only about the diffusing-like ones, as the one we are proposing here falls in that family, but here [Kim et al., 2010] is a more exhaustive, even though a little out of date, review. It is interesting to notice, that these systems, like the one shown in Figure 4.3, that closely resembles the one we later introduce, have been mostly used to investigate co-cultures, vascularisation, and capillary morphogenesis [Saadi et al., 2007] [Kim et al., 2013] [Carrion et al., 2010], or in this other version, to stimulate cells with two different media [Zheng et al., 2019], rather than to expose cells to a gradient, as we will later do.

These devices, despite more or less important technical differences, share the same functioning principle. As said they rely on diffusion, which is the process by which a change of concentration of some particle along one direction leads to a flux of particles directed toward the less concentrated region, to equilibrate the concentration. Fick's first law translates this observation into maths, and gives, for isotropic diffusion:

$$\vec{J} = -D\nabla C \tag{1}$$

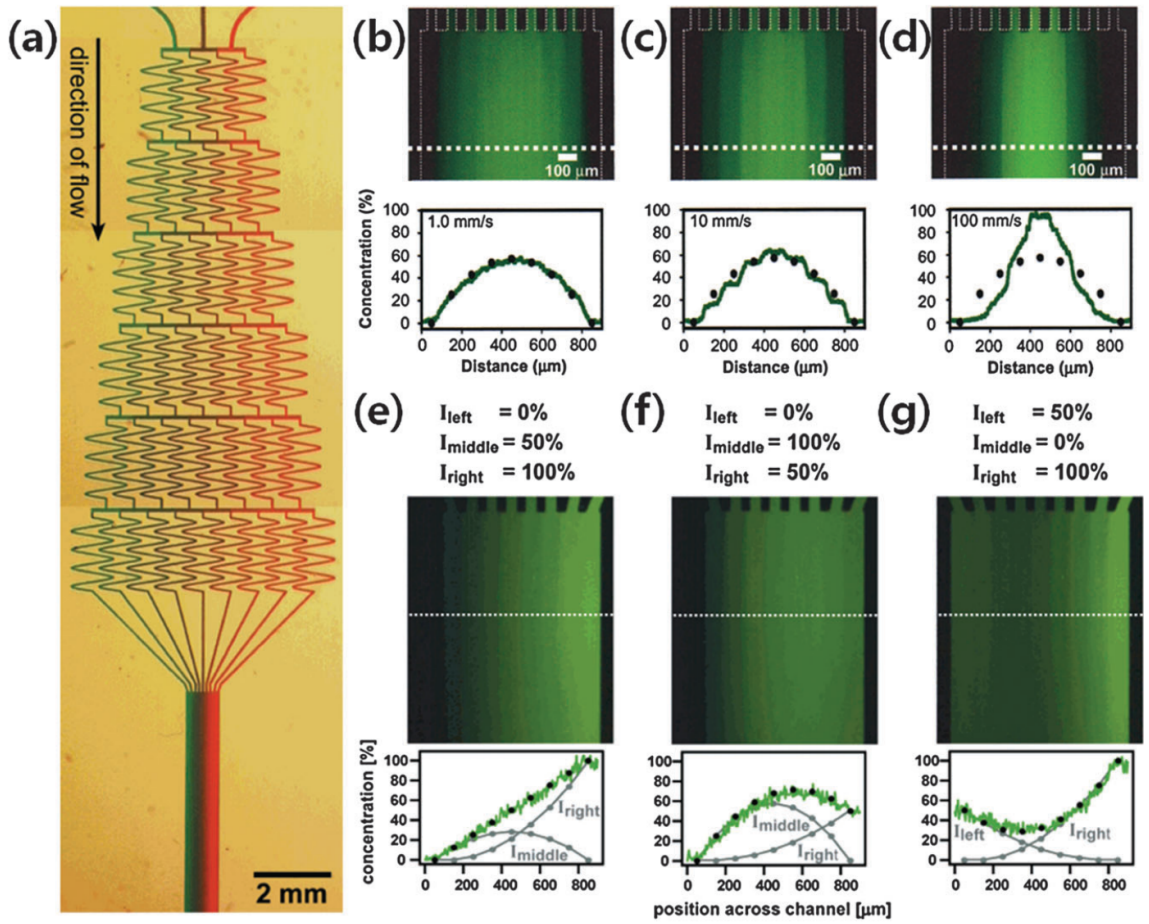

Figure 4.2: **Gradient device based on co-flowing of media with different chemical composition** Devices based on co-flowing different media, allow for almost instantaneous time control over the dynamics of the gradient. Moreover, by changing media composition at the different inlets, they allow different gradient profile, not only the linear profile allowed by diffusion-based devices. On the other hand, they expose cells to a shear stress, that can be damaging in certain conditions. Adapted from [Stephan K. W. Dertinger et al., 2001]

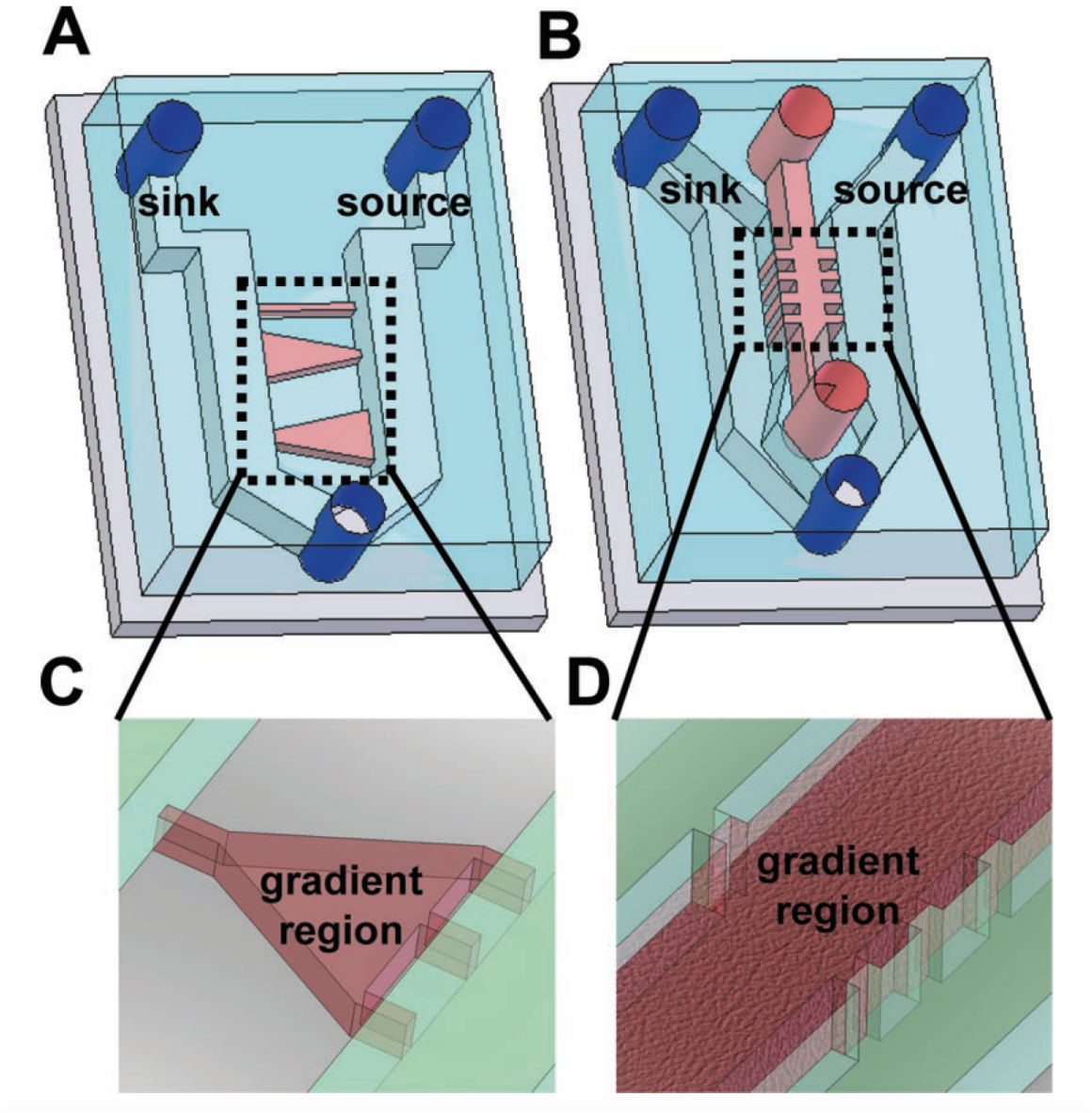

Figure 4.3: **Gradient device based on diffusion from a source toward a sink** Gradients devices based on diffusion rely on the difference of concentration of some chemicals between a source and a sink. Drawbacks are that diffusion being a slow process, it can take time to establish a linear gradient, depending on the length scale over which the gradient is needed. They do not allow then a fast dynamical control, plus the only profile possible to be obtained is the linear one. On the other hand they do not expose cells to any shear stress, permitting to meet more easily optimal cell culture conditions. Adapted from [Mosadegh et al., 2007]

where $\vec{J}$ is the flux of particles, C = C(x) is the concentration and D is the diffusivity (of diffusion coefficient), defined as the proportionality coefficient between the Flux and the Concentration gradient and that depends on the characteristics of the particles and the environment they are diffusing in. So these systems exploit Fick's law to establish a linear gradient of some chemicals. To do so, two elements are needed, a continuous source of molecules and a sink, separated by a distance along which these molecules diffuse. This distance is usually filled with some gel to allow diffusion, but prevent crossflow. Alternatively, a barrier filled in with some gel is interposed between the source/sink channels and the chamber allocated for cells. To have a continuous source and a perfect sink two main options are available: providing a continuous flow along two channels of two media with different chemical composition or featuring two reservoirs for the media whose volume is much bigger than the volume over which diffusion takes place.
Our system belongs to the first class, as we will see later in detail.

Now that we have summed up the basic features of the existing gradient devices, we can see some representative and most recent examples and discuss what results have been obtained with them.

4.1.2 Patterning Stem cells by exposing them to a gradient of morphogens

The first study we are introducing [Zheng et al., 2019] is the closest to the one we discuss in Section 4.2, and we already presented its results in Section 2.1, when describing how it helped increasing reproducibility and frequency of observation of the interesting polarised phenotype. Here, we focus more on the technical aspects, because the device we are introducing later closely resembles in working principles this one. As shown in Figure 4.4, they use this three-channels device to accurately position human Embryonic Stem cells in the space between pillars that separate the gel channel from the other two, and they use one of the two external media channel to stimulate the cysts on one side, resulting in very reproducible differentiation toward

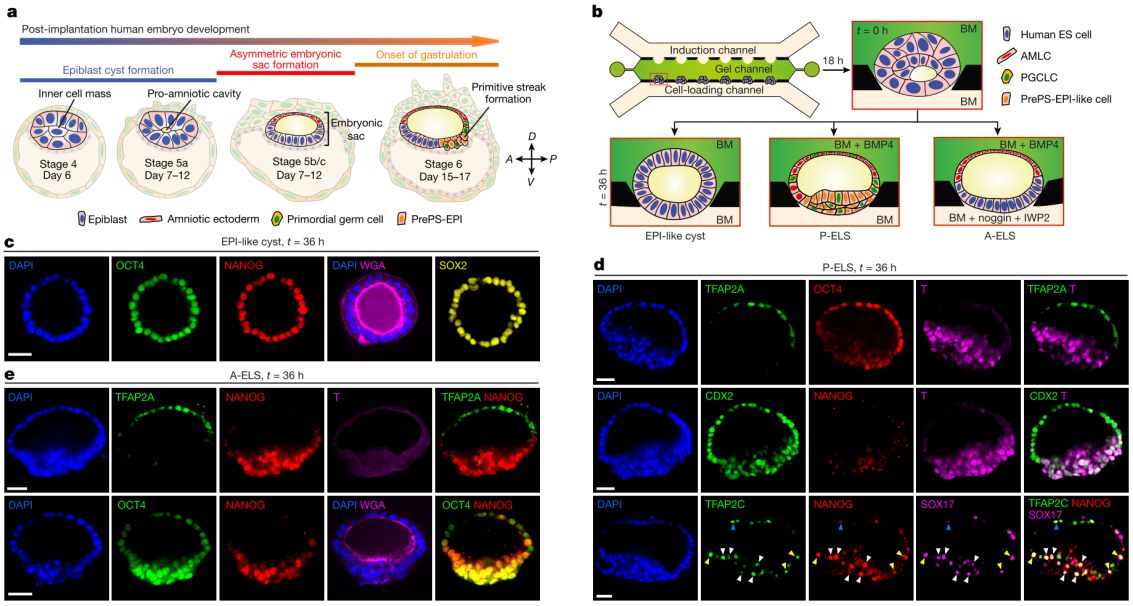

Figure 4.4: .**A microfluidic device for controlling the formation of asymmetric hES cysts recapitulating the amniotic sac formation** The device features three channels: in the inner one a gel is inserted, that cross-linking and shrinking will form some sort of wells between the pillars that separate the gel from the two media channels. Cells can then be deposited in this wells and fed by the external channel with media with different composition. Adapted from [Zheng et al., 2019]

asymmetric cysts, that recapitulate amnion formation, presenting both embryonic and extra-embryonic tissues.

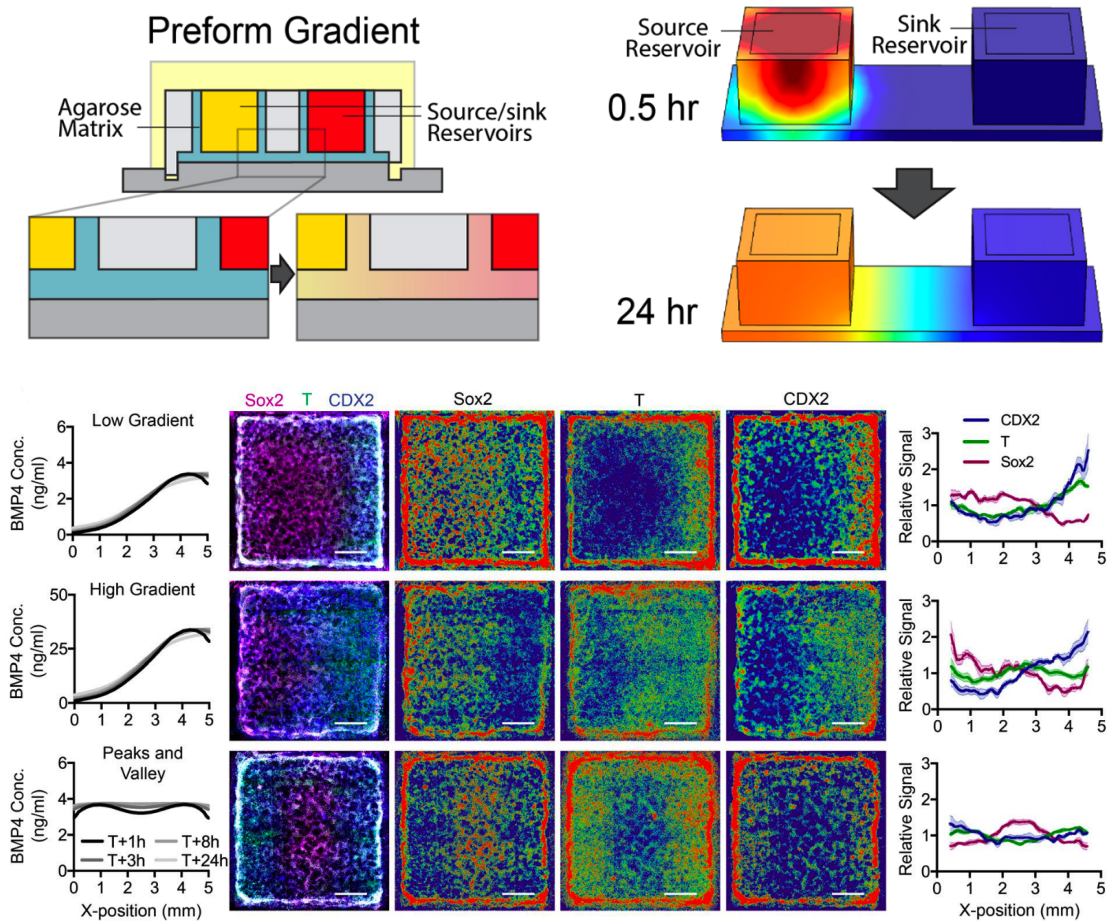

Figure 4.5: **Diffusion based device for patterning of human Embryonic Stem Cells** This device based on diffusion from a source toward a sink allows for patterning hES in response to BMP. Different profile translate to different patterning, presenting from time to time the appearance of different markers knowing to be induced by BMP, like Cdx2 (Extra-embryonic Mesoderm) or Brachyury (Embryonic Mesoderm) which interestingly appear in a concentration dependent fashion. Adapted from [Regier et al., 2019]

Another example [Regier et al., 2019], illustrated in Figure 4.5, shows the patterning of human Pluripotent Stem Cells (hPSCs) when stimulated with a gradient of BMP. They observed the emergence of the mesoderm/Primitive Streak marker Brachyury, as well as the extra-embryonic mesoderm one Cdx2, in a concentration-profile dependent way.

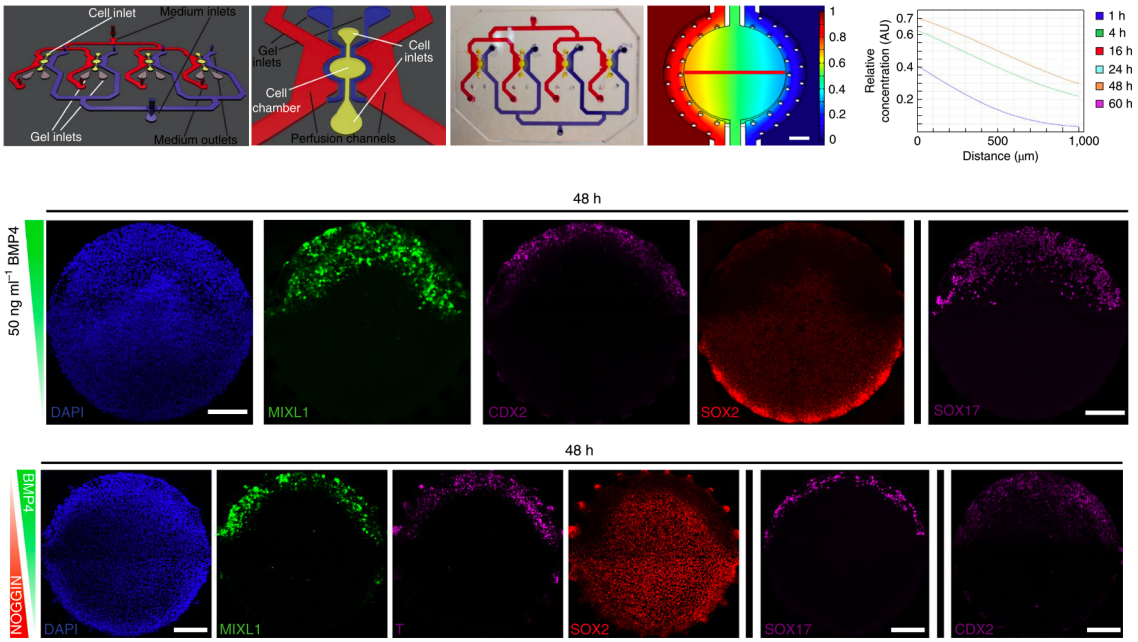

Figure 4.6: **Microfluidic device for exposing human Pluripotent Stem Cells micropatterned colonies to a gradient of BMP4** This device allows for a gradient stimulation with BMP, that can be coupled to an opposite gradient of BMP inhibitor Noggin. This way it is possible to obtain patterning of the micropatterned colonies in a way that is not only BMP concentration dependent, but also cell density dependent. Adapted from [Manfrin et al., 2019]

Last, we present [Manfrin et al., 2019], where they stimulate human Pluripotent Stem Cells with a gradient of BMP4, or a double opposite gradient of BMP4 and its inhibitor Noggin, and show, as reported in figure 4.6, and obtain a concentration dependent, cell density dependent, emergence of different differentiation markers. The gradient in this case is applied apically, and due to positioning of BMP receptors on the baso-lateral side, cells seem to respond to the distance from the edge more than to the gradient itself.
Taken all together, these results show two important aspects: cells can sense different concentration of morphogens, and differentiate accordingly, and, as is shown in the first example [Zheng et al., 2019], a localised source can be determinant to faithfully reproduce symmetry breaking in 3D *in vitro* models of human embryo.
In what follows we will try to test these ideas on our 3D model of the mouse Epiblast.

4.2 First step: setting up the gradient device

We designed a microfluidic device (see Appendix C) that allows us to grow Embryonic Stem cells organoids in a chemically controlled environment. The idea was to be able to provide morphogens, such as BMP, to induce cell differentiation, in a locally controlled manner, instead of providing them uniformly together with culture media. Particularly, we wanted to provide morphogens locally and have them free to diffuse to establish a linear gradient, as is hypothesised to occur in the mouse embryo around E4.5 where BMP, that is provided from the Extra-embryonic Ectoderm, sustain the expression of Nodal and Wnt in the Epiblast and induce the formation of the Primitive Streak and of the Extra-embryonic Mesoderm [Arnold and Robertson, 2009]. The requirements to be fulfilled then are:

- to have a device where cells can be grown for two days in order to form cysts that will be later stimulated
- to be able to stimulate them with a gradient of morphogens
- to be able to obtain a gradient over a timescale of minutes and a length scale

of the order of magnitude of the size of a cyst, i.e. D $\approx$ 100μm , and be able to have it stable over the timescale of days

The final design we ended up with, which is an adaptation from [Saadi et al., 2007] and [Zheng et al., 2019], is the one you can find in Figure 4.1 and is made of three elements:

- a central channel that is filled in with a suspension of cells and Geltrex
- some hexagonal pillars that hold the gel in place and avoid it to spill on the external channels
- two external channel where two media, with different chemical composition, are provided, that share the same outlet to balance the pressure in the two channels and prevent backflow (see Appendix C)

The device has two inlets for the two different media, and one outlet. It is important to avoid the formation of bubbles that can modify the gradient, and, in the worst case, damage the gel. In order to do so, we pressurised the outlet with a pressure between 30-80mbar.
The single outlet is important to avoid pressure imbalance on the two sides of the gel, that, being very soft (Matrigel is about 400Pa), could be easily broken by a pressure gradient, that would lead to the establishment of a crossflow that would make the gradient unpredictable and the experiment to be discarded.

All diffusion-driven gradient devices described in our overview share with the one we propose here the same underlying functional mechanism. A central channel is filled in with a gel. Some pillars prevent the gel from spilling out into the two flow channels. Providing two media with two different concentrations of some morphogens or chemical in general, a gradient of such a chemical will be established over some time across the gel. All these device respond then to the first two requirements we have stated at the beginning of this paragraph. What pushed us toward designing our own device was the third requirement. In fact, all these devices present a central chamber

that has a width of the order of magnitude of few millimetres. Diffusion being a slow process, it means that to establish a stable gradient over such a distance, few hours would be needed.
Moreover, the typical size of our synthetic Epiblast ($\approx 50 - 100\mu m$) is two orders of magnitude smaller that the size of these channels, whereas we aim to obtain a gradient over a length scale that compares to the size of our system.

To overcome these problems, we designed a device where the central chamber is 200μm wide so that the size of our cysts could be comparable to this distance, still allowing us to have cysts in different configuration in the same experiment. Reducing the size, reduced dramatically also the time needed to establishing the gradient bringing it from few hours to few minutes.
The timescale for establishing the gradient will be discussed thoroughly in Section 4.3, but for now we can just convince ourselves that it is important to reduce the cross section length of the middle channel, by considering that diffusion processes rely on random walk. Random walk equation for the one dimensional case we are considering gives us the following relationship between time and distance

$$< r^2 >= 2Dt$$

where $< r^2 >$ is the mean square distance, D is the diffusion coefficient and t is the time.
As we can see, time varies with the distance squared, so increasing the distance (which in our case is the width of the cell channel of our device) by one order of magnitude results in increasing the time needed to establish the gradient by two orders of magnitude. We show in the Section dedicated to the characterisation of the device an estimation for the time needed to reach a stable gradient.

4.2.1 Protocol: filling the gradient device

To start an experiment, the culture media have to be prepared first. Possibly they need to equilibrate their pH in the incubator at 37°C and 5%CO_2. In the meantime,

the syringes and the tubing need to be cleaned, by flushing through them Ethanol 70%, and then rinsed with PBS, to ensure that no Ethanol is left over. Then the syringes need to be filled in, and the air to be removed. Then the tubing can be connected to the syringes. It is important to use glass syringes (here, Hamilton® syringe, 1000 series GASTIGHT®, PTFE luer lock 1ml) and PTFE tubing to reduce to the minimum the elasticity of the system, in order to avoid any capacitance that would translate to possibly backflow and disrupting the correct functioning of the device. At this point, it is critical to avoid any bubbles presence in the system syringes plus tubing. There might be some bubbles arising in the tubing, though. In this case flick the tubing gently handling the tip upward and let them rise until the tip. Let the tubing rest in this position fro 10 minutes to half an hour to ensure that all the bubbles reached the tip and the remove them, by giving a pulse to the syringe piston. When it is ensured that there are no bubbles in the tubing, syringes have to be mounted on the syringe pump (here, PhD ULTRA Harvard Apparatus, where we custom made a holder to host up to six syringes at a time, so to push the two syringes at the same speed to avoid pressure imbalance).

The setup being ready, it is possible to prepare the cells and insert them in the central channel of the microfluidic chip. To do so, cells are trypsinised for 5 minutes and resuspended as single cells at a density of 1million/ml. At this point cells need to be added to the Geltrex. Since Geltrex would gelify at room temperature, it is necessary to work on ice, so cool down the cells before adding them to the matrix by letting them staying in ice for 5 minutes. Then, add 20-25µl of cells resuspended in N2B27 (it is needed at least 80k cells) to 100µl Geltrex and mix thoroughly. This step is delicate as you risk to gelify the gel that would then be of no use for the experiment, so it is recommended to use pipettes and cones that are stored at -20°C and to keep working on ice through all the process. To carefully mix the gel and the cells aspire 50-60µl of the mix from the bottom and release it on the top, taking care of not introducing bubbles (to be sure, do not pipette the mixture out until the end, or alternatively reverse pipette the first time you upload the pipette). Mix the gel until the colour is uniform. At this point, upload a P10 with 3µl of gel and place the

tip inside one of the inlets of the gel chamber of the chip and fill it. The volume of this chamber is less than 0.5µl so it is not necessary to push the plunger until the end. To fill in the chamber, push the pipette extremely gently, and stop increasing the pressure applied when you see the gel starting filling the chamber (but do not release the pressure , otherwise you will aspire back the gel). The filling will keep on going by wetting and capillarity and the pillars will provide a barrier for the gel to stay in place and not to spill out in the flow channels. If the filling stops around half of the channel, remove the pipette from the inlet, while not releasing the plunger, and fill the other half of the channel in the same way from the other inlet. When the cells are in place, check under the microscope that the gel did not spill out and that there is a good density (an example is later shown in Figure 4.12) of cells with a uniform distribution. Due to small volume, and to the difficulty of mixing uniformly cells and Geltrex, density could sensibly varying from chip to chip. Then place the chip on a Petri dish with a PBS reservoir so that the gel stay hydrated and do not dry and place it in the incubator for 6 minutes to let the gel solidify.

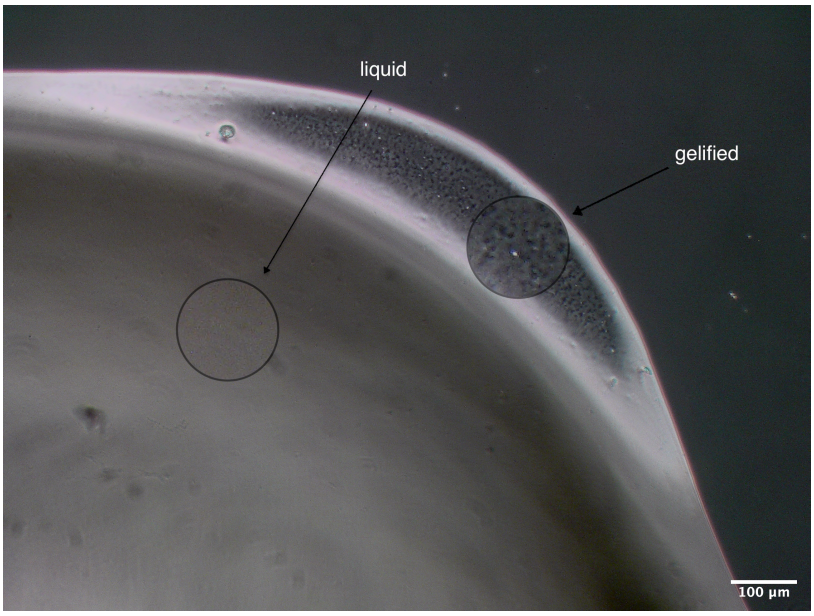

Figure 4.7: **Geltrex appears transparent when liquid, but structures are visible when solidified** This picture shows a drop of Geltrex on a glass slide and how the gel appears after solidification. When loading the device, a 5-10 minutes time in the incubator at 37°C is needed for the gel to solidify and avoid crossflow, when plugging in to the syringes and starting the flow.

To assess if the gel is solidified, it is possible to establish that by looking at it on the microscope with a 10x (cf. Figure 4.7): when the gel is first uploaded it is transparent and only the interface between gel and air is visible. When the gel is correctly solidified, structures arise, that are visible at the 10x magnification. If these structures are homogeneous, it will mean that the gel nicely filled in the channel. Then two full pins have to be placed at the inlets of the gel chamber to close them and avoid later the media flowing through the gel. To place them, insert them very gently otherwise you will push the gel into the flow channels. There is no need to push the pins through the inlets completely as having them right on top will prevent any crossflow already. At this point, the two tubes connecting the syringes can be plugged in the two inlets, provided that they are dripping and media are flowing through them. The final flow rate we run the experiment with is 10µl/h, but it is better to start with a higher flow rate (before plugging the tubes to the chip!) and let the fluid drip from the tip, and only when media are flowing to plug them to the chip. Again, this is to ensure that we are not inserting bubbles in the device. Inlet tubings have to be plugged in first, then the outlet will be pressurised only when the media filled in the two channels. If the experiment is not run directly under the microscope, the outlet has to be pressurised as soon as it is possible to observe some media going out at the outlet. Pressurising the outlet is important for two reasons: it will avoid bubbles being nucleated and if bubbles are present it will help getting rid of them through the PDMS that is porous to gasses. To pressurise the outlet there are two options: to carefully control the pressure at the outlet it is possible to use a pressure controller such as Fluigent MFCS-EZ. But here, such a precise controlling is not necessary, so we connect the outlet to a vial filled in with PBS with a hole and top of it, that is then placed at a height of 30-40cm with respect to the device, thus applying a pressure of 30-40mbar. When plugging in the outlet, it is important to check that the inlet pin is dripping, but having the vial at roughly the same height as the chip, in order not to apply the pressure abruptly. Then the vial can be gently raised up and placed to its final position. The final flow rate of 10µl/h ensures that the medium is changed 20 times every hour given that the volume of the flow channels

in contact with the cells channel is approximately 0.5μl. This configuration ensures that we are in the condition of having a perfect source and sink.

4.3 Characterisation of the device

By means of this device, a scheme of which is represented in Figure 4.1, a gradient is established by diffusion through the gel in the middle channel, as two media with different chemical composition flow in the external channels.
The single outlet was preferred to a 2-outlets options to balance the pressure in the two flow channels and avoid backflow issues, that would compromise the stability of the gradient.

As the two flow channels can be considered a perfect source and a perfect sink, after a certain amount of time a linear gradient is established between them. This linear function represents the stationary solution of the equation of diffusion in one dimension :

$$\frac{\partial \mathrm{C}}{\partial \mathrm{t}} = \mathrm{D}\frac{\partial^2 \mathrm{C}}{\partial \mathrm{x}^2} \tag{2}$$

After a certain time t^*, the solution of 2 across the channel is of the type:

$$\mathrm{C(x)} = \frac{\mathrm{C_0}}{\mathrm{L}}\mathrm{x} \tag{3}$$

where C_0 is the concentration at the source and L is the length of the channel.

We were then interested in an estimate of t^*, to understand the order of magnitude of the time needed to establish a stable gradient across our device, and to be able to compare it to the relevant time scale along which the expression dynamics unfolds, as observed in our previous bulk experiments.
To get it, we face two possibilities: the theoretical approach would lead us to solve (2) and get the characteristic time of the system, while the experimental approach would take us to measure the time needed for the system to stabilise.
We start analysing what we can estimate as a theoretical characteristic time, and then we compare it with what we could observe in our experimental setup.

An analytical solution for the equation (2 for diffusion between a source at a certain concentration C_0 and a sink can be found [Crank, 1975] by separation of variables and gives an infinite convergent series of the form:

$$C(x,t) = C_0 \left(1 - \frac{x}{L} - \frac{2}{\pi} \sum_{n=1}^{\infty} \frac{\sin(\frac{n\pi x}{L})}{n} \exp - \frac{Dn^2\pi^2}{L^2} t \right) \tag{4}$$

By means of this equation, some estimations can be done. For us, the interest is in extrapolate from it the characteristic time t^* of the system:

$$t^* = \frac{L^2}{\pi^2 D} \tag{5}$$

For our system, considering $L = 200\mu m$ and $D \approx 80\mu m^2/s$ we obtain a characteristic time $t^* = 50s$. We got the value for D from [Kihara et al., 2013], where they study the diffusion coefficient for molecules with different molecular weight through collagen. The value reported here corresponds to Alexa488 Dextran [10kDa], while the value measure for FICT dextran [40kD] is $D \approx 45\mu m^2/s$. In what follows we use dextran 20kDa and 40kDa.

By using this estimated value for diffusion through Geltrex, we can anticipate then, that the time needed to establish a stable gradient across our device is two orders of magnitude smaller that the relevant time needed to observe the consequences of the stimulation, which is between 24h and 48h.

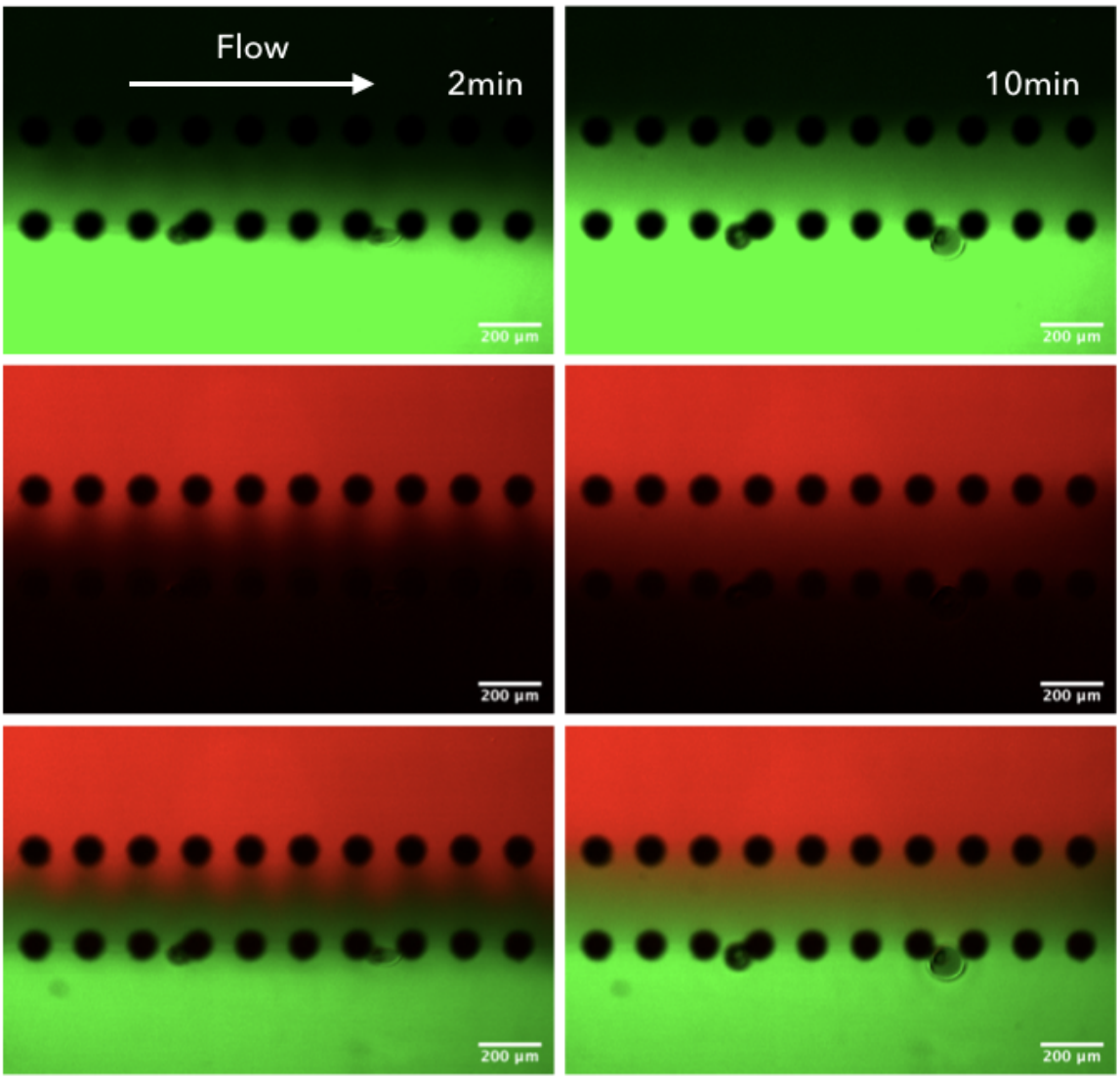

Figure 4.8: **Gradient device characterisation**. The time needed to establish the gradient has been analysed by means of two different fluorophores diluted in the two flow channels. Here the picture show 3 steps in establishing a gradient along 8minutes

We proceeded then to estimate the time needed experimentally. To do so we loaded the chip's inner channel of with Geltrex, as we would do in our cells experiments. To visualise the gradient forming, we loaded the two flow channels with media in which we would have dissolved some dextran, labelled with some fluorescent molecules. To ensure that what we would measure was reasonably close to what we would obtain when providing a gradient of morphogens, we choose dextran whose molecular weight was around 10-40kDa. Particularly in what follows, the molecular weight of the

dextran labelled with Rhodamine is 20kDa, while that of the one labelled with FITC is 40kDa. This difference explains for the shift in timescale observed between the two.

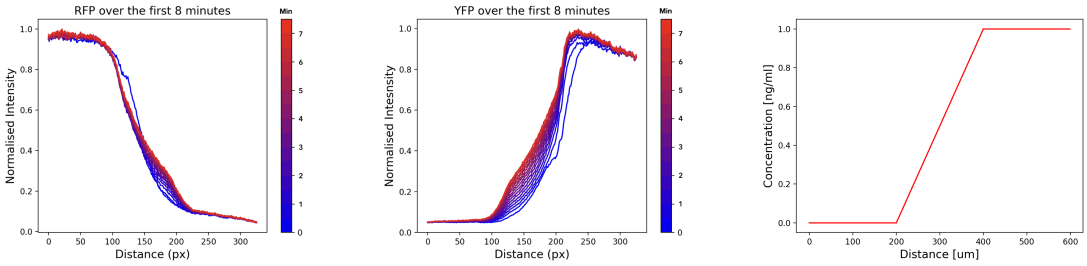

Figure 4.9: **Gradient device: quantification of the characteristic time of the system**. The plot shows the intensity of the two fluorophores across the device for a total time of 8 minutes. A picture is being acquires every 30 seconds. On the right the theoretical stationary solution of the 1D equation for diffusion is represented

Figure 4.8 shows the gradient establishing over 8 minutes. Analysing these data, Figure 4.9, we can conclude that 8 minutes are already sufficient to observe a linear gradient between the source and the sink. We have to consider though that two this time, another 2 minutes need to be added, as the acquisition starts once everything (tubing, syringes) is already connected and a flow is established correctly.
Another check of the timescale needed to observe a linear gradient, is to plot the value of a single pixel at a fixed distance over time. Here, we considered the value of a pixel situated at x $\approx$ 0.75L, and we follow the pixel dynamics over t $\approx$ 30mins. This is meant to establish the time needed for the gradient device to establish a stable value at a given point. The results of this experiment can be visualised in Figure 4.10.
An important remark to be made here is that are image acquisition always starts 1-2minutes after the flow has been established, because the start of the fluid flowing is a critical point that needs checking that the gel does not break following a pressure imbalance or adjusting the flow rate to get rid of a bubble. This is to explain the high fluorescence value for t = 0 in the charts in Figure 4.10.

Nonetheless, two main aspects can be appreciated from these graphs. First, when acquisition starts, the initial values is already $\approx$ 90% of the final value, meaning that

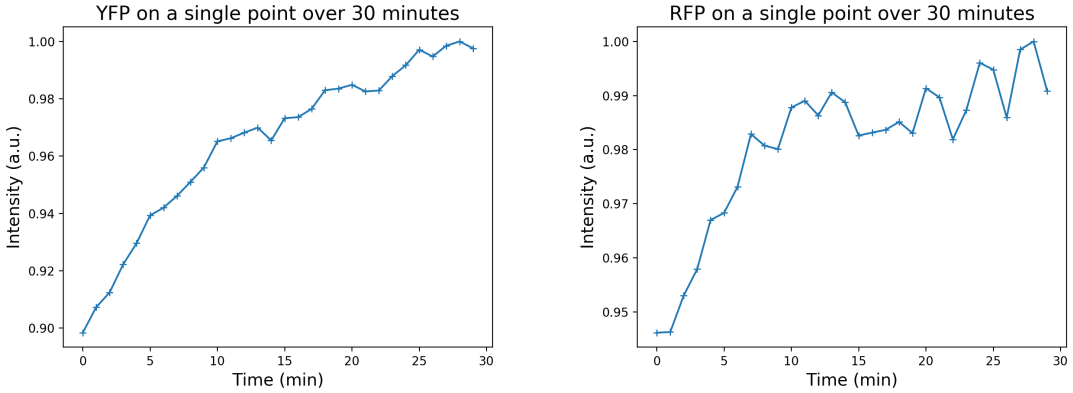

(a) (b)

Figure 4.10: **Evaluation of the characteristic time of the gradient device**. Checking the intensity value of a single point, situated at x ≈ 0.75L from the respective source, over a time t = 30mins reveals that 2 minutes after the acquisition, the intensity value is already ≈ 90% of the final intensity value

few minutes are already enough to reach a decent linear gradient. Then, the stable final value is reached between 10-25 minutes depending on the molecular weight of the chemical under consideration.

To conclude, we finally checked the stability of the gradient after 20h, following the dynamics of the dynamics of the intensity across the whole device, and at a single point located at x ≈ 75%L for a total of 3h long experiment. As shown in Figure 4.11, the gradient, once established can stay stable over a long time, upon providing a continuous and stable flow of chemicals. As a last comment, the timescale observed for establishing a gradient ensures that even in the event of a bubble blocking the device, a gradient can be re-established in a reasonable amount of time, that is still an order of magnitude smaller than the timescale of the whole experiment.

4.4 Cells seeding in the gradient device

As in our bulk experiments, the experiment protocol runs over 4 days. During the first two days, cells are kept in N2B27 supplied with FgF and KSR. The first thing to check was then that they could grow, divide and develop into cysts, in the same

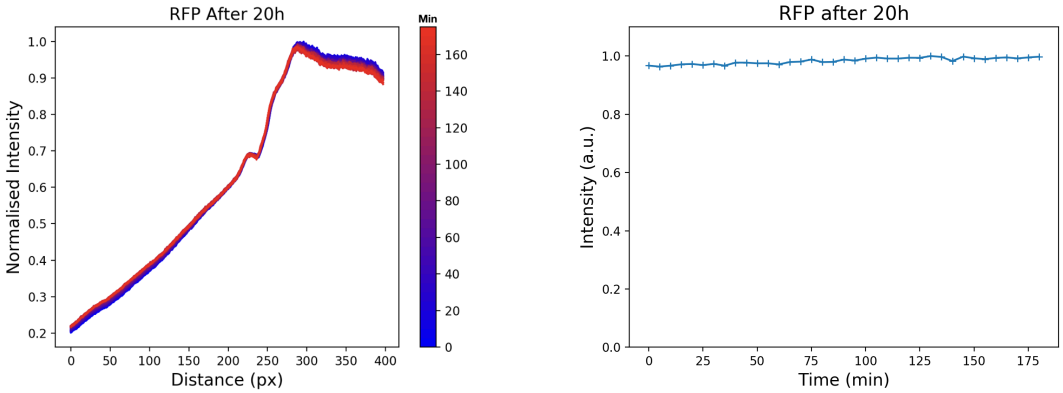

(a) (b)

Figure 4.11: **gradient stability after 20h**. Repeating the measure after 20h, and along 3 hours, every 5 minutes shows that is possible to keep the gradient stable across the timescale of our whole experiment. As in the previous analysis, the graph refers to the intensity value of a single point, situated at x $\approx$ 0.75L from the source.

way that was observed in bulk. Indeed no significant difference could be noticed in morphology, even though we will need in the future some further experiments to assess precisely that the growth rate is the same as when plated on big surfaces. The growth along the first two days inside the microfluidic chip is shown by the three pictures shown in Figure 4.12.

After the first two days, we proceed stimulating the cysts with BMP. This was done by loading the medium in one of the two flow channels with BMP4 at the concentration of 1ng/ml, which is the minimal concentration we found reliably sustaining Nodal and inducing Brachyury in the bulk counterpart of this experiment (cf. Figures 3.6, 3.7, 3.10).

Again, we were able to appreciate a degree of communication between cysts, that we have not investigated any further yet, as also in this configuration cyst might attract each other and fuse together. An interesting example of this phenomenon is shown in Figure 4.13, where 3 cysts, initially separated by a distance of several typical cyst diameter, fuse together over 48h. What is interesting to notice in the pictures that the cysts fusing together are not necessarily the closest neighbours, proving that their interaction is not motivated only by proximity nor lack of space, but relies on

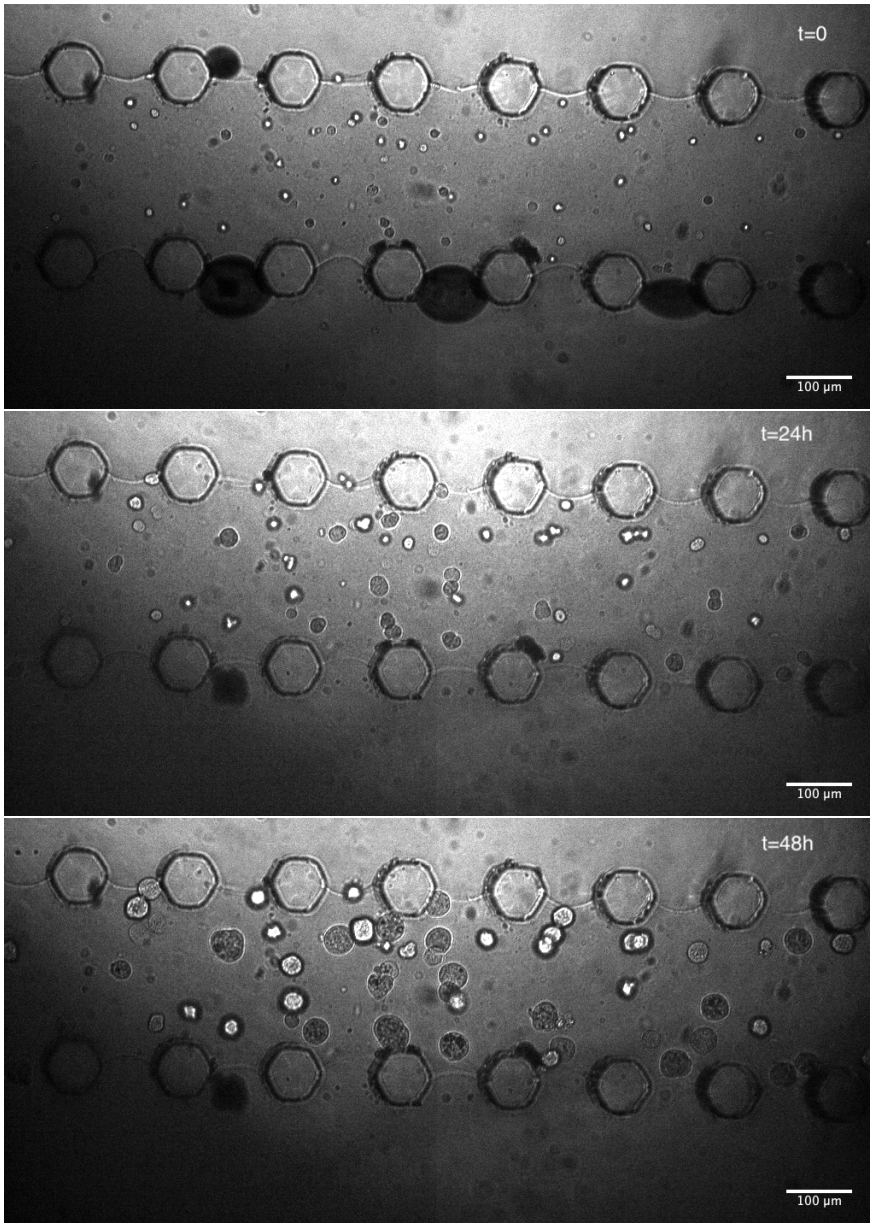

Figure 4.12: **Cells growing for the first 2 days in the gradient**. The pictures show the cells, during the first two days protocol, behaving in the microfluidic chip as they would when plated onto Petri dishes, growing and developing into compacted cysts. During the first 2 days no gradient is applied, and both channel are filled with N2B27.

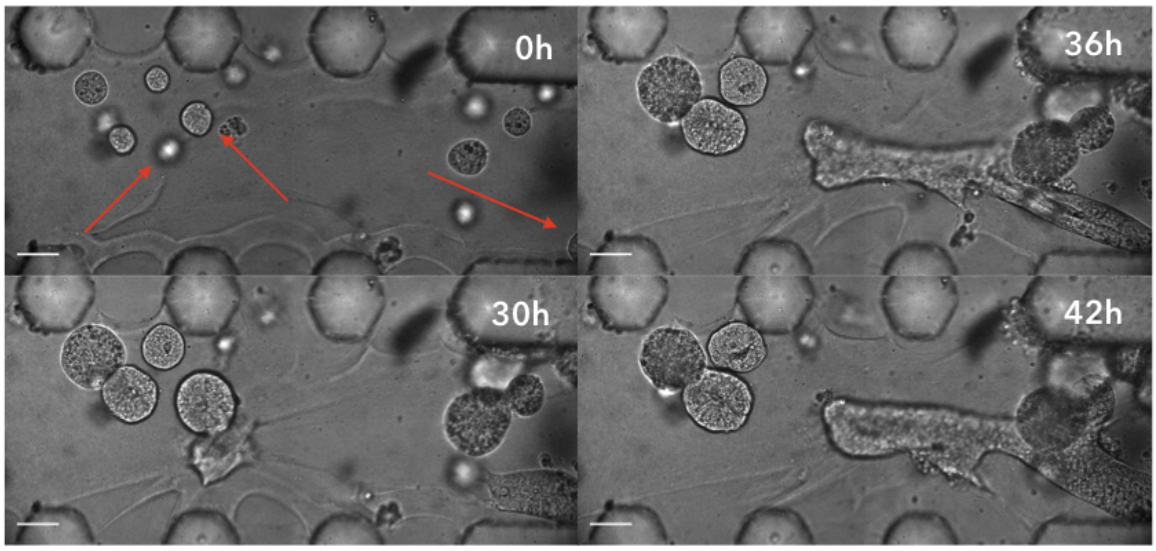

Figure 4.13: **Cysts attracting each other and finally fusing**. The pictures highlight the presence of a crosstalk between different organoids, as, over two days, they are able to attract each other and fuse together. The fact that this happens even when the distance separating them is of the order of magnitude of several cyst diameter proves that is not only a closest neighbour effect, nor it derives purely from some lack of space or over-density issue.

some other communication mechanism that might be connected to some signalling released by the cells themselves.

4.4.1 Validating the gradient device with Hoechst and Smad2 staining

In order to visualise the gradient and to prove that cells were getting an asymmetric stimulation, we ran some preliminary experiments. First, we used Hoechst stain, a blue fluorescent dye that binds to DNA, to visualise the cysts being stained accordingly to the gradient. In Figure 4.14, we can see different cysts getting stained over few minutes and particularly we can appreciate a cyst being asymmetrically stained. Hoechst though accumulates in the cells, so soon enough every cyst in the device was fully stained and signal saturated. Nonetheless this was important to visualise the gradient (as we did with the Rhodamine and FITC dextran) arising, and being able to observe live its effect on the cells.

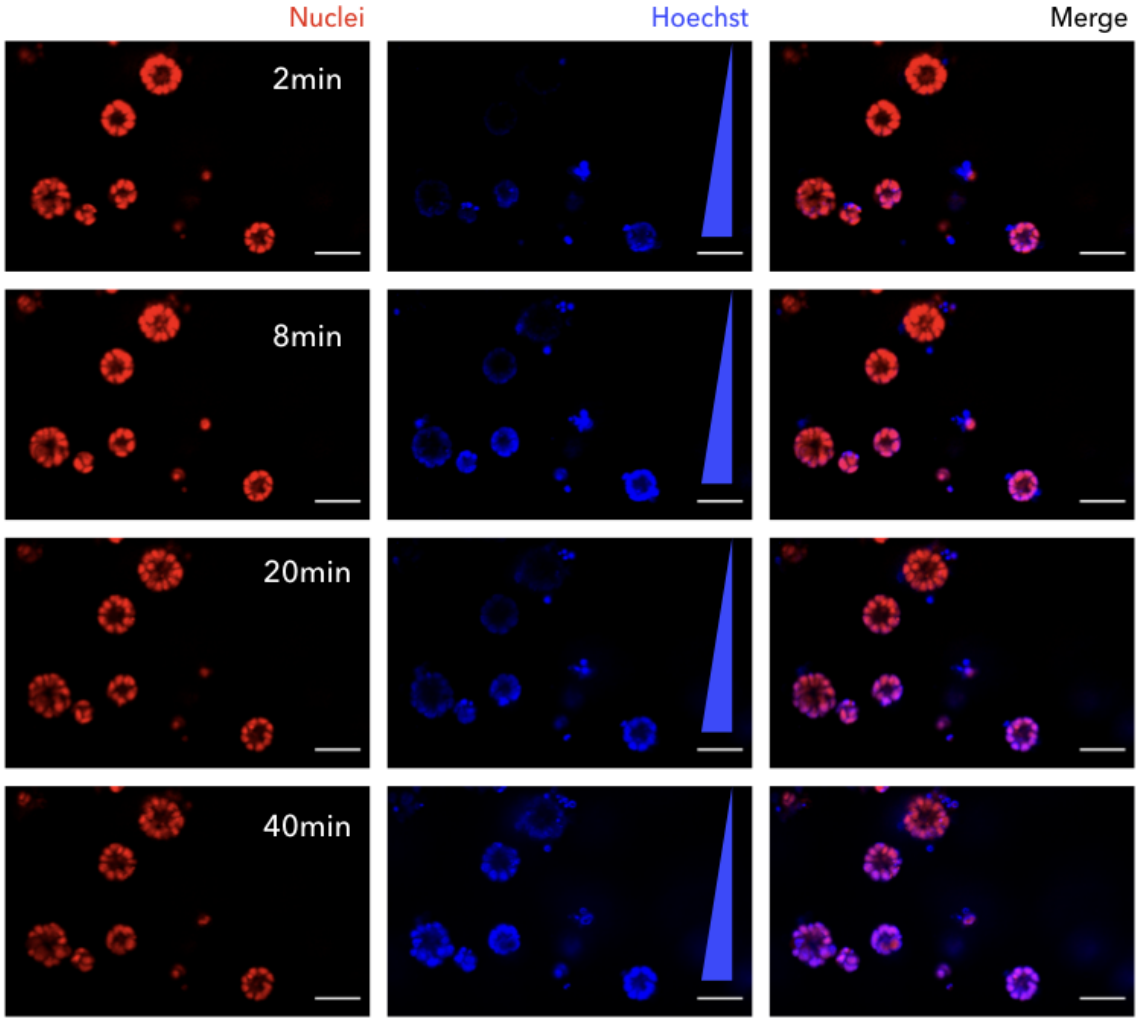

Figure 4.14: **Hoechst staining in the gradient device** The gradient is visualised by means of Hoechst staining. The cysts are asymmetrically stained over 40 minutes. Finally, Hoechst accumulates and every cyst is stained. Scale bar is 50μm

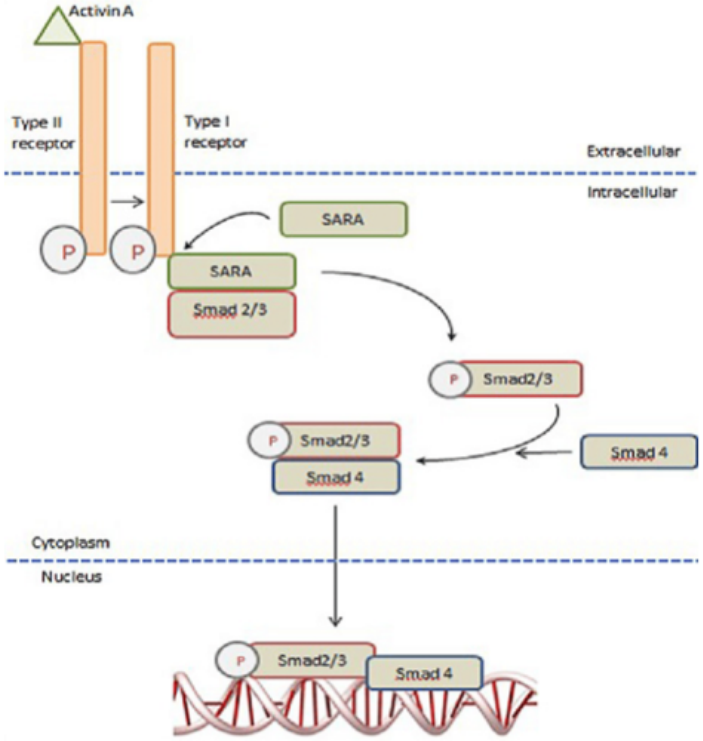

Figure 4.15: **Activin/Smad2 signalling pathway** When a Activin molecule binds to a membrane receptor, the transcription factor Smad2 is phosphorilated and can enter the nucleus

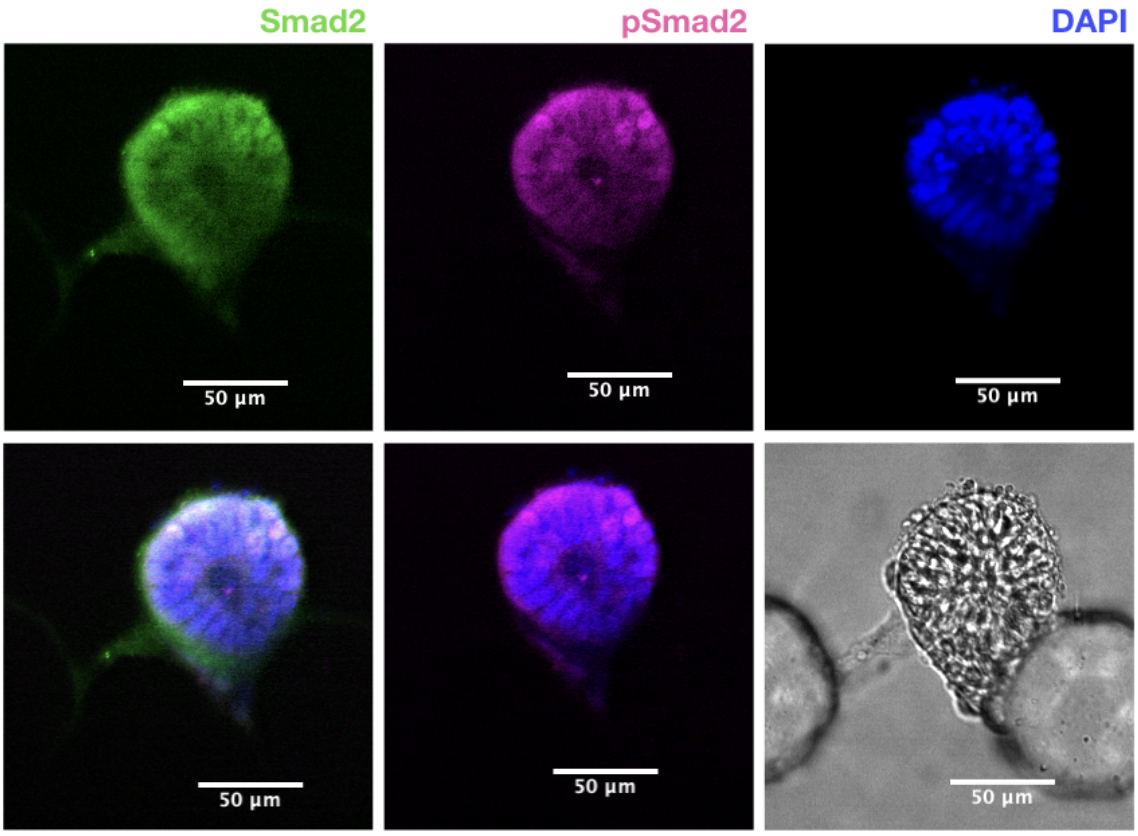

Figure 4.16: **Smad2 staining in the gradient device** The staining shows the asymmetric stimulation of a cyst with Activin. Activin has being provided from the top. Nuclear Smad2 is only found on top external cells. Scale bar is 50µm

After having validated the device with the Hoechst staining, we proceeded with stimulating the cells inside the device. To be able to visualise a direct readout for the stimulation, we stimulated the cysts with Activin (20ng/ml) for 24h and then stained for Smad2 a transcription factor that gets phosphorilated when Activin binds to the membrane receptors (see Figure 4.15). We stained for Smad2 and phosphoSmad2, to be able to tell in what condition Smad2 is also nuclear, and when it is only cytoplasmic. In Figure 4.16, a cyst is shown that presents asymmetric nuclear Smad2, correspondent to the direction of the Activin gradient (Activin being provided from top in picture).

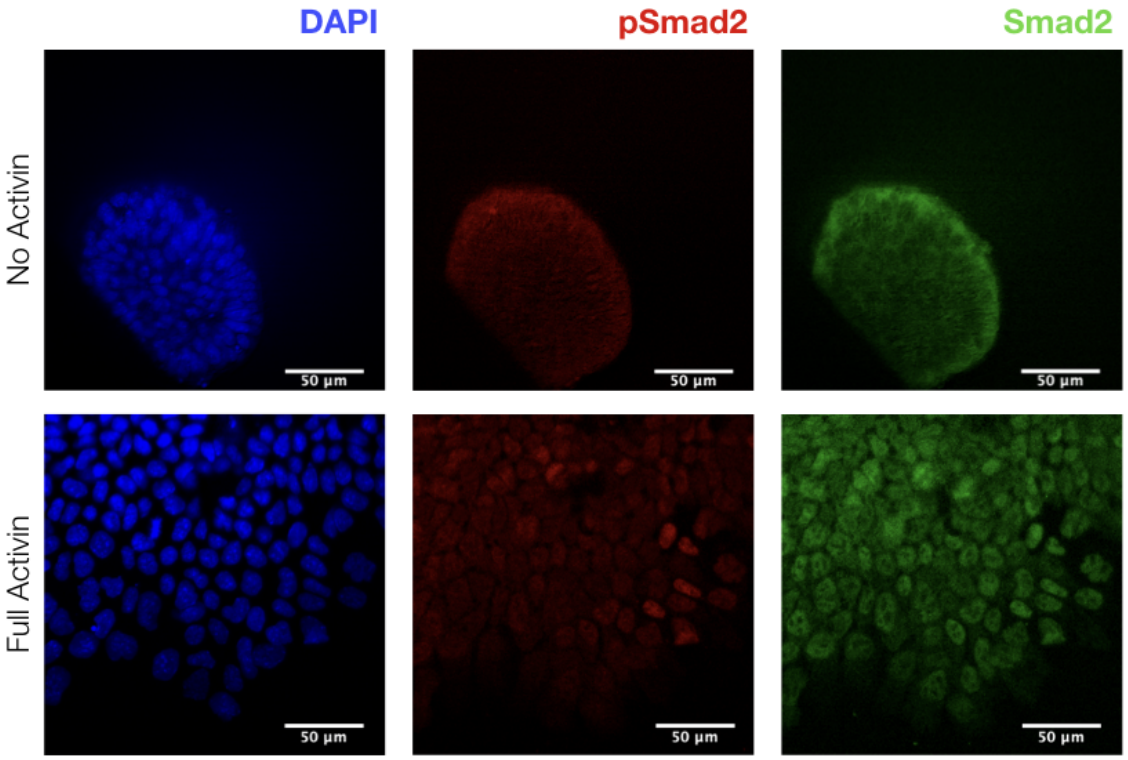

Figure 4.17: **Control for the Smad2 staining** The staining shows that when Activin is provided uniformly, all cells show nuclear Smad2, while when in no Activin condition, Smad2 is fully cytoplasmic. Scale bar is 50µm

As a control, we observed cysts that were growing outside the central channel of the microfluidic chip, in condition of no Activin and uniform Activin. As shown in Figure 4.17, when no Activin is provided Smad2 is found to be only cytoplasmic. On the other hand, when grown in full Activin, cysts are more likely to undergo EMT and spread on the substrate and Smad2 is found to be clearly nuclear.
From these preliminary experiments, we concluded that our device was able to asymmetrically stimulate the cells, so we moved on to observe the patterning of Nodal and Brachyury upon 48h stimulation with BMP, or Wnt.

4.5 Differentiating mES cysts in a gradient

After, having established that cysts could grow in our device as they were growing and organising when plated on Petri dishes, we moved on to stimulate them.

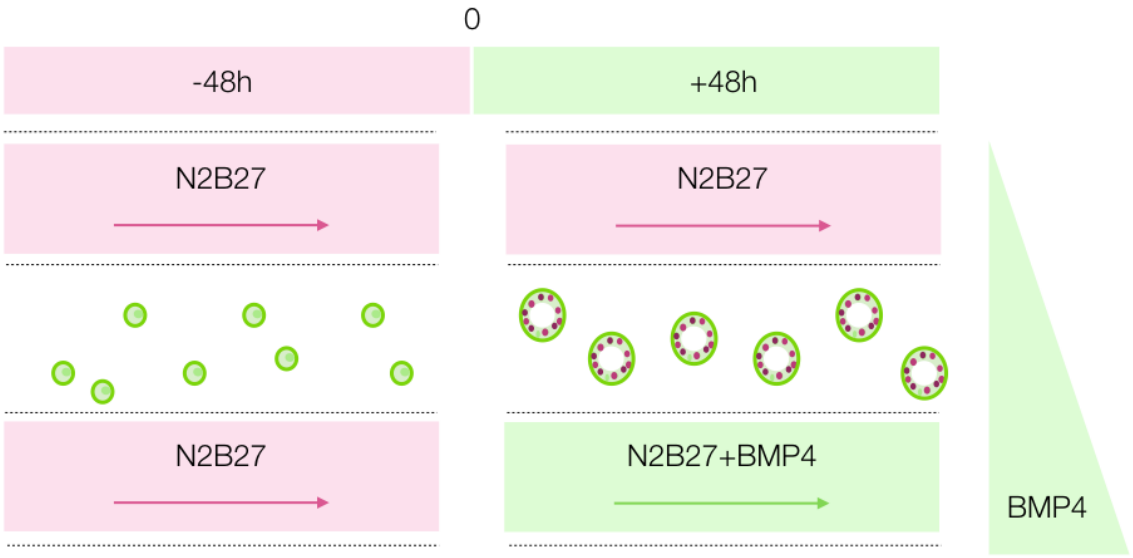

Figure 4.18: **Differentiation protocol in the gradient device** mESCs are grown on chip for 48h in N2B27, during which they proliferate, and form the cysts. Then they are stimulated on one side with BMP4 for other 48h

We recall in Figure 4.18 the differentiation protocol: we grow the cells for 2 days in N2B27, they proliferate, polarise and undergo luminogenesis. Then BMP4 is added to one flow channel of the microfluidic device.

We mainly stimulated the cysts with BMP 1ng/ml, provided that we proved from our experiments done in bulk, that it was inducing a reproducible expression dynamics for Nodal and Brachyury. We ran though also collateral experiments with Wnt or Chir, which is a Wnt agonist, proved Wnt role in patterning the posterior side of the embryo as discussed in Section 2.1.

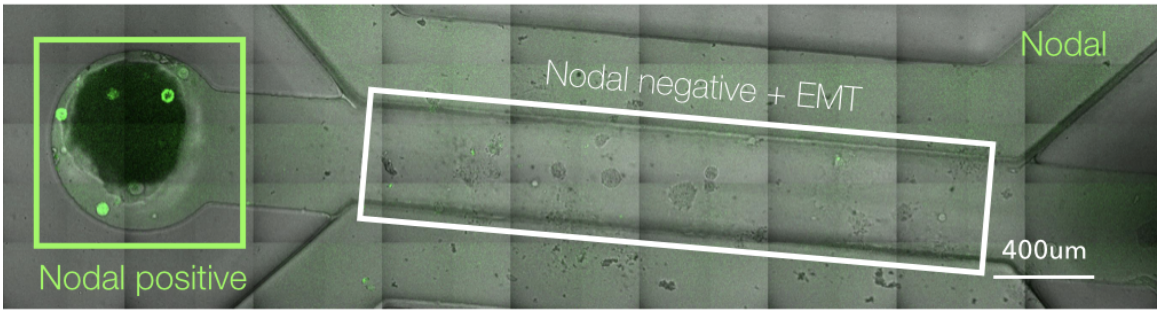

Figure 4.19: **Different behaviours in different parts of the device**. The picture show that, upon 48h stimulation with Wnt, only cysts located far from the flowing channels are expressing Nodal, while those located in the middle of the device are consistently Nodal negative. This hints at the fact that continuous flow removes from the cells something that is crucial to observe Nodal expression

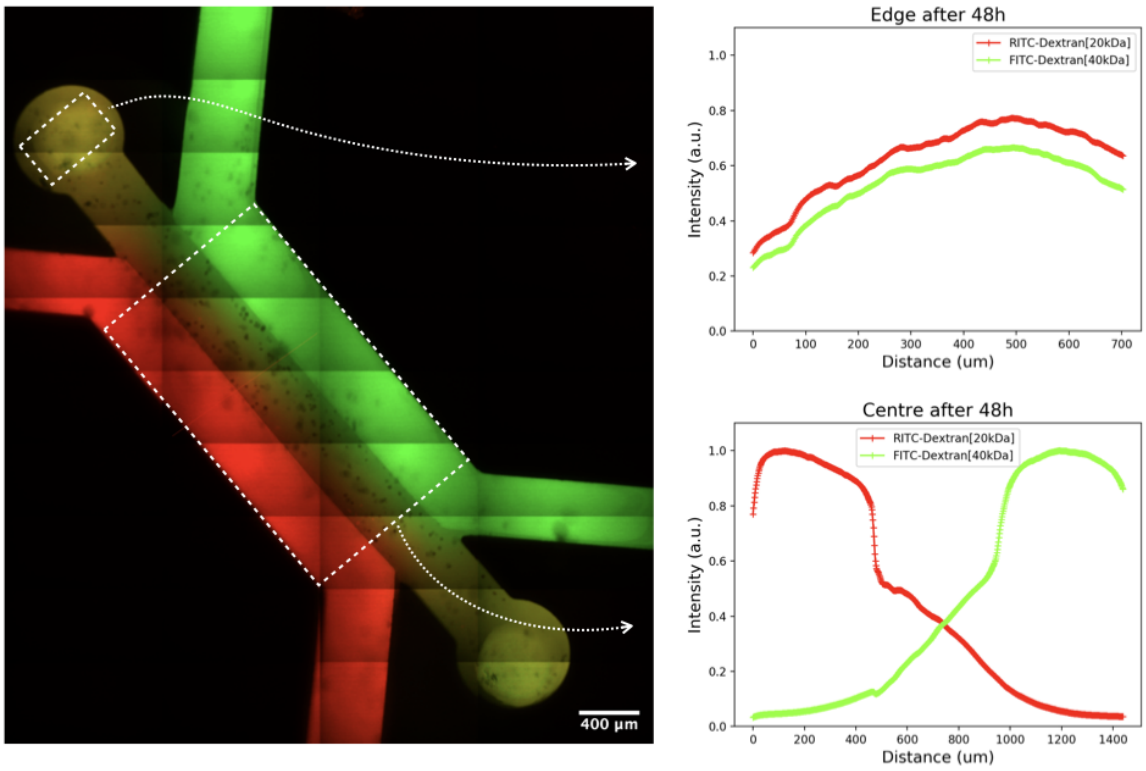

Figure 4.20: **On the edges of the gradient device the gradient is not maintained** While the gradient is table across the section of cell channel, which is in contact with the flow channels, on the edges the gradient is not established nor maintained. They present rather a more homogeneous and intermediate concentration, that show some accumulation toward the centre.

Remarkably, we realised at a certain moment that a difference of behaviour was found in two segments of the device, the part of the cell channel which is in contact

with the two flow channels and the two ends that host the inlets by which the gel is inserted in the chamber. What we could notice (an example where cysts have been stimulated with Wnt is shown in Figure 4.19) is that upon stimulation the behaviour of the cysts in these two parts of the channel was critically different: cysts located in the middle of the device, where there is a gradient, would coherently be Nodal negative, and showing massive EMT that would lead them to flatten out spreading on the glass slide, while cysts in the corner would preserve their spherical structure and would consistently express Nodal in a uniform way. In following experiments, we could confirm this observation also with BMP: we observed having a stronger Nodal expression in the two corners, and a smaller one in the main part of the channel. Mainly, the negative phenotype was the only present across the cell chamber (except in the corners), in strong opposition to what observed in bulk. Figure 4.20 highlights by means of RITC-Dextran and FITC-Dextran the difference in diffusion between this two parts of the gradient device: the gradient is only established in the part of the central channel which is in contact with the flow channels, while the two edges present a more homogeneous concentration, with some accumulation toward the centre, due to a less efficient wash out from the sink.

This observation was reproducible over several repeats of the experiments except one time, when in one of our experiments, the N2B27 flow channel was filled with some air bubble, that blocked the device over few ours (the exact length it is impossible to estimate, because for avoiding phototoxicity, only the cells part of the device is imaged in few spots and not more often than every 6 hours). When this happens some flow is still allowed circumnavigating the walls of the bubble, so the experiment kept running, but the dispersion in the sink is clearly slowed down. We present here the results we obtained in this experiment, and we discuss later how we interpreted them and along what direction we changed the device to reproduce it.

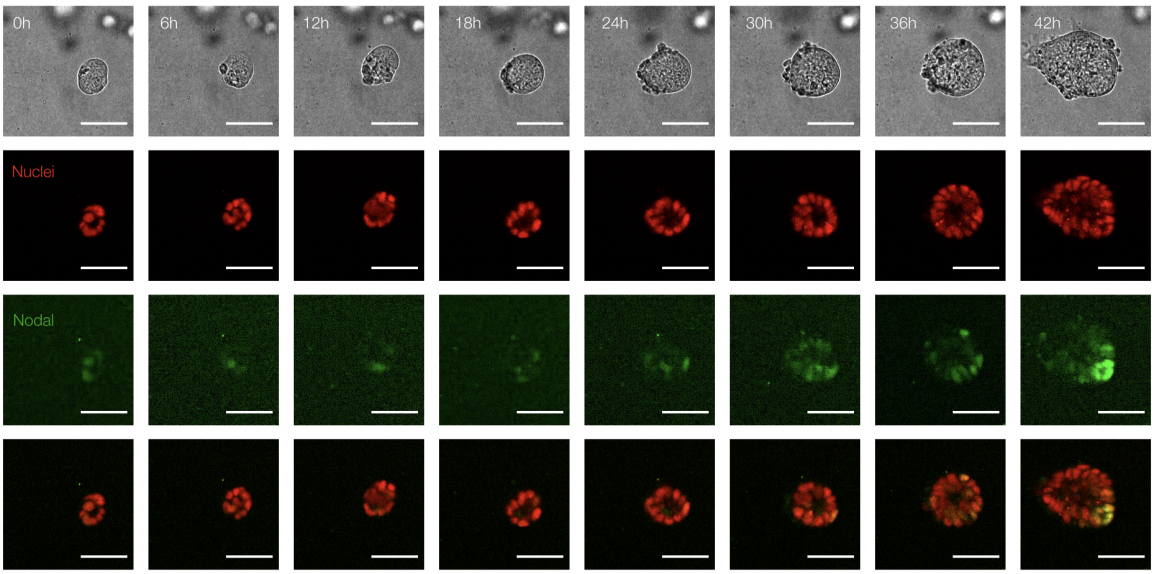

Figure 4.21: **Polarised Nodal emerges over 42h in BMP**. The pictures show the dynamical expression of Nodal that becomes polarired over 36-42h in BMP. It has to be noticed that this polarisation actively arises from a previous state of uniform or unpolarised Nodal, which suggests an active mechanism of restriction to one side of the synthetic epiblast, in a way that is reminiscent of what takes place *in vivo*.

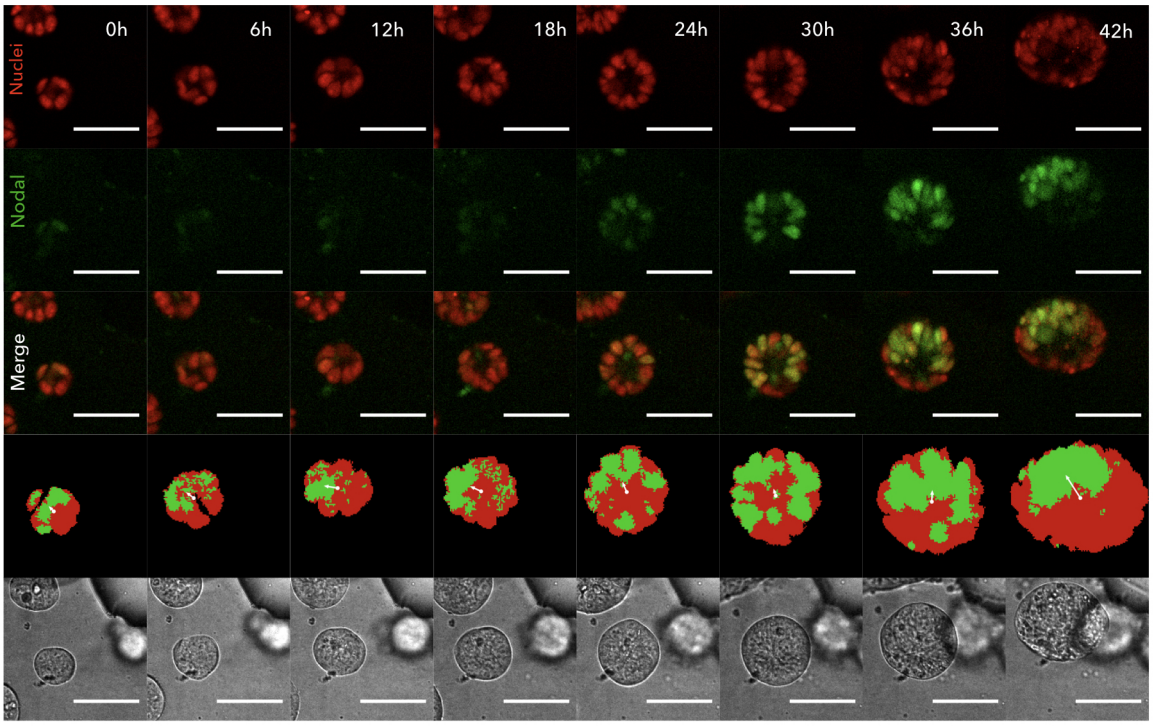

Figure 4.22: **Nodal polarisation emerging over 42h in BMP**. The picture show the formation of a polarised expression of Nodal over 42h in BMP. On the bottom line an algorithm is used to calculate the polarisation vector at the different time points. This shows that the polarity is not prepatterned, as a polarised Nodal expression is preceded by a uniform or isotropic expression

As it is shown in Figure 4.21 and 4.22, during this experiment we were able to observe and track the polarisation of Nodal being established in a sub-ensemble of cysts, upon stimulation with BMP4 at the concentration of 1ng/ml over 42h. We describe here the characteristic of the establishment of the polarisation, and later what we hypothesised being the mechanism behind it.

Being able to observe the polarisation establishing dynamics, we remarked that this is not established along a biased direction from the beginning. Nor we could find any particular correlation with the direction along which BMP was provided (in all pictures shown, BMP is provided from the top). On the opposite, we could observe a real restriction of Nodal to a posterior-like domain, while until 30h after stimulation began, the expression of Nodal was distribute isotropically all over the cyst. To visualise the polarisation, we develop a Python algorithm that segment the nuclei and the positive cells as a population and calculate the Polarisation vector as the

difference of the two centres of mass (this is shown at the bottom of Figure 4.22).

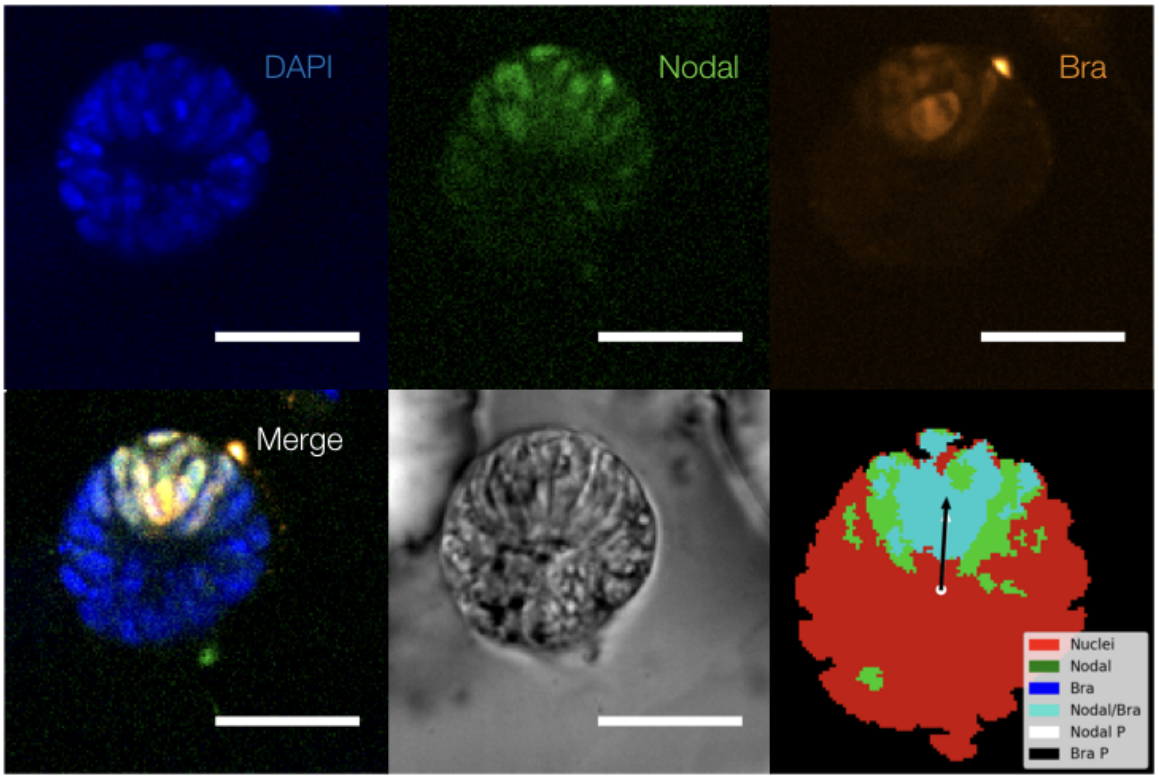

Figure 4.23: **Nodal and Brachuyry are found colocalised after 45h in BMP**. The overlap of the two domain is highlighted by means of our segmentation algorithm. Brachyury domain is completely included inside Nodal domain

To confirm that this Nodal positive domain was actually showing posterior-like fate markers, we imunostained the cells for Brachyury, and found that Brachyury colocalised with Nodal. Particularly Brachyury domain was included inside the Nodal domain. This is shown in Figure 4.23, where the algorithm is being adapted to highlight the overlap of the two domains and show that they both present a polarisation vector along the same direction.

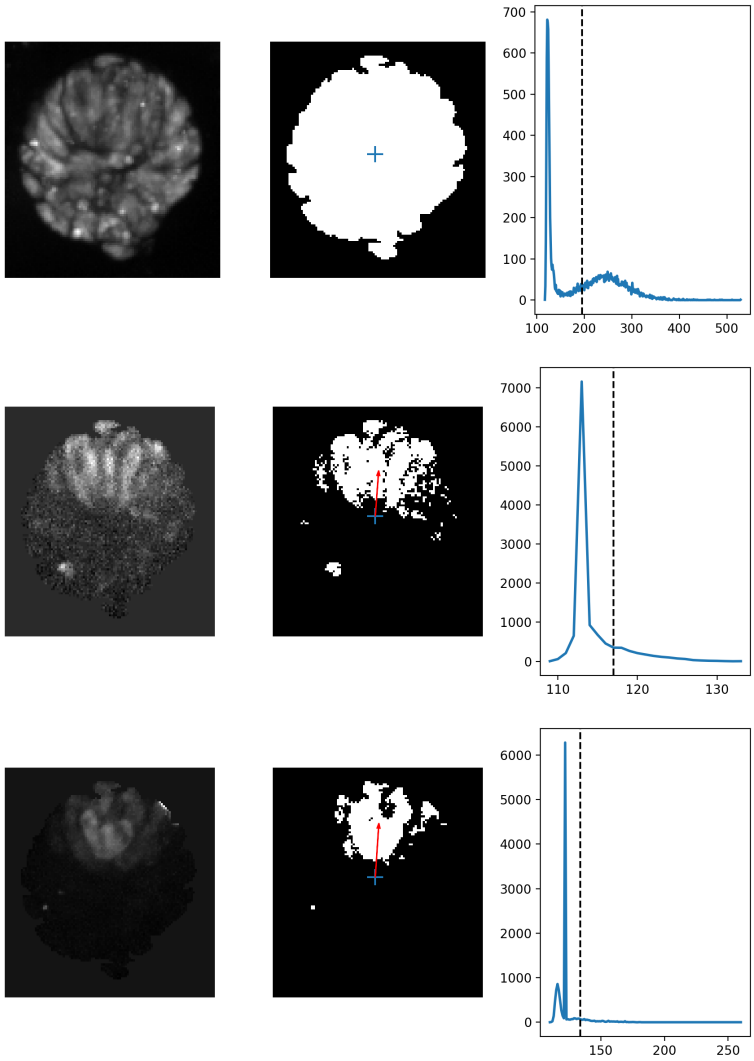

Figure 4.24: **Segmentation algorithm**. The pictures show how the algorithm extracts a mask for the Nuclei by applying the Otsu thresholding algorithm to the original image projected along z. Then the resulting mask is applied to the signal images and a new mask is extracted for Nodal and Brachyury. The polarisation vector is established as the distance in between the center of mass of the Nuclei mask and of the Nodal or Brachyury mask

As a remark, Figure 4.24 shows how the algorithm works to detect the positive cells from the negative ones. First of all, it has to be noticed that the algorithm works in 2D, and this is not only due to simplification reasons. At first, we hypothesised that providing a stimulus along an axis lying on the x-y plane, we thought that it would have been reasonable to expect the polarisation vector lying on the same plane. Indeed this this was later confirmed by the observation, where we never observed any

significant polarisation along the z-axis. Nonetheless, it will be interesting in the future to generalise the algorithm to detect any polarisation along z, for confirming this observation.

So to remove the third dimension the first thing is to project the maximum intensity along z. The the Otsu algorithm is applied to the nuclei microscope image to extract the mask. The way the Otsu algorithm works to divide the pixels whose value varies between 0 and 255 in two classes of values 0 and 1, is to find the two sub-classes whose inter-class variance is the minimum possible. Once the Nuclei mask is obtained (Figure 4.24, top), it is applied to the signal images and to remove some background noise from around the image. Then the signal is extracted again by means of the Otsu algorithm.

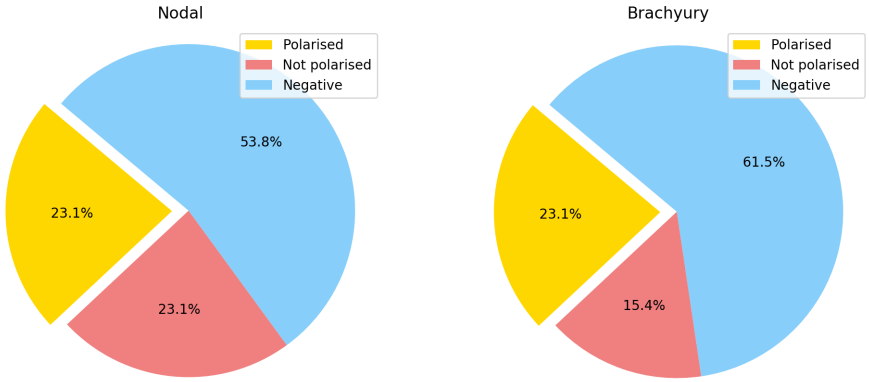

Figure 4.25: **Quantification of the relative amount of Nodal and Brachyury phenotypes after 45h in BMP, n=26** The polarised Nodal phenotype represents half of the total positive phenotype. Polarised synthetic Epiblasts also show the polarised expression of the posterior marker Brachyury, as assessed by immunofluorescence

After describing qualitatively the phenomenology of the polarisation, we examined the experiment in its entirety and we evaluated the respective amount of polarised, not polarised but still positive and negative cysts. We quantify and show the result in Figure 4.25.

Here are a few things to be noticed. First of all, it is important to comment on the

fact that this experiment leads necessarily to a throughput that is much smaller to what it is much more easily obtained in previous bulk experiment.
That taken into account, by comparing the two experiments, we can note that the frequency at which the polarised phenotype is observable is much higher than the one it is possible to get by applying an isotropic stimulus. Moreover, here, the polarised phenotype frequency is comparable to the full positive one, which was not the case in the bulk experiment, where the polarised mostly represented a fraction of $\approx 10\%$ of the total positive organoids group.
The second aspect to be noticed is that the total amount of Nodal positive cysts is comparable to what obtained in bulk for the same condition of BMP concentration (1ng/ml) and also the same dynamical pattern is reproduced, meaning a strong Nodal induction around 24h after stimulation.

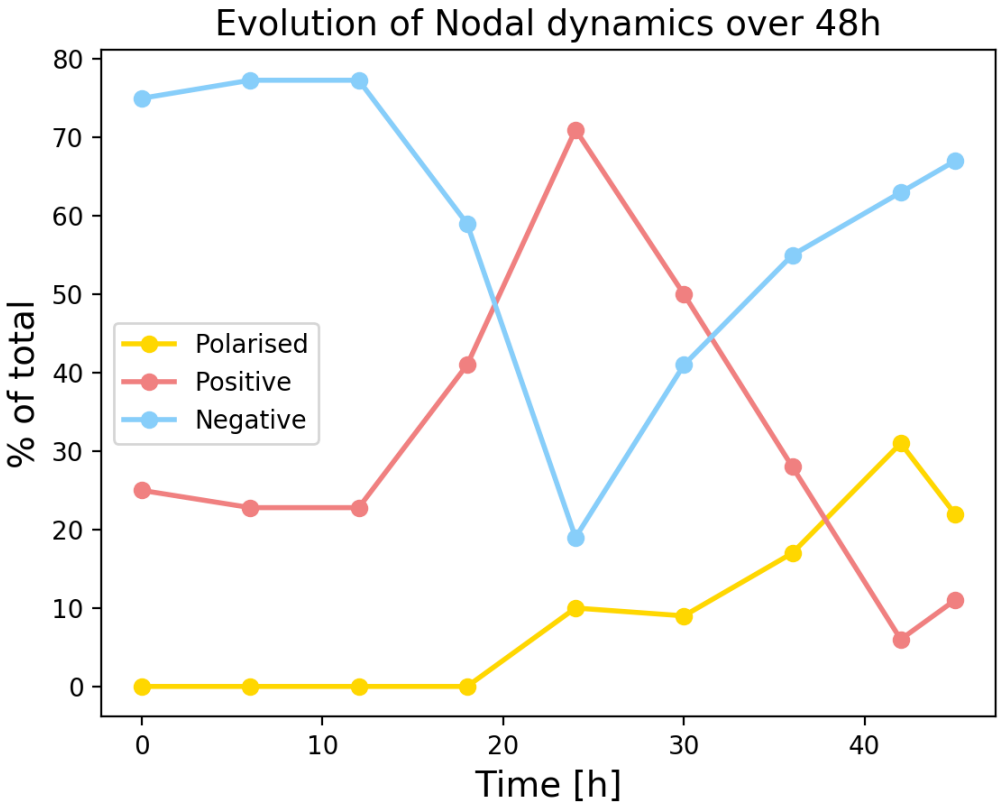

Figure 4.26: **Temporal evolution of Nodal polarised, fully positive and negative cysts relative amount over 45h days in BMP**. Corresponding to the decreasing of the Positive phenotype, the number of polarised cysts raises, confirming that the establishment of the polarity is active and follows from a previously unpolarised configuration, n varies between 16 and 22.

To better visualise the dynamical recurrence of the different phenotypes, we quantified the relative amount of each of them and show their temporal evolution in Figure 4.26. The difference between the uniform stimulus and the localised one though is that corresponding to a the decreasing amount of the full positive phenotype we found an increase in the polarised one, suggesting that, as we showed by a representative example in Figures 4.21 and 4.22, the mechanism underlying the establishment of the polarisation of Nodal is an active restriction to a localised domain of a previously uniform or not polarised Nodal expression overall the synthetic Epiblast.

To conclude on this, and before describing our interpretation of this result, the

fact of visualising the formation of a rudimentary Antero-posterior polarity in absence of any Extra-embryonic tissue suggests the existence of a self-regulated mechanism in the Epiblast itself that does not necessarily needs inhibitors to be present. Moreover, we could probably think of the role of the AVE as reinforcing this already existing mechanism, to ensure the robustness of the axis formation. To confirm this hypothesis further experiments will be needed, but it will be important to be able to uncouple Embryonic and Extra-embryonic tissues to fully unveil the mechanisms by which the Epiblast can break its symmetry. Finally it is important to remark that the amount of polarised cysts observed is much higher, $\approx 25\%$ of the total in the gradient device $\approx 5-10\%$ of the total in bulk. And even more informative it is probably to consider that the polarised cysts in the gradient represents half of the total positive ones, condition that we were not able to reproduce in bulk.

That said, it is important to ask ourselves why we could not observe this result, until we had a blockage in our device. We provided a possible answer and we proposed a modification of the device to test it. Our hypothesis was suggested by the observation discussed at the beginning of this Section, where we detailed the loss of Nodal expression for cysts in the part of the cell channel in contact with the flow channels, while Nodal was kept on in the cysts located in the two channel o-ends. We hypothesised that a continuous flow, beside providing a stable source of BMP, was also acting as a double-sided sink for something the cells were secreting and releasing that sustains Nodal expression, which is lost if this element is not present anymore. From embryology literature, we can hypothesise it being Nodal itself or Wnt, being the two downstream of BMP, and being known, as discussed in Section 2.1, that the two of them play a role in the early posterior patterning of the embryo, and control Nodal expression through the ASE and PEE enhancers, respectively.

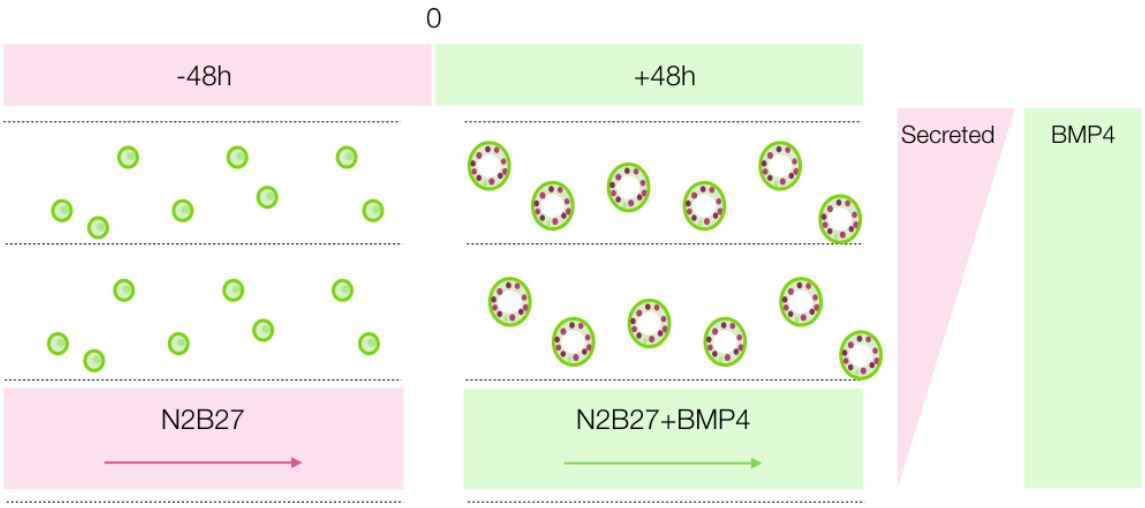

Figure 4.27: **Modified differentiation protocol and setup to accommodate for the washing out effect of the gradient device** We modified the protocol, filling two channels of the device with cells, and feeding them from one side only. We hypothesise that that translates to a uniform BMP stimulation, but produces a gradient of secreted molecules

To test the hypothesis that a washing out effect was what was preventing the system to work, and that the blockage we had was solving this issue, we ran another experiment, keeping providing BMP from one flow channel, at the same flow rate as before, but filling the other channel with cells and gel as we do for the middle channel. We hypothesised that this solution would provide a uniform stimulation with BMP, because the concentration of BMP through the gel will quickly reach the provided concentration, due to removal of the sink. On the other hand, this configuration also provides a sink for, and therefore establish a gradient of, the molecules that are secreted and released from the cysts. In the future, further experiments and solutions could be imagined, that keep also the BMP gradient. We give some hints of how we plan to do that in the conclusions of this chapter. A scheme of the modified set up and the new differentiation protocol is illustrated in Figure 4.27.

Despite this solution not solving all the issues presented, it is interesting to observe that, with this modified setup, we could reproduce faithfully the results in terms of observing the polarised cysts.

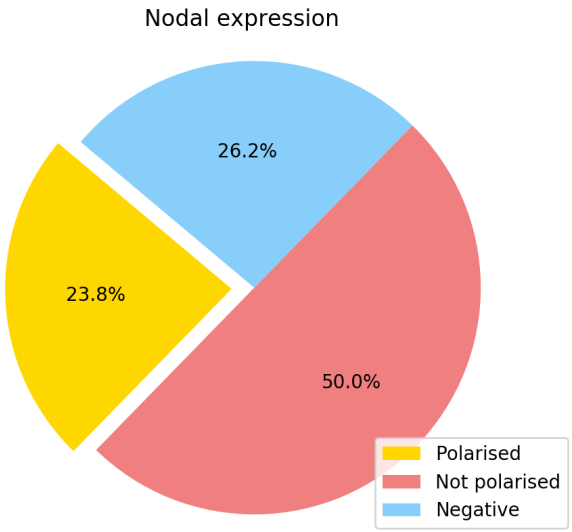

Figure 4.28: **Quantification of the relative amount of Nodal and Brachyury phenotypes after 45h in BMP, in the modified gradient device**. The total amount of polarised cysts is consistent with precious experiment. In this configuration, though the total amount of Nodal positive cysts is bigger, confirming that limiting the loss of secreted molecules, sustains Nodal expression. n=42

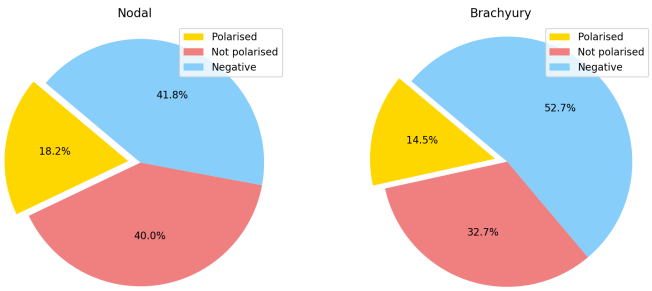

Figure 4.29: **Quantification of the relative amount of Nodal and Brachyury phenotypes, in the modified gradient device**. The experiment confirms that Nodal polarised cysts present the characteristics of antero-posterior polarity as demonstrated by the colocalised expression of the Posterior marker Brachyury. n=55

The quantification for it is shown in Figure 4.28 and 4.29, where the difference in the two comes from the fact that they are two different data sets of the same experiments, the first figure comes from live-imaging data and the second from immunofluorescence. Moreover the total amount of Nodal positive phenotype cysts is

consistently higher than in the previous gradient experiment, and closer to what observed in bulk, hinting again to Nodal expression relying on something the cells secrete and our original setup was continuously washing out.

4.6 Perspectives and what to improve

In conclusion, we have shown that growing the synthetic Epiblast in the gradient device results in a complete loss of Nodal expression. We motivated that, with the fact that BMP indirectly induces Nodal through activating Wnt and that this could be lost due to continuous flow. We have shown, that in conditions that limit this loss, not only Nodal expression is rescued, almost to the same levels at which we found it expressed in our uniform stimulation experiments, but, more interestingly, a polarised Nodal phenotype is observed in a more consistent way that we were previously able to with the uniform stimulation scenario.

Moreover, we have shown that this polarity is not pre-patterned: before being polarised, Nodal is expressed uniformly of in a 'salt and pepper' fashion all over the Epiblast-like cysts. This polarity arises only upon 40h stimulation. By means of immunofluorescence staining, we were able to assess that the polarity observed is reminiscent of the Antero-posterior polarity established in the embryo before gastrulation takes over, as the Nodal positive polarised domain was found to be Brachyury positive (Brachyury being a known posterior/Primitive Streak marker).

We can conclude that, biasing the direction of stimulation, by providing a gradient of secreted molecules downstream of BMP, might be a relevant mechanism of symmetry breaking in the Epiblast. This suggests the presence in the embryo of multiple mechanisms that cooperate to ensure a robust axis formation. We highlighted also that Nodal expression needs to be sustain by some signalling produced by the Epiblast cells themselves downstream of BMP, and that these molecules were being washed out by our original experimental design.

We have proposed a modification of such design to solve the washing out issue, but this solution disrupts the establishment of a linear gradient.

We believe these preliminary results to be encouraging, but experiments had to be

stopped to allow the writing of this manuscript. In the future, we think it will be relevant to identify by means of single cells analysis techniques clearly the identity of these molecules. We anticipated that it was possible to hypothesised, based on the literature, that Wnt and Nodal itself could be the missing signalling part. We envision that a possible solution, that we have not been able to test yet, would be to provide exogenous Nodal or Wnt, by directly adding to the media Wnt and/or Activin, in order to compensate for the washing-out effect of having a constant flow. Multiple configurations could be tested, and the impact of Wnt and Activin provided uniformly (on both flow channels) or in a gradient (only one channel) could be assessed.

Another possible strategy, that we intend to pursue is to switch from a syringe pumps-driven system to a reservoir system, in order to obtain a static gradient. This way we would still have these elements diffusing out inside the reservoir (as it happens in bulk where the total volume is much bigger than the actual volume occupied by the cysts), but we would cut off the washing out due to advection. To convince ourselves that this represents a relevant change in our system we can look at the Péclet number, which is a dimensionless number that compare the relevance of transport by advection with respect to diffusion. The Péclet number, that tells the dominant phenomenon between active transport and diffusion, is given by:

$$\mathrm{Pe} = \frac{\mathrm{L} < \mathrm{v} >}{\mathrm{D}} \tag{6}$$

Here, L is a typical distance, $< \mathrm{v} >$ is the mean transport velocity and D is the diffusion coefficient. For our system, considering $\mathrm{L} = 100\mu\mathrm{m}$, $< \mathrm{v} > \approx 23\mu/\mathrm{s}$ and $\mathrm{D} = 81.7\mu^2/\mathrm{s}$, we obtain $\mathrm{Pe} = 28.3$. This means that the time it takes for a molecule to travel a certain distance by diffusion is ≈ 28 times bigger than the it needs to travel the same distance by advection (given our conditions of flow rate). This is maybe clearer if we consider that these two characteristic times are given by:

$$\mathrm{t_{Diff}} = \frac{\mathrm{L}^2}{\mathrm{D}} \tag{7}$$

$$t_{Adv} = \frac{L}{< v >} \tag{8}$$

Then we can see Péclet number as the ratio between this two quantities:

$$Pe = \frac{t_{Diff}}{t_{Adv}} \tag{9}$$

Of course, to conclude that this change will remove the problem we would need to know the production rate at which cells release this molecule, but this is an unknown parameter, and we are left with the only possibility to find out empirically.

Along our experiments, in bulk as well as in the microfluidic chip, we have observed clear hints of cross-talk between different organoids. This apart from being interesting and still unresolved, introduces a degree of complexity, as in our current setup, we have no control on the positioning of the cysts relative to each other. This effect could concur to the variability that we accounted for in the last two chapter of this thesis.

To uncouple and study the effect of such interaction, it will be necessary to implement in the system a way to control cell positioning, in a way that all of them are as much as possible in the same condition of not only media availability but also of receiving signalling from their neighbour. This way we aim to reduce or understand the variability observed. In this direction, it is worth citing the previous work and the recent advancement done in Fu's lab [Shao et al., 2017] [Zheng et al., 2019], already presented in the Section 2.1 to this thesis. They make use of a device which has the same features of our gradient device to position the cells at a fixed distance between each other. This only modification increased dramatically the reproducibility of their experiment with human asymmetric cysts formation, with respect to their bulk counterpart. We anticipate that it could help narrowing down the requirements for establishing the Antero-posterior polarity also in our scenario.

Moreover, our device could be also used to infer the relevance of certain inhibitors, by providing them in a gradient opposite to the direct stimulation. Also it will be interesting in the future to study the relevance of different and more complicated

stimulation dynamics, establishing whether pulses of BMP, instead of the continuous stimulation presented here, could also trigger the dynamics of the gene expression here considered. In fact we envision that BMP pulses would activate system, but also allow to build up the secreted signalling once the flow is stopped.

5 Uncoupling confinement and bio-chemical stimulation: the Capsules Technology

As discussed in the Section 2.1, Extra-embryonic tissues, present in the mouse embryo at the egg-cylinder stage, have two roles, a mechanical and a chemical one. They provide the embryo with morphogens that promote or prevent cell differentiation toward a certain fate. On the other hand, particularly the Visceral Endoderm confines the Epiblast to a closed space. In Figure 2.10, we can see a section of the embryo that seems to buckle under the stress applied from the Extra-embryonic tissue. This role for the Extra-embryonic tissue has been less investigated in the literature. Recently, [Hiramatsu et al., 2013] it has been shown that a prerequisite to get mouse embryos grown *in vitro* to establish the A-P polarity was to grow them inside narrow agarose microwells that would apply a confining constraint on them. The authors conclude that confinement applied *in vivo* by maternal tissues plays an important role in patterning the embryo. Their results have been later challenged by [Bedzhov et al., 2015], where they report being able to grow mouse embryos *in vitro* and being able to observe the A-P polarity in the absence of maternal tissues. Nonetheless, we think it would be interesting to study the role of confinement applied by the VE, possibly uncoupling it from its role as a source of Nodal inhibitors. In many 3D systems, already introduced in the Section 2.1 of this thesis, like Gastruloids [van den Brink et al., 2014] or human Embryonic Stem Cell organoids [Simunovic et al., 2019], whenever cells are differentiating toward mesendoderm fate, it has been noticed that a pool of Brachyury positive cells would, as expected, undergo Epithelial-to-Mesenchymal transition, and leave the aggregate. Cells leaving the aggregate disrupt the organisation of the structure and prevent any further reorganisation. In the mouse embryo, cells undergoing EMT in the Primitive structure will form the mesoderm layer in between the Epiblast and the Visceral Endoderm. We hypothesised that the lack of Visceral Endoderm in systems described is accountable for preventing the possibility of an organised migration of the cells. We believe it would be important, to build a system

that allows to couple the possibility of inducing differentiation by directly providing morphogens, to the presence of a confinement mimicking the boundary conditions imposed by the Extra-embryonic tissues.

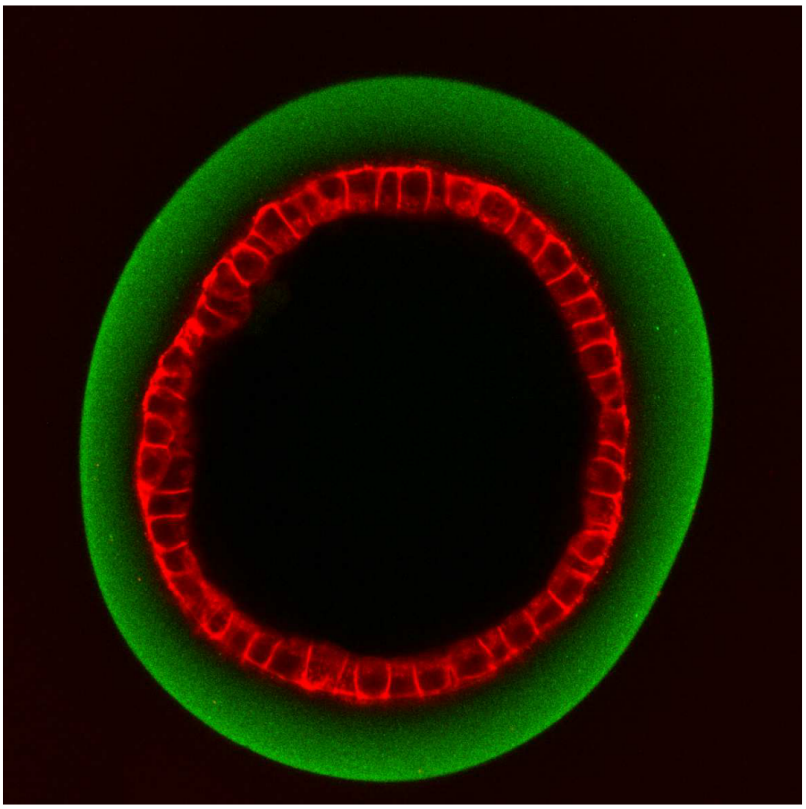

Figure 5.1: **Section of an MDCK cyst inside an alginate capsule** MDCK reaching confluence form epithelial cysts inside alginate capsules. Image adapted from [Alessandri, 2013]

Here, we propose to adapt from [Alessandri et al., 2013] [Alessandri et al., 2016] the culture system, they originally developed to encapsulate MDCK, to encapsulate Embryonic Stem cells. Doing so, we expect to provide a closed manifold on which Stem cells can adhere and grow as an epithelium, in order to mimic the Epiblast growing in contact with the Visceral Endoderm. An example of a cyst in a capsule is reported from [Alessandri, 2013] in Figure 5.2. The Capsules Technology consists in encapsulating cells in alginate capsules. Once inside such capsules, cells can adhere on the capsule's walls if proteins from the Extra-Cellular Membrane are provided. Here, we mix cells with Geltrex, that, as observed by Alessandri (2013, PhD thesis),

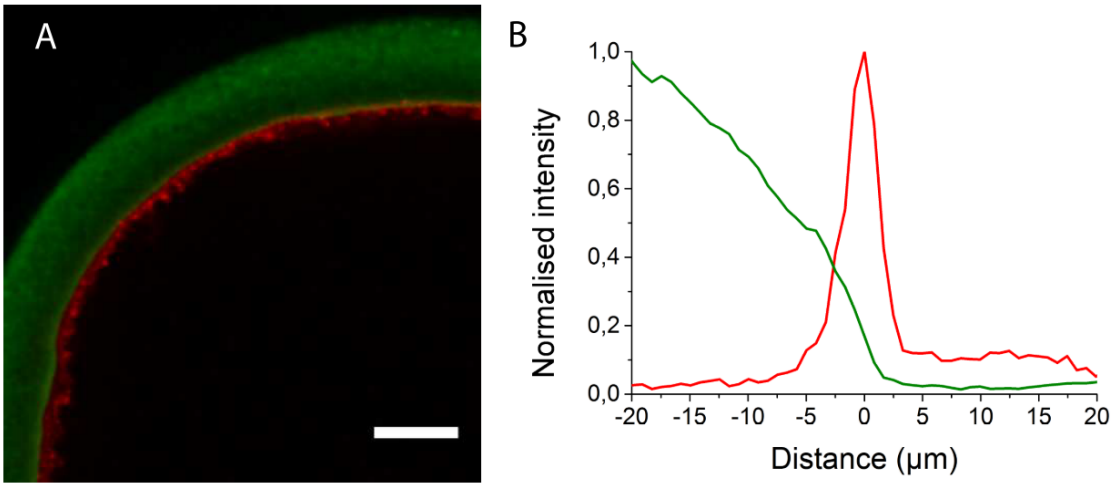

Figure 5.2: **Matrigel spontaneously coating the inner wall of an alginate capsule** Matrigel is found to spontaneously accumulate on the inner wall of the alginate capsule, even though is provided together with the cell mix. In figure Matrigel is red, and alginate is green. Image adapted from [Alessandri, 2013]

spontaneously forms a thin layer in contact with the capsule's walls, even if provided mixed with cell suspension.

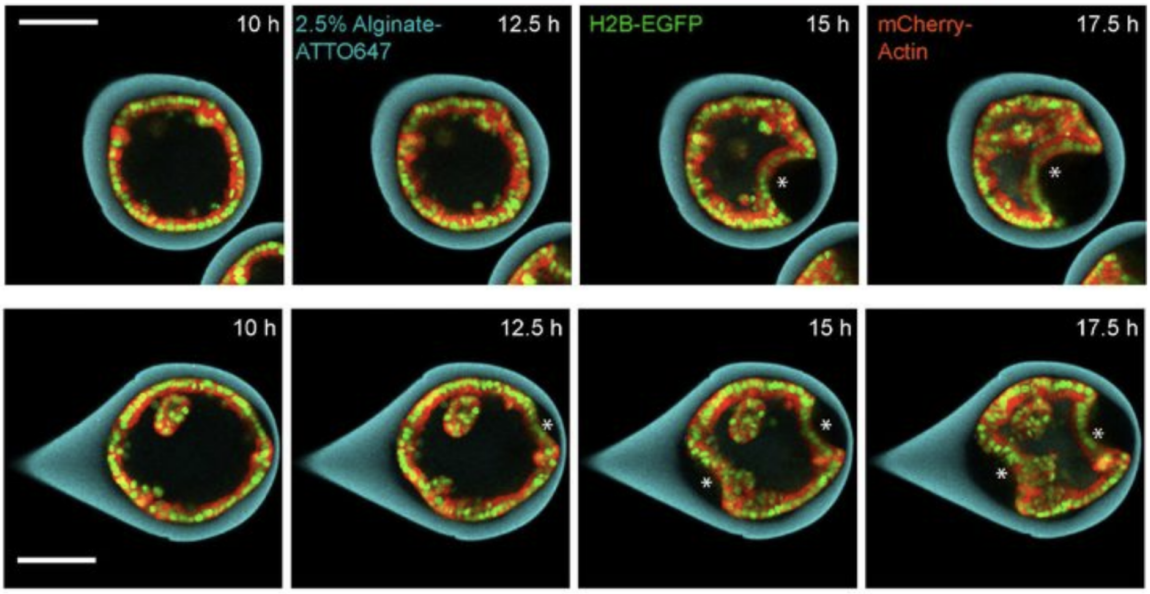

Figure 5.3: **MDCK buckling under confinement** Adapted from [Trushko et al., 2019]

This method has been recently exploited in Roux's lab [Trushko et al., 2019] to study the buckling of MDCK epithelia under confinement due to cell proliferation, as

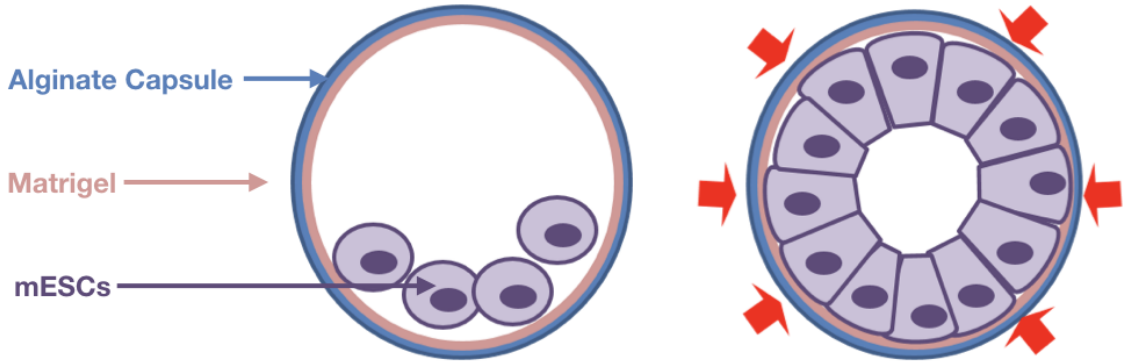

Figure 5.4: **Encapsulating mouse Embryonic Stem Cells to study their differentiation behaviour under confinement**

shown Figure 5.3.

We would like to implement something similar here (cf. Figure 5.4), to study how the confinement imposed by the capsule impact the reorganisation of the Stem cells epithelium. The system proposed here would still allow us to feed and stimulate cells, as alginate is permeable to proteins, but still provides a semi-rigid confining substrate to investigate confinement. Alginate is a biopolymer, soluble in water, that croslinks in presence of divalent ions. Calcium Chloride is used here to this purpose. The stiffness of alginate gels depends on many parameters like concentration of the solution and concentration of Calcium Chloride used to cross-link it. [Kaklamani et al., 2014] have measured an elastic modulus E $\approx$ 150kPa for Sodium Alginate 2.5% (w/v) and Calcium Chloride 1M. In what follows though, we use a Calcium Chloride bath which is 100mM, to meet cell culture conditions. Moreover, it has already being observed [Alessandri, 2013] that removing the capsules from the reservoir and keeping them at the lower Calcium concentration present in culture media, could also have a role in determining the stiffness of the capsules.

We show in the following how we adapted the existing method, and how mouse Epiblast Stem cells and human induced Pluripotent Stem cells grow in this configuration. We discuss the issues encountered, along with possible solutions that need to be implemented to overcome them.

5.1 Encapsulating Stem cells in Alginate Capsules

The encapsulation method is extensively decribed in [Alessandri, 2013] and is based an co-extrusion of different solutions through a set of aligned and centered glass microcapillaries connected to syringe pumps. The original system consists of three glass capillaries, while here we simplified the system to two, provided that we could obtain satisfactory results.

A scheme of the device functioning principles is shown in Figure 5.5, while an image of the actual device is shown in Figure 5.6.

Here, one micro-glass pipette is inserted inside to a bigger one, whose tip is pulled to get a diameter of $\approx 100\mu$m. In contrast to what done by [Alessandri, 2013], we only use two pipettes here instead of three, but the third one might be important to improve the shape of the capsules, even though it fairly complicates the fabrication process. To obtain closed and hollow capsules it is crucial to have the two pipettes well aligned and kept coaxial. To ensure that, we printed by photolithography some centering pearls that we glued with Epoxy glue on the inner pipette. These pearls have the diameter of the hole the size of the inner pipette and the diagonal as the diameter of the outer pipette. The gluing part needs to be done under the binocular, due to the very small amount of glue needed. In the outer pipette alginate is pushed through while the inner one is dedicated to a cells suspension of cells, media and Matrigel.

The two-phase solution is extruded in a Calcium Chloride bath where the cross-linking takes place. This device can be used to encapsulate cells inside alginate tubes as well, if the device is plunged directly into the Calcium reservoir (an example of cells encapsulated in alginate tubes is provided later in Figure 5.10).

Otherwise if a distance is allowed between the tip and the bath the stream will break into droplets under the effect of the Rayleigh-Plateau instability, which also fixes the size of the capsule radius to 2-4 nozzle diameters. In fact we can distinguish two regimes: a dripping regime at low flow rate, and a jetting regime at high flow rate. We want to be in between this two regimes, and have the stream breaking

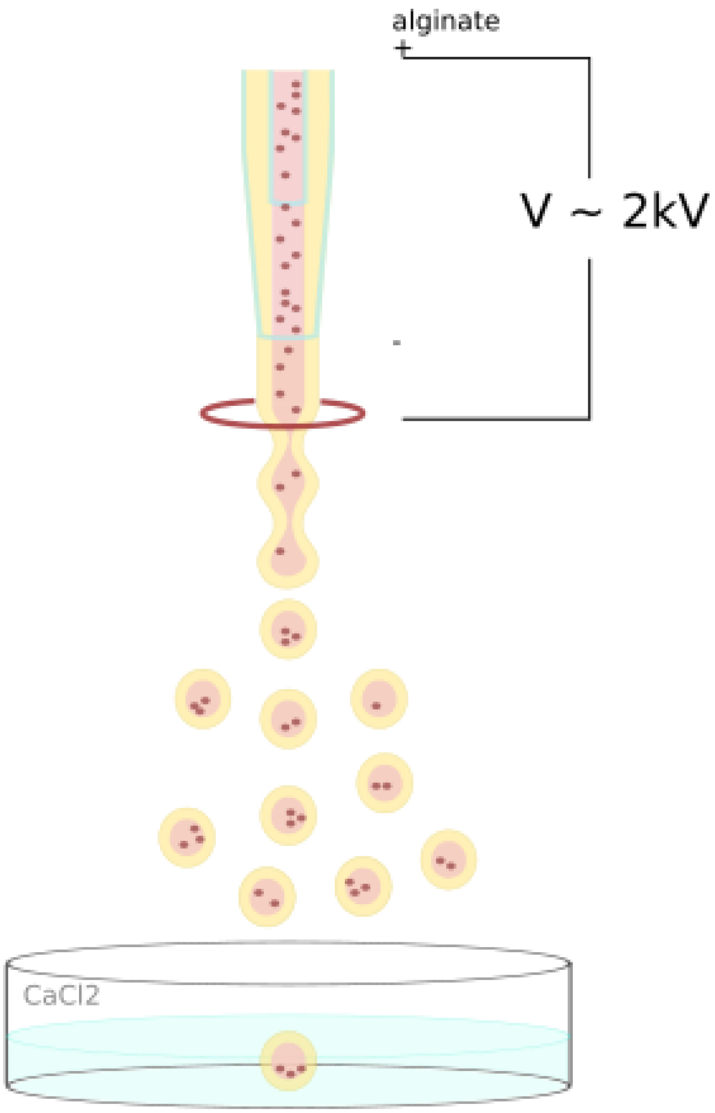

Figure 5.5: **Scheme of the microencapsulation device** Our device is composed of two coaxial capillary glass pipettes. The tip of the outer one is pulled by means of a micro-puller to reach a diameter of 100μm. Pipettes are connected to syringe pumps that push the alginate solution through the outer one and a solution of cells, media and Geltrex to the inner one. The two phase solution is extruded on a Calcium Chloride bath where the cross-linking takes place

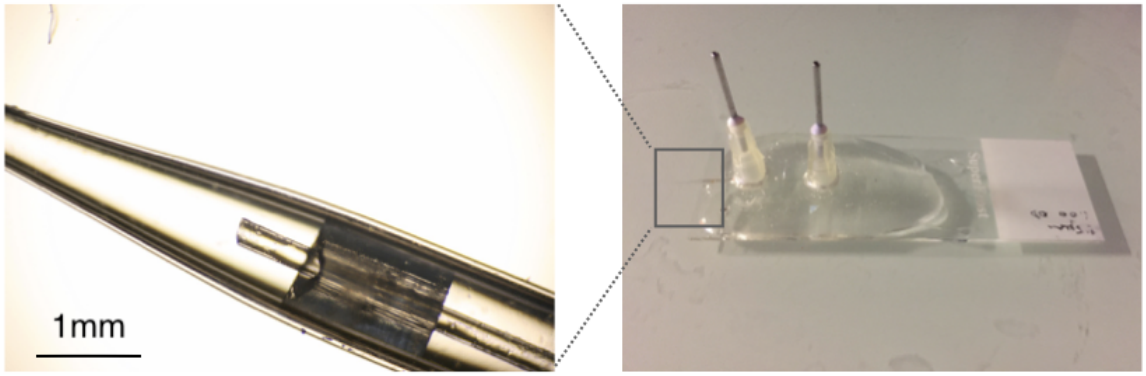

Figure 5.6: **Microencapsulation device** The figure shows the device on the right and on the left a magnification of its nozzle. To ensure the pipettes to be coaxial, which is crucial to obtain hollow and closed capsules, we printed micro-pearls by mean of photolythography

into droplets before getting to the reservoir. The distance between the nozzle and the reservoir needs to be adjusted to minimise coalescence and the breaking of the capsules. The reservoir is placed at a distance D $\approx$ 40cm from the nozzle. Then to avoid mixing eect and the breaking of the capsules at the surface of the Calcium bath, surfactants can be added to the alginate solution and the reservoir. Here, as done by [Alessandri, 2013], we use Sodium Alginate at a concentration of 2% (w/v) and we add SDS 0.5mM to it. Plus, we add a drop of Tween20 to approximately 100ml Calcium bath.

As we said, the radius of the capsules is set by the Rayleigh-Plateau instability to a multiple of the nozzle diameter. To reduce the capsules diameter we tried to reduce the diameter of the outer pipette, but noticed, that when this was the same or smaller than the size of the inner pipette, the surface of the capsules obtained was much more irregular. To reduce it further then, beyond reducing the nozzle diameter, alginate in solution is connected to the positive pole of a voltage supply, while a copper ring is placed two centimetres from the nozzle and connected to the negative pole. By means of a Voltage multiplier we get a voltage V=2kV. The effect is that of an electro-spray. The jet is thinned and the capsules are sprayed on the Calcium reservoir. Moreover, the size of the capsules results more monodisperse than when no electric field is applied. Having capsules sprayed in the air makes the system quite

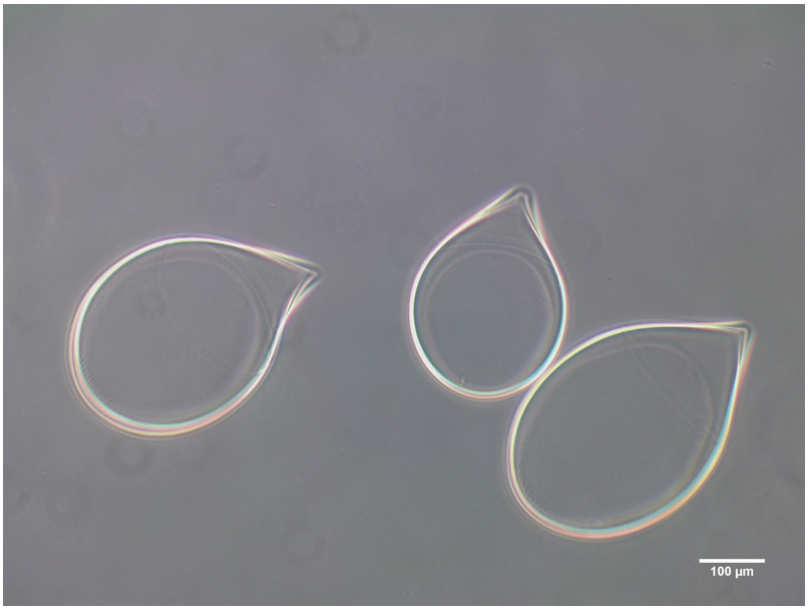

Figure 5.7: **Alginate Capsules** An example of capsules is shown. Here, as inner solution, distilled water has been shown. Therefore, the inner surface of the capsules is smooth and spherical. When Geltrex is provided, the surfaces are more irregular.

sensitive to infections, so it is crucial to work under a sterility hood.

In Figure 5.7 a sample of capsules is shown when only distilled water is used as inner solution. The size in the range of few hundreds micrometers is still bigger that what we would ideally aim, in order to be in the same range of the embryo at the egg-cylinder stage, which would be D $\approx$ 150µm.

Another possibility to act on the diameter would be to vary the flow rate as the outer and inner diameter are connected to the flow rates of the inner and outer solution by conservation of volume:

$$\frac{h}{R_{out}} = 1 - \left(\frac{\frac{q_{in}}{q_{out}}}{1 + \frac{q_{in}}{q_{out}}} \right)^{\frac{1}{3}} \tag{10}$$

where q_{out} is the alginate flow rate, q_{in} is the cell suspension flow rate, h is the thickness of the capsule wall, and R_{out} its outer diameter. Here, we use q_{out} = 40ml/h and q_{in} = 30ml/h as we found this regime to be the most stable, but it could in principle be increased the alginate flow rate in order to have thicker capsules, with smaller inner diameter.

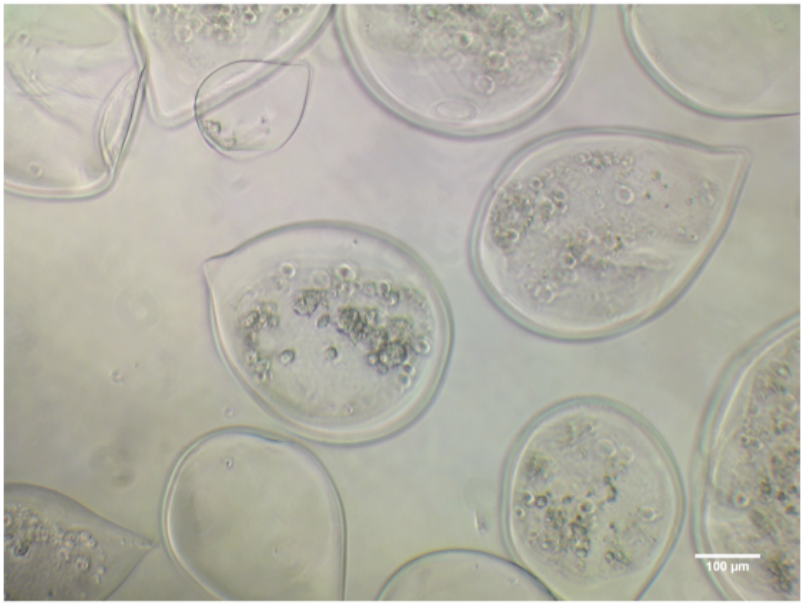

Figure 5.8: **Epiblast Stem Cells seeded in alginate capsules** Just after seeding, cells sediment on the bottom of the capsule.

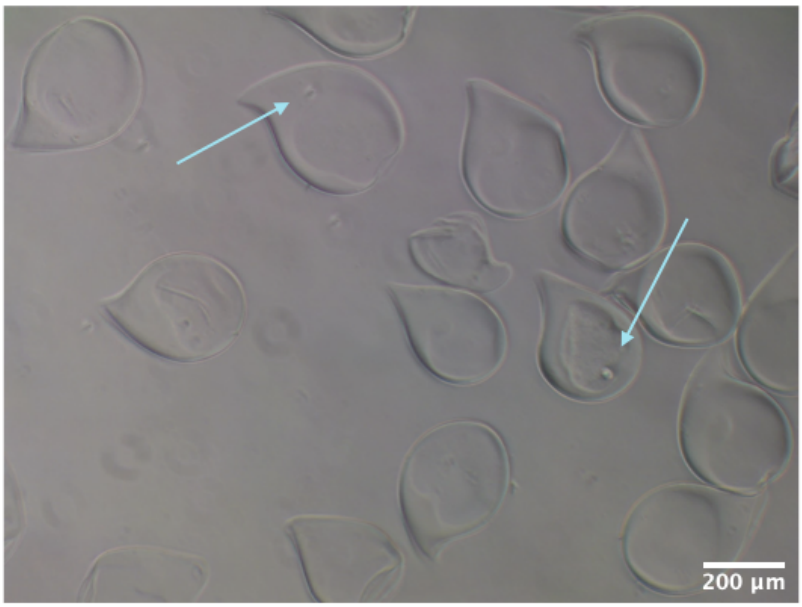

Figure 5.9: **Encapsulating single cells in alginate capsules** We tried to encapsulate single cells, in order to get monoclonal epithelia, but this reduces the rate of success of the encapsulation, and only few capsules feature a cell in them. Moreover getting to confluence requires a much longer time

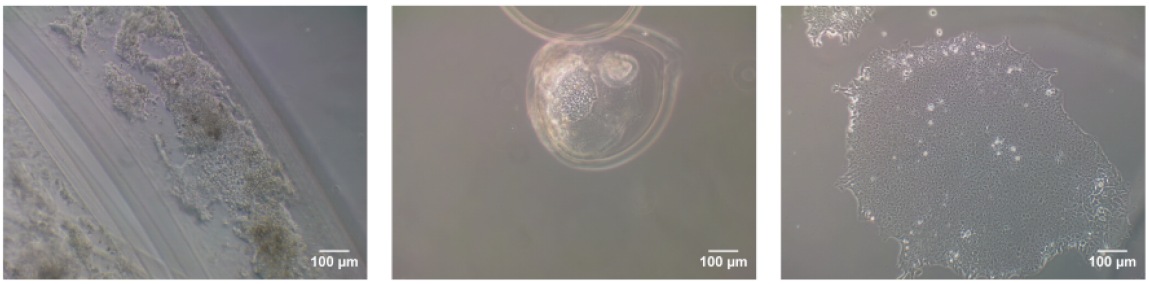

Figure 5.10: **Epiblast Stem Cells inside an alginate capsule and tube, compared to their growth on a Petri dish** Compared to the configuration in which EpiSCs are grown on a Petri dish, cells look less flattened, and more three-dimensional, as they are not fully spreading.

Once we set up the system, we proceeded to encapsulate cells with it. Figure 5.8 shows capsules with mouse Epiblast Stem cells just after seeding.
To encapsulate cells, they need to be resuspended in a solution that contains 50% medium and 50% Geltrex. As already explained, Geltrex is extremely sensitive to temperature, so it is crucial to do the mixing on ice. In fact, solidified gel would be deadly to the experiment, as it would slow down the flow and make it unstable, resulting in rotten capsules, highly irregular and much bigger than usual. Moreover, solidified gel could clog the device and make it unusable anymore. Here, we mix 50µl of Geltrex to 50µl of medium containing approximately 100k cells. When mixed, the gel is inserted in a six-port injection valve connected to a syringe containing PBS and the inner capillary of the device. In fact, due to small volumes, we first reach a stable dripping-jetting regime by flowing PBS, and we only switch to cell suspension, when a stable flow is ensured. Again, the switch has to be kept on ice.
In order to get monoclonal epithelia, we also tried to reduce the cell density in order to get single cells encapsulated, as shown in Figure 5.9. Clearly that reduced the encapsulation succes rate, as the majority of the capsules would be empty. Also, we always managed to get capsules that have a diameter around $\approx 300 - 400$µm, that makes it really slow to get to confluence starting with a single cell.

In contrast to mouse Embryonic Stem cells, that when plated in Geltrex self-organise as cysts, mouse Epiblast Stem Cells and induced Pluripotent Stem cells are

epithelial cells. When seeded inside the capsule they grow as epithelia on this curved surface (see Figure 5.10), in a way that is similar to the way they grow on Petri dishes. Though they seem to present a more three-dimensional morphology, that would maybe hint to a less efficient spreading on this substrate.

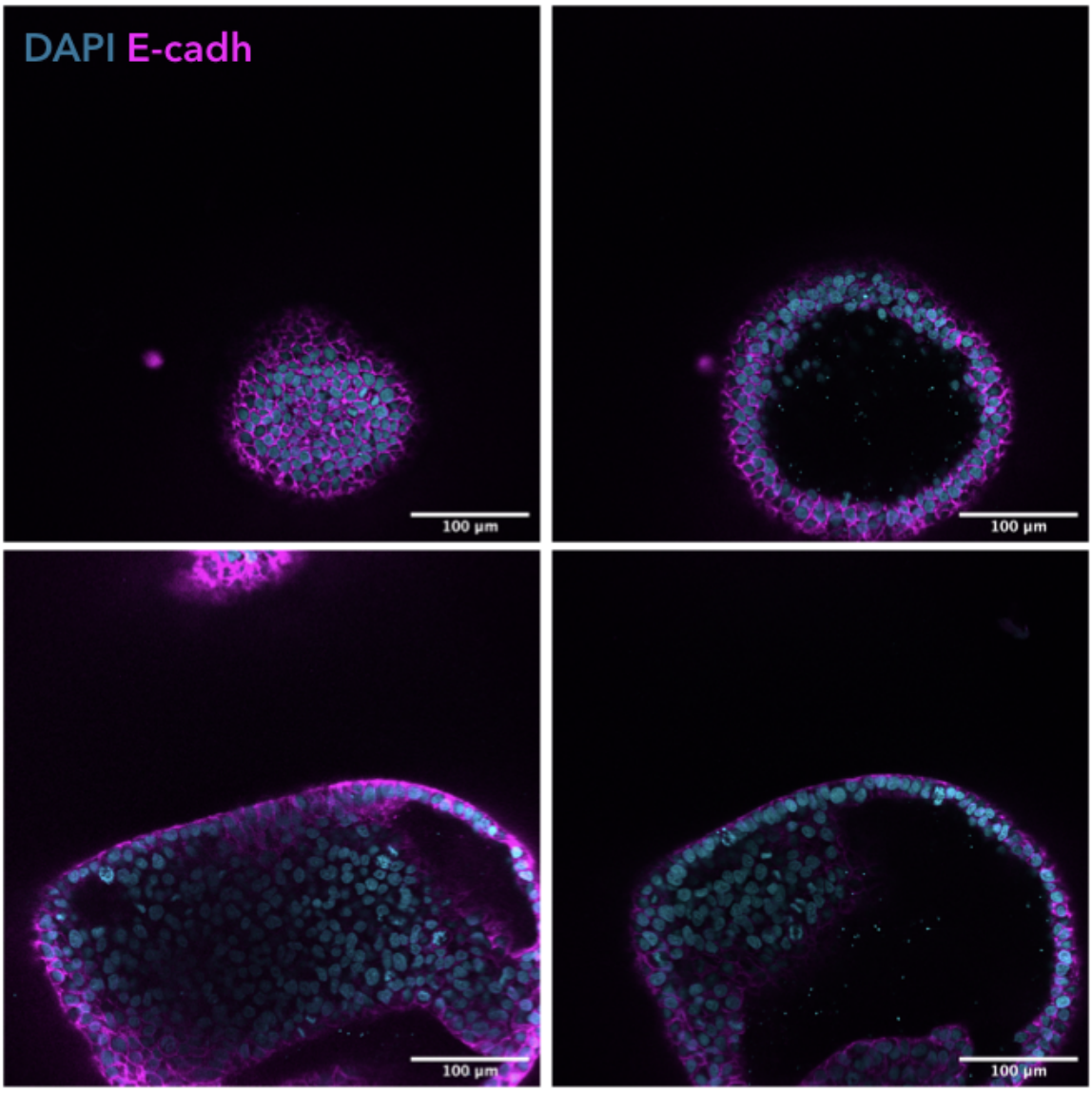

Figure 5.11: **Different focal views of hiPSCs inside an alginate capsule** hiPSCs have been grown inside the capsule for 5 days to reach confluence. Then they have been stimulated for 48h with BMP (50ng/ml) for 48h. Perfect confluence is not reached as cells start to pile up, before completely covering the capsule.

Cells grow as an epithelium, to almost cover the whole surface of the capsule. As

shown in Figure 5.11, where different sections of hiPS cells covering a capsule are shown, they do not reach perfect confluence, and after several days of culture instead of spreading on the surface, they pile up on several layers(Figure 5.11 bottom right).

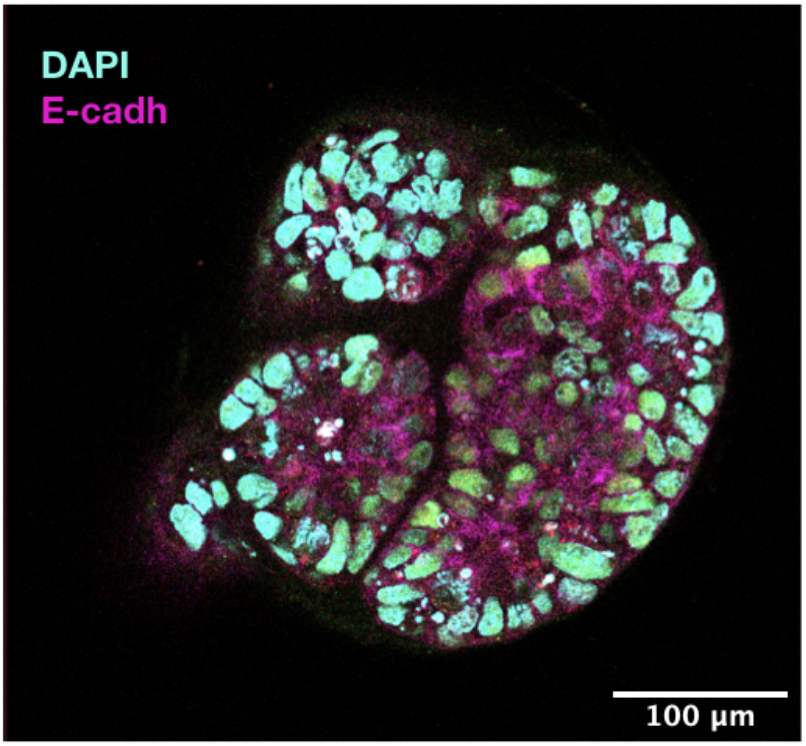

Figure 5.12: **hiPSCs inside an alginate capsule** Sometimes multiple epithelia are found developing insiede a capsule and forming complicated structure whose behaviour is difficult to forsee and conrtol

Moreover, and especially if the inner surface of the capsule is rather irregular, multiple epithelia can grow inside the same capsule (an example of this is shown in Figure 5.12).

Finally, when stimulated with BMP4 cells in a capsule showed a rather disorganised expression of Brachyury, an example of which is shown in Figure 5.13. Up to now we were not able to observe any particular organisation of cells in this system. The disorganised and seemingly random Brachyury expression that we report in Figure 5.13 is similar to what is obtained colonies of hiPSCs are stimulated on Petri dishes: BMP induces Brachyury, but Brachyury positive cells do not show any degree of symmetry breaking nor polarisation. We hypothesised that the underlying reason could

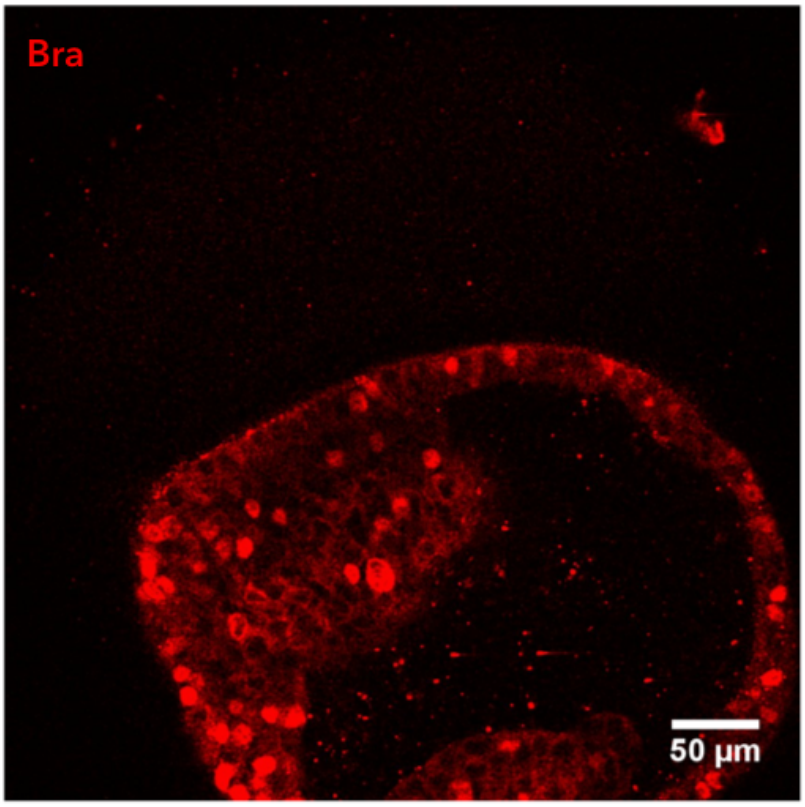

Figure 5.13: **Brachyury immunostaining of hiPSCs in an alginate capsule** Cells have being grown in mTeSR for 5 days to reach confluence, and then have been stimulated with BMP (50ng/ml) for 48h. Brachyury positive cells are spread all over the colony, without any manifest reorganisation

be connected to the fact that cells growing inside the capsules reproduce the same morphology of those grown on flat standard culture condition. It would be interesting to be able to grow the synthetic Epiblast we described in Section 3. Ideally we would have the cysts forming directly inside the capsule, and growing up to the size of the capsule they would get confined. We also tried though to encapsulate directly the cysts, releasing them from Geltrex, with Cornig Cell Recovery solution, which is meant to dissolve it, but we found that that was damaging the structure of the cysts. Up to now, though we did not manage to get capsules of the relevant size, and our organoids our too small to get confined by the capsules we got.

5.2 Discussion: possible ways to improve it and fix the issues

We believe that there is a lack of studies investigating the mechanical role of the Extra-embryonic tissues in confining the embryo and driving the rearrangements that it undergoes during gastrulation. To run these experiments *in vivo* is challenging. To overcome these difficulties, we proposed to adapt the encapsulation method firstly developed by [Alessandri et al., 2013]. Here we show that mouse Epiblast Stem cells and induced Pluripotent Stem cells can grow inside such alginate capsules when Geltrex is provided, and they form Epithelia covering the interior walls of the capsules, even if not completely nor uniformly. We were not able yet to observe any reorganisation of the tissue in terms of morphogenesis nor expression patterns. The recent results presented in [Trushko et al., 2019], where they study the buckling of MDCK are encouraging and suggesting that a similar method could be adapted to ESCs.
To do so, the first issue to overcome is the size of the capsules: with our glass capillary device we could obtain capsules whose diameter was few hundred of micrometers order of magnitude. With the new 3D printed version of the device presented by Nassoy's lab in [Alessandri et al., 2016], they were able to reduce the size to $D_{caps} \approx 100\mu m$, which we believe would be more relevant to us. A possible amelioration we envision would be to encapsulate the organoids that we grow in Geltrex and that we presented in Section 3. We ran a first attempt at doing so, by dissolving the Geltrex with Cornig Cell Recovery solution. Probably the protocol needs adjusting (a smaller incubation

time could be advisable, and cooling the solution down could increase its efficiency) as we observed that doing that was also damaging cell-cell junctions. Being able to encapsulate cysts, would allow to remove the problem of getting uniform confluence inside the capsule, and get an actual confinement when the organoid reach the size of the capsule. The organoids being much smaller in size than the capsules, getting smaller capsules is a fundamental prerequisite. Moreover, to observe symmetry breaking in the expression of posterior markers such a Brachyury, we could envision the possibility to grow our capsules inside the gradient device, in order to re-couple the confinement to a localised source of signal.

6 Conclusions

The establishment of the antero-posterior polarity is a fundamental step in development as it will set the locus of the Primitive Streak and therefore start Gastrulation which will end up with the formation of the three germ layers and the setting up of the future body plan. The mechanisms that regulate the symmetry breaking in gene expression that results in the antero-posterior polarity have been described in the literature and rely on the cross-talk between the Extra-embryonic tissues and the Epiblast: the Extra-embryonic Ectoderm through BMP sustains the expression of Nodal and induces posterior gene expression such as Brachyury and Cdx2 at the proximal side of the Epiblast, while the Visceral Endoderm feeds the Epiblast with Nodal inhibitors Lefty1 and Cerberus, while migrating toward the prospective anterior pole. These two mechanisms cooperate to ensure the restriction of Nodal to the posterior side and the formation at the posterior side of the Primitive Streak.

The interactions between these three tissue being complex to resolve, we proposed here a minimal model for the Epiblast to allow us to uncouple the role of the Extra-embryonic tissues from their secreted morphogens. We have described how Embryonic Stem cells, when induced to differentiate to Epiblast-like Stem Cells, while embedded in a gel, which contains the main basal proteins, recapitulate the morphogenesis of the early Epiblast: they indeed compact, polarise along the apico-basal direction and undergo luminogenesis. We have used this system to investigate the gene expression under uniform stimulation with BMP. We have confirmed that BMP sustains Nodal expression and induce Brachyury, and that the dynamics of the expression is BMP dose dependent. We have also observed spontaneous polarisation of Nodal and Brachyury, which suggests the existence in the Epiblast of some self-regulated mechanism to establish polarisation. The limited frequency at which this polarisation is induced though suggests the necessity for more robust mechanisms to ensure the polarity.

We have hypothesised the necessity for a localised source to induce a stronger polarisation, and we have developed a microfluidic system to stimulate the synthetic

Epiblast with a gradient of BMP. We have noticed though the loss of Nodal expression when mESCs organoids were grown on chip, which never occurred when growing them in bulk. We attributed this to the continuous flow necessary to keep the gradient stable. We hypothesised that continuously flowing resulted in washing out secreted molecules, that appear to be necessary to sustain Nodal expression. We modified the system to counteract this effect, and we hypothesised that this new configuration was corresponding to stimulating the Epiblast-like organoids with a uniform concentration of BMP, while establishing a gradient of secreted molecules. In this configuration we could observe the establishment of a polarisation of Nodal, that, as we could assess by immunofluorescence experiments corresponds to a polarisation in Brachyury that co-localise with the Nodal domain. Interestingly, the polarisation establishing process seems to be active, meaning that the organoids evolve from a situation where Nodal is all over expressed to reach a configuration where the polarisation is specified, which resembles what takes place *in vivo*, where before the antero-posterior polarity is established, Nodal is expressed all over the Epiblast. These preliminary experiments seem to confirm the hypothesis of a redundancy of mechanisms in the embryo that cooperate to ensure the robustness of the body plan formation. To confirm these results we have sketched up the future experiments plan. We have hypothesised the secreted molecules needed to keep Nodal expression to be Wnt and Nodal itself, for they are both known to induce Nodal and to be downstream of BMP. To prove this hypothesis we propose to come back to the original design of the gradient experiment and to feed Activin and/or Wnt together with BMP to make up for the loss of secreted factors due to continuous flowing. Alternatively we propose to set up a different device to establish a static gradient that relies on reservoirs instead of continuous flow, to act as source and sink. We expect this to solve the washing out issues and to restore the expression of Nodal. Furthermore, we believe that different temporal patterns for the BMP stimulation could be explored, as to substitute continuous stimulation over the 48h with repeated pulses that would also solve the washing out issue.

Lastly, we observed that another relevant feature of the Visceral Endoderm could be to confine the embryo into a closed space and we hypothesised that this could have an

impact on the early development, driving the migration of the mesoderm. This aspect being less investigated, we proposed to adapt the cellular capsules technology to grow Embryonic Stem cells in order to model a confined Epiblast. We have shown that Epiblast Stem cells could grow inside such capsules if ECM proteins were provided. The growing inside the capsules though was rather disorganised and resulted in cells piling up in multiple layers before reaching confluence. Moreover reaching confluence was slowed down by the dimension for capsule diameter we were able to obtain. We anticipate that to keep improving this system it will be crucial tor educe the capsules diameter to $50 - 100\mu$m, while we obtained capsules in the range $200 - 300\mu$m. We have also shown that preliminary experiments in stimulating the capsules with BMP result in random expression for Brachyury. It is reasonable to assume that also in this scenario, a localised signalling source could be necessary to the consistent induction of symmetry breaking.

Appendices

A Cell lines

All experiments presented in Sections 3 and 4 have been run with mouse Embryonic Stem cells WT HM1, provided by Jerome Collignon's lab , and two reporter lines mESCs Nodal-YFP (CK35 background) also from Jerome Collignon's lab, and mESCs Bra-2A-GFP (a gift form Hiroshi Sasaki)[Imuta et al., 2013]. For live imaging experiments, a nuclear marker was added to the cells, either nls-mCherry or H2B-iRFP for the nodal-yfp or Bra-GFP cell lines, respectively. the nuclear marker expression is driven by the CAG constitutive promoter. Stable cell lines were generated using the ePiggyBAC system of transportable elements. For the Bra-GFP line, cells were also transfected with the CRE recombinase to excise the selection cassette and allow GFP expression. Experiments presented in Section 5 have been run with mouse Epiblast Stem Cells (mEpiSCs) FT 129.1 provided by Alice Jouneau's lab and human induced Pluripotent Stem Cells (hiPSCs) V, clone C17 provided by Bertrand Pain's lab.

A.1 Cell culture

A.1.1 mouse Embrionic Stem Cells

Mouse Embryonic Stem Cells are plated on Petri dishes coated with Gelatin. The dishes need to be coated with a solution 0.15% Gelatin, 15-30 minutes prior to plating cells. Gelatin solution has to be just sufficient to cover the whole surface, here we coated with 600µl a well in a 6-wells plate.

Successively cells are grown in N2B27 provided with 2i/LIF. N2B27 medium is a mix of equal doses of Neurobasal medium (Lifetech #21103-049) and DMEM/F12 (Lifetech #21331-020), supplied with 0.5x N2 (Lifetech #17502-048), 1x B27 (Lifetech #17504-044), 1x L-Glutamin, 0.65x BSA 7.5%, and 1x Penstrep. Then, 0.1mM $\beta-$mercaptoethanol, that is added directly when feeding cells. Cells are passaged 2-3

times a week by tripsinising them for 5 minutes and around 50k cells are seeded on a well in a 6-wells plate. Medium is replaced every day.

A.1.2 mouse Epiblast Stem cells

EpiSCs are plated on Petri dishes coated for 30 minutes with DMEM 10%FBS (not Heat Inactivated). They are fed with a Chemically Defined Medium whose composants for 50ml medium are: 25ml IMDM (Invitrogen 31980-32), 25ml F12 (Invitrogen 31765-027), BSA 0.25gr (5mg/ml), Lipid 100X (Invitrogen 11905-031) 0.5ml (1%), Monothioglycerol (Sigma M6145, ready to use) 2µl(450µM), Insulin 10mg/ml 35µl(7µg/ml), Transferin 25µl(15µg/ml). To this, when feeding cells Activin (20ng/ml final concentration) and FgF (12ng/ml final concentration.) Medium is replaced every day. Cells are passaged twice a week with Collagenase II for 1 minute at room temperature.

A.1.3 human induced Pluripotent Stem Cells

hiPSCs are plated on Petri dishes coated with Matrigel. They are kept pluripotent and expanded using the mTeSR1 chemically defined medium, acording to manufacturer's instructions. hiPSC are passaged in clumps using RelesR reagent, according to manufacturer's instructions. To load iPSC in alginate capsules, cells need to be detached form their substrates as single cells. this is done with accutase. ROCK inhibitor Y27... is added to the culture medium the day after cell seeding to improve cell survival

A.2 Experiment protocol in bulk and in the gradient

To run the experiments described in Sections 3 and 4, 50-100k cells resuspended in 20µl N2B27 are mixed with 100µl Geltrex. For the bulk experiments 10µl of suspension is plated and spread on a surface equivalent to a well of a 96-wells plate. They are grown for 48h in N2B27 supplied with FgF (10ng/ml) and KSR. Then they are

induced to differentiate for 48h in BMP4. For bulk experiments following BMP concentrations have been tested: 0.1ng/ml, 1ng/ml, 10ng/ml. Gradient experiments have been performed at 1ng/ml BMP concentration. Medium is replaced every day. For gradient experiments µl of cell suspension is inserted in the cell chamber of the gradient device.

A.3 Immunostaining protocol

For the bulk experiments, the culture medium is rinsed with two washes in PBS. Then cells are fixed for 30 minutes in PFA 4%. Cells are washed three times for 10 minutes in PBS to remove the PFA. Cells are permeabilised in PBS 1% Triton for 10 minutes. Blocking is done for 1h in PBS 0,3% Triton + 1%BSA. Then primary antibodies are diluted (1:300) in PBS 0,3% Triton 0,1%BSA overnight at 4°C. Then primary antibodies are washed six times for 10 minutes in PBS 0,3% Triton. Blocking is done in PBS 0,3% Triton 1%BSA for 1h. Then secondaries antibodies are diluted (1:500) in PBS 0,3% Triton 0,1% BSA for 2h at room temperature or overnight at 4°C.

For the gradient experiments, the medium is washed on chip, by flushing PBS three times for 10 minutes. Cells are fixed in PFA 4% for 10 minutes. PFA is washed three times for 10 minutes in PBS. Then permeabilisation is done in PBS Triton 0.1% for 10 minutes. Then blocking is done in PBS Triton 0.1% 1% BSA. Primary antibodies are diluted (1:300) in PBS Triton 0.1% 1% BSA and incubated overnight at 4°C. They are then washed 3 times in PBS Triton 0.1% for 10 minutes. Secondary antibodies are diluted (1:500) in PBS Triton 0.1% 1% BSA and incubated for 2h at room temperature or overnight at 4°C.

B Image Analysis

Image analysis has been done with Fiji-ImageJ software and Python for the segmentation of the polarised cysts images and the analysis of the dynamics in the gradient device.

Basic features of the code for segmenting the organoids are described in Section 4.

Given the functioning of this gradient, based on calculating the center of mass of a two-dimensional binary image, a small polarisation would be calculated for every signal whose centre of mass is shifted with respect to the nuclei.

To make up for this, in all experiments presented in Section 3 and 4 we have considered polarised all cysts where it would be possible to trace a line that separates the positive cells from the negative ones.

C Device Fabrication

In this section we described how to make the gradient chip, from its design to the photolythography steps needed to the PDMS moulding. To design the outline of the device, it is needed a vectorial design software such as AutoCAD or Inkscape. The relevant dimensions to take into account are the width of the channels, 200μm for the gel channel and 400μm for the flow channels. The size of the pillars is 100μm diameter and the spacing between them is 70μm. This spacing is crucial, because having it too wide would limit the trapping ability of these pillars.

Then the design has to be transferred on a transparent mask, with a resolution of the order of 10μm, in order to be used during the photolythography.

To obtain a mould for PDMS we used the SU8 2150 photoresist (MicroChem) and we aimed to adjust the parameters in order to get a channel height of 200-300μm. The photoresist has to be spin coated on a Silicon Wafer previously cleaned with Ethanol or Acetone. The spin coater velocity needs to be adjusted to reach a height of $200 - 300$μm.

Then the resin is baked in two steps at 65°C and 95°C. The device design is printed on the Silicon wafer, by exposing it to UV light through a mask. The wafer is then baked again in two steps at 65°C and 95°C. Then the wafer need to be developed by soaking it in a SU-8 developer bath, until the uncured resin is fully removed. To speed up the process, in order not to damaged the edges of the mould, a shaker or a sonicator can be used. After developing, the wafer needs to hard baked to remove any traces of solvent. To do so bake it at 65°C and raise gently the temperature of the hot plate until 200°C.

References

Alessandri, K. (2013). *The Cellular Capsules technology And its applications to investigate model tumor*. PhD thesis.

Alessandri, K., Feyeux, M., Gurchenkov, B., Delgado, C., Trushko, A., Krause, K.-H., Vignjević, D., Nassoy, P., and Roux, A. (2016). A 3D printed microfluidic device for production of functionalized hydrogel microcapsules for culture and differentiation of human Neuronal Stem Cells (hNSC). *Lab Chip*, 16(9):1593–1604.

Alessandri, K., Sarangi, B. R., Gurchenkov, V. V., Sinha, B., Kießling, T. R., Fetler, L., Rico, F., Scheuring, S., Lamaze, C., Simon, A., Geraldo, S., Vignjevic, D., Doméjean, H., Rolland, L., Funfak, A., Bibette, J., Bremond, N., and Nassoy, P. (2013). Cellular capsules as a tool for multicellular spheroid production and for investigating the mechanics of tumor progression in vitro. *Proceedings of the National Academy of Sciences of the United States of America*, 110(37):14843–8.

Arnold, S. J. and Robertson, E. J. (2009). Making a commitment: cell lineage allocation and axis patterning in the early mouse embryo. *Nature Reviews Molecular Cell Biology*, 10(2):91–103.

Atencia, J., Morrow, J., and Locascio, L. E. (2009). The microfluidic palette: A diffusive gradient generator with spatio-temporal control. *Lab on a Chip*, 9(18):2707.

Beccari, L., Moris, N., Girgin, M., Turner, D. A., Baillie-Johnson, P., Cossy, A.-C., Lutolf, M. P., Duboule, D., and Arias, A. M. (2018). Multi-axial self-organization properties of mouse embryonic stem cells into gastruloids. *Nature*, 562(7726):272–276.

Bedzhov, I., Bialecka, M., Zielinska, A., Kosalka, J., Antonica, F., Thompson, A. J., Franze, K., and Zernicka-Goetz, M. (2015). Development of the anterior-posterior axis is a self-organizing process in the absence of maternal cues in the mouse embryo. *Cell Research*, 25(12):1368–1371.

Bedzhov, I. and Zernicka-Goetz, M. (2014). Self-Organizing Properties of Mouse Pluripotent Cells Initiate Morphogenesis upon Implantation. *Cell*, 156(5):1032–1044.

Boxman, J., Sagy, N., Achanta, S., Vadigepalli, R., and Nachman, I. (2016). Integrated live imaging and molecular profiling of embryoid bodies reveals a synchronized progression of early differentiation. *Scientific Reports*, 6(1):31623.

Brennan, J., Lu, C. C., Norris, D. P., Rodriguez, T. A., Beddington, R. S. P., and Robertson, E. J. (2001). Nodal signalling in the epiblast patterns the early mouse embryo. *Nature*, 411(6840):965–969.

Britton, G., Heemskerk, I., Hodge, R., Qutub, A. A., and Warmflash, A. (2019). A novel self-organizing embryonic stem cell system reveals signaling logic underlying the patterning of human ectoderm. *Development (Cambridge, England)*, page 518803.

Burkert, U., von, T. R., and Wagner, E. (1991). Early fetal hematopoietic development from in vitro differentiated embryonic stem cells. *The New biologist*, 3(7):698–708.

Carrion, B., Huang, C. P., Ghajar, C. M., Kachgal, S., Kniazeva, E., Jeon, N. L., and Putnam, A. J. (2010). Recreating the perivascular niche ex vivo using a microfluidic approach. *Biotechnology and Bioengineering*, 107(6):1020–1028.

Cockburn, K. and Rossant, J. (2010). Making the blastocyst: Lessons from the mouse. *Journal of Clinical Investigation*, 120(4):995–1003.

Crank, J. (1975). *The Mathematics of Diffusion*. OXFORD UNIVERSITY PRESS.

De Clerq, F. and Schmelz, J. (1983). *Ethnographische Beschrijving van de West- en Noordkust van Nederlandisch Nieuw-Guinea*. Leiden.

Demers, C. J., Soundararajan, P., Chennampally, P., Cox, G. A., Briscoe, J., Collins, S. D., and Smith, R. L. (2016). Development-on-chip: In vitro neural tube patterning with a microfluidic device. *Development (Cambridge)*, 143(11):1884–1892.

Diao, J., Young, L., Kim, S., Fogarty, E. A., Heilman, S. M., Zhou, P., Shuler, M. L., Wu, M., and DeLisa, M. P. (2006). A three-channel microfluidic device for generating static linear gradients and its application to the quantitative analysis of bacterial chemotaxis. *Lab on a Chip*, 6(3):381–388.

Doetschman, T. C., Eistetter, H., Katz, M., Schmidt, W., and Kemler, R. (1985). The in vitro development of blastocyst-derived embryonic stem cell lines: formation of visceral yolk sac, blood islands and myocardium. *Development*, 87(1).

Dumortier, J. G., Le Verge-Serandour, M., Tortorelli, A. F., Mielke, A., de Plater, L., Turlier, H., and Maître, J.-L. (2019). Hydraulic fracturing and active coarsening position the lumen of the mouse blastocyst. *Science*, 365(6452):465–468.

Etoc, F., Metzger, J., Ruzo, A., Kirst, C., Yoney, A., Ozair, M., Brivanlou, A., and Siggia, E. (2016). A Balance between Secreted Inhibitors and Edge Sensing Controls Gastruloid Self-Organization. *Developmental Cell*, 39(3):302–315.

Evans, M. J. and Kaufman, M. H. (1981). Establishment in culture of pluripotential cells from mouse embryos. *Nature*, 292(5819):154–156.

Gaztelumendi, N. and Nogués, C. (2014). Chromosome instability in mouse embryonic stem cells. *Scientific reports*, 4:5324.

Guo, G., Yang, J., Nichols, J., Hall, J. S., Eyres, I., Mansfield, W., and Smith, A. (2009). Klf4 reverts developmentally programmed restriction of ground state pluripotency. *Development (Cambridge, England)*, 136(7):1063–9.

Harrison, S. E., Sozen, B., Christodoulou, N., Kyprianou, C., and Zernicka-Goetz, M. (2017). Assembly of embryonic and extraembryonic stem cells to mimic embryogenesis in vitro. *Science*, 356(6334):eaal1810.

Heemskerk, I., Burt, K., Miller, M., Chhabra, S., Guerra, M. C., Liu, L., and Warmflash, A. (2019). Rapid changes in morphogen concentration control self-organized patterning in human embryonic stem cells. *eLife*, 8.

Hiramatsu, R., Matsuoka, T., Kimura-Yoshida, C., Han, S.-W., Mochida, K., Adachi, T., Takayama, S., and Matsuo, I. (2013). External Mechanical Cues Trigger the Establishment of the Anterior-Posterior Axis in Early Mouse Embryos. *Developmental Cell*, 27(2):131–144.

Imuta, Y., Kiyonari, H., Jang, C. W., Behringer, R. R., and Sasaki, H. (2013). Generation of knock-in mice that express nuclear enhanced green fluorescent protein and tamoxifen-inducible Cre recombinase in the notochord from Foxa2 and T loci. *Genesis*, 51(3):210–218.

Kaklamani, G., Cheneler, D., Grover, L. M., Adams, M. J., and Bowen, J. (2014). Mechanical properties of alginate hydrogels manufactured using external gelation. *Journal of the Mechanical Behavior of Biomedical Materials*, 36:135–142.

Keller, G. (2005). Embryonic stem cell differentiation: Emergence of a new era in biology and medicine. *Genes and Development*, 19(10):1129–1155.

Kihara, T., Ito, J., and Miyake, J. (2013). Measurement of biomolecular diffusion in extracellular matrix condensed by fibroblasts using fluorescence correlation spectroscopy. *PloS one*, 8(11):e82382.

Kim, S., Kim, H. J., and Jeon, N. L. (2010). Biological applications of microfluidic gradient devices. *Integrative Biology*, 2(11-12):584–603.

Kim, S., Lee, H., Chung, M., and Jeon, N. L. (2013). Engineering of functional, perfusable 3D microvascular networks on a chip. *Lab on a Chip*, 13(8):1489.

Lancaster, M. A. and Knoblich, J. A. (2014). Organogenesis in a dish: Modeling development and disease using organoid technologies. *Science*, 345(6194):1247125–1247125.

Lenhoff, H. M. (1991). Ethel Browne, Hans Spemann, and the Discovery of the Organizer Phenomenon. *The Biological Bulletin*, 181(1):72–80.

Li Jeon, N., Baskaran, H., Dertinger, S. K. W., Whitesides, G. M., Van De Water, L., and Toner, M. (2002). Neutrophil chemotaxis in linear and complex gradients of interleukin-8 formed in a microfabricated device. *Nature Biotechnology*, 20(8):826–830.

Lu, C. C. and Robertson, E. J. (2004). Multiple roles for Nodal in the epiblast of the mouse embryo in the establishment of anterior-posterior patterning. *Developmental Biology*, 273(1):149–159.

Maître, J.-L., Niwayama, R., Turlier, H., Nédélec, F., and Hiiragi, T. (2015). Pulsatile cell-autonomous contractility drives compaction in the mouse embryo. *Nature Cell Biology*, 17(7):849.

Maître, J.-L., Turlier, H., Illukkumbura, R., Eismann, B., Niwayama, R., Nédélec, F., and Hiiragi, T. (2016). Asymmetric division of contractile domains couples cell positioning and fate specification. *Nature*, 536(7616):344–348.

Manfrin, A., Tabata, Y., Paquet, E. R., Vuaridel, A. R., Rivest, F. R., Naef, F., and Lutolf, M. P. (2019). Engineered signaling centers for the spatially controlled patterning of human pluripotent stem cells. *Nature Methods*, 16(7):640–648.

Martin, G. R. (1981). Isolation of a pluripotent cell line from early mouse embryos cultured in medium conditioned by teratocarcinoma stem cells. *Proceedings of the National Academy of Sciences of the United States of America*, 78(12):7634–8.

Martyn, I., Brivanlou, A. H., and Siggia, E. D. (2019). A wave of WNT signaling balanced by secreted inhibitors controls primitive streak formation in micropattern colonies of human embryonic stem cells. *Development*, 146(6):dev172791.

Matsumoto, H. (2017). Molecular and cellular events during blastocyst implantation in the receptive uterus: clues from mouse models. *The Journal of reproduction and development*, 63(5):445–454.

Meinhardt, A., Eberle, D., Tazaki, A., Ranga, A., Niesche, M., Wilsch-Br??uninger, M., Stec, A., Schackert, G., Lutolf, M., and Tanaka, E. M. (2014). 3D reconstitu-

tion of the patterned neural tube from embryonic stem cells. *Stem Cell Reports*, 3(6):987–999.

Morgani, S. M., Metzger, J. J., Nichols, J., Siggia, E. D., Hadjantonakis, A.-K., Pera, M., Morgani, S. M., Metzger, J. J., Nichols, J., Siggia, E. D., and Hadjantonakis, A.-K. (2018). Micropattern differentiation of mouse pluripotent stem cells recapitulates embryo regionalized cell fate patterning. *eLife*, 7.

Mosadegh, B., Huango, C., Park, J. W., Shin, H. S., Chung, B. G., Hwang, S. K., Lee, K. H., Kim, H. J., Brody, J., Jeon, N. L., Bobak Mosadegh, Carlos Huang, Jeong Won Park, Hwa Sung Shin, Bong Geun Chung, Sun-Kyu Hwang, Kun-Hong Lee, Hyung Joon Kim, James Brody, , and Noo Li Jeon*, 2007). Generation of stable complex gradients across two-dimensional surfaces and three-dimensional gels. *Langmuir*, 23(22):10910–10912.

Murry, C. E. and Keller, G. (2008). Differentiation of Embryonic Stem Cells to Clinically Relevant Populations: Lessons from Embryonic Development. *Cell*, 132(4):661–680.

Nallet-Staub, F., Yin, X., Gilbert, C., Marsaud, V., BenMimoun, S., Javelaud, D., Leof, E. B., and Mauviel, A. (2015). Cell Density Sensing Alters TGF-β Signaling in a Cell-Type-Specific Manner, Independent from Hippo Pathway Activation. *Developmental Cell*, 32(5):640–651.

Needham, J. (1959). *A History Of Embryology*. Cambridge University Press.

Perea-Gomez, A., Camus, A., Moreau, A., Grieve, K., Moneron, G., Dubois, A., Cibert, C., and Collignon, J. (2004). Initiation of Gastrulation in the Mouse Embryo Is Preceded by an Apparent Shift in the Orientation of the Anterior-Posterior Axis. *Current Biology*, 14(3):197–207.

Perea-Gomez, A., Vella, F. D., Shawlot, W., Oulad-Abdelghani, M., Chazaud, C., Meno, C., Pfister, V., Chen, L., Robertson, E., Hamada, H., Behringer, R. R., and

Ang, S. L. (2002). Nodal antaginists in the anterior visceral endoderm prevent the formation of multiple primitive streaks. *Developmental Cell*, 3(5):745–756.

Poh, Y.-C., Chen, J. J., Hong, Y., Yi, H., Zhang, S., Chen, J. J., Wu, D. C., Wang, L., Jia, Q., Singh, R., Yao, W., Tan, Y., Tajik, A., Tanaka, T. S., and Wang, N. (2014). Generation of organized germ layers from a single mouse embryonic stem cell. *Nature Communications*, 5.

Ranga, A., Girgin, M., Meinhardt, A., Eberle, D., Caiazzo, M., Tanaka, E. M., and Lutolf, M. P. (2016). Neural tube morphogenesis in synthetic 3D microenvironments. *Proceedings of the National Academy of Sciences of the United States of America*, 113(44):E6831–E6839.

Regier, M. C., Tokar, J. J., Warrick, J. W., Pabon, L., Berthier, E., Beebe, D. J., and Stevens, K. R. (2019). User-defined morphogen patterning for directing human cell fate stratification. *Scientific Reports*, 9(1):6433.

Riethmacher, D., Brinkmanni, V., and Birchmeier, C. (1995). A targeted mutation in the mouse E-cadherin gene results in defective preimplantation development. *Proceedings of the National Academy of Sciences of the United States of America*, 92(3):855–859.

Rivron, N., Pera, M., Rossant, J., Martinez Arias, A., Zernicka-Goetz, M., Fu, J., van den Brink, S., Bredenoord, A., Dondorp, W., de Wert, G., Hyun, I., Munsie, M., and Isasi, R. (2018). Debate ethics of embryo models from stem cells. *Nature*, 564(7735):183–185.

Rossant, J. (2004). Lineage development and polar asymmetries in the peri-implantation mouse blastocyst. *Seminars in Cell and Developmental Biology*, 15(5):573–581.

Saadi, W., Rhee, S. W., Lin, F., Vahidi, B., Chung, B. G., and Jeon, N. L. (2007). Generation of stable concentration gradients in 2D and 3D environments using a microfluidic ladder chamber. *Biomedical Microdevices*, 9(5):627–635.

Sagy, N., Slovin, S., Allalouf, M., Pour, M., Savyon, G., Boxman, J., and Nachman, I. (2018). Prediction and control of symmetry breaking in embryoid bodies by environment and signal integration. *bioRxiv*, page 506543.

Shahbazi, M. M. N., Scialdone, A., Skorupska, N., Weberling, A., Recher, G., Zhu, M., Jedrusik, A., Devito, L. G., Noli, L., Macaulay, I. C., Buecker, C., Khalaf, Y., Ilic, D., Voet, T., Marioni, J. C., and Zernicka-Goetz, M. (2017). Pluripotent state transitions coordinate morphogenesis in mouse and human embryos. *Nature*, 552(7684):239.

Shahbazi, M. N., Siggia, E. D., and Zernicka-Goetz, M. (2019). Self-organization of stem cells into embryos: A window on early mammalian development. *Science*, 364(6444):948–951.

Shahbazi, M. N. and Zernicka-Goetz, M. (2018). Deconstructing and reconstructing the mouse and human early embryo. *Nature Cell Biology*, 20(8):878–887.

Shamloo, A., Ma, N., Poo, M.-m., Sohn, L. L., and Heilshorn, S. C. (2008). Endothelial cell polarization and chemotaxis in a microfluidic device. *Lab on a Chip*, 8(8):1292.

Shao, Y., Taniguchi, K., Gurdziel, K., Townshend, R., Xue, X., Yong, K., Sang, J., Spence, J., Gumucio, D., and Fu, J. (2016). Self-organized amniogenesis by human pluripotent stem cells in a biomimetic implantation-like niche. *Nature Materials*, 16(4):419–425.

Shao, Y., Taniguchi, K., Townshend, R. F., Miki, T., Gumucio, D. L., and Fu, J. (2017). A pluripotent stem cell-based model for post-implantation human amniotic sac development. *Nature Communications*, 8(1):208.

Silva, J., Nichols, J., Theunissen, T. W., Guo, G., van Oosten, A. L., Barrandon, O., Wray, J., Yamanaka, S., Chambers, I., and Smith, A. (2009). Nanog Is the Gateway to the Pluripotent Ground State. *Cell*, 138(4):722–737.

Simunovic, M., Metzger, J. J., Etoc, F., Yoney, A., Ruzo, A., Martyn, I., Croft, G., You, D. S., Brivanlou, A. H., and Siggia, E. D. (2019). A 3D model of a human epiblast reveals BMP4-driven symmetry breaking. *Nature Cell Biology*, 21(7):900–910.

Soofi, S. S., Last, J. A., Liliensiek, S. J., Nealey, P. F., and Murphy, C. J. (2009). The elastic modulus of Matrigel as determined by atomic force microscopy. *Journal of structural biology*, 167(3):216–9.

Sorre, B., Warmflash, A., Brivanlou, A. H., and Siggia, E. E. (2014). Encoding of temporal signals by the TGF-β Pathway and implications for embryonic patterning. *Developmental Cell*, 30(3):334–342.

Sozen, B., Amadei, G., Cox, A., Wang, R., Na, E., Czukiewska, S., Chappell, L., Voet, T., Michel, G., Jing, N., Glover, D. M., and Zernicka-Goetz, M. (2018). Self-assembly of embryonic and two extra-embryonic stem cell types into gastrulating embryo-like structures. *Nature Cell Biology*, 20(8):979–989.

Stephan K. W. Dertinger, Daniel T. Chiu, Jeon, N. L., , and Whitesides*, G. M. (2001). Generation of Gradients Having Complex Shapes Using Microfluidic Networks. *Analytical Chemistry*.

Taniguchi, K., Shao, Y., Townshend, R. F., Tsai, Y. H., Delong, C. J., Lopez, S. A., Gayen, S., Freddo, A. M., Chue, D. J., Thomas, D. J., Spence, J. R., Margolis, B., Kalantry, S., Fu, J., O'Shea, K. S., and Gumucio, D. L. (2015). Lumen Formation Is an Intrinsic Property of Isolated Human Pluripotent Stem Cells. *Stem Cell Reports*, 5(6):954–962.

ten Berge, D., Koole, W., Fuerer, C., Fish, M., Eroglu, E., and Nusse, R. (2008). Wnt Signaling Mediates Self-Organization and Axis Formation in Embryoid Bodies. *Cell Stem Cell*, 3(5):508–518.

Thomas, P. and Beddington, R. (1996). Anterior primitive endoderm may be respon-

sible for patterning the anterior neural plate in the mouse embryo. *Current Biology*, 6(11):1487–1496.

Trushko, A., Meglio, I. D., Merzouki, A., Blanch-Mercader, C., Abuhattum, S., Guck, J., Alessandri, K., Nassoy, P., Kruse, K., Chopard, B., and Roux, A. (2019). Buckling of epithelium growing under spherical confinement. *bioRxiv*, page 513119.

Turner, D. A., Girgin, M., Alonso-Crisostomo, L., Trivedi, V., Baillie-Johnson, P., Glodowski, C. R., Hayward, P. C., Collignon, J., Gustavsen, C., Serup, P., Steventon, B., P Lutolf, M., Arias, A. M., Lutolf, M. P., Arias, A. M., P Lutolf, M., and Arias, A. M. (2017). Anteroposterior polarity and elongation in the absence of extra-embryonic tissues and of spatially localised signalling in gastruloids: mammalian embryonic organoids. *Development (Cambridge, England)*, 144(21):3894–3906.

van den Brink, S. C., Baillie-Johnson, P., Balayo, T., Hadjantonakis, A.-K. A.-K., Nowotschin, S., Turner, D. A., and Martinez Arias, A. (2014). Symmetry breaking, germ layer specification and axial organisation in aggregates of mouse embryonic stem cells. *Development*, 141(22):4231–42.

Vanderhooft, J. L., Alcoutlabi, M., Magda, J. J., and Prestwich, G. D. (2009). Rheological Properties of Cross-Linked Hyaluronan-Gelatin Hydrogels for Tissue Engineering. *Macromolecular Bioscience*, 9(1):20–28.

Vickerman, V., Blundo, J., Chung, S., and Kamm, R. (2008). Design, fabrication and implementation of a novel multi-parameter control microfluidic platform for three-dimensional cell culture and real-time imaging. *Lab on a chip*, 8(9):1468–77.

Wallingford, J. B. (2019). We Are All Developmental Biologists. *Developmental Cell*, 50(2):132–137.

Warmflash, A., Sorre, B., Etoc, F., Siggia, E. D., and Brivanlou, A. H. (2014). A method to recapitulate early embryonic spatial patterning in human embryonic stem cells. *Nature Methods*, 11(8):847–854.

Xue, X., Sun, Y., Resto-Irizarry, A. M., Yuan, Y., Aw Yong, K. M., Zheng, Y., Weng, S., Shao, Y., Chai, Y., Studer, L., and Fu, J. (2018). Mechanics-guided embryonic patterning of neuroectoderm tissue from human pluripotent stem cells. *Nature Materials*, 17(7):633–641.

Yamamoto, M., Saijoh, Y., Perea-Gomez, A., Shawlot, W., Behringer, R. R., Ang, S.-L., Hamada, H., and Meno, C. (2004). Nodal antagonists regulate formation of the anteroposterior axis of the mouse embryo. *Nature*, 428(6981):387–392.

Yoney, A., Etoc, F., Ruzo, A., Carroll, T., Metzger, J. J., Martyn, I., Li, S., Kirst, C., Siggia, E. D., and Brivanlou, A. H. (2018). WNT signaling memory is required for ACTIVIN to function as a morphogen in human gastruloids. *eLife*, 7:1–28.

Yoshinaga, K. (2013). A sequence of events in the uterus prior to implantation in the mouse. *Journal of assisted reproduction and genetics*, 30(8):1017–22.

Zhang, S., Chen, T., Chen, N., Gao, D., Shi, B., Kong, S., West, R. C., Yuan, Y., Zhi, M., Wei, Q., Xiang, J., Mu, H., Yue, L., Lei, X., Wang, X., Zhong, L., Liang, H., Cao, S., Belmonte, J. C. I., Wang, H., Han, J., Carlos, J., Belmonte, I., Wang, H., and Han, J. (2019). Implantation initiation of self-assembled embryo-like structures generated using three types of mouse blastocyst-derived stem cells. *Nature Communications*, 10(1):496.

Zhang, Z., Zwick, S., Loew, E., Grimley, J. S., and Ramanathan, S. (2018). Embryo geometry drives formation of robust signaling gradients through receptor localization. *bioRxiv*, page 491290.

Zheng, Y., Xue, X., Shao, Y., Wang, S., Esfahani, S. N., Li, Z., Muncie, J. M., Lakins, J. N., Weaver, V. M., Gumucio, D. L., and Fu, J. (2019). Controlled modelling of human epiblast and amnion development using stem cells. *Nature*.